This is to certify that the

dissertation entitled

NON-LINEAR INTERACTIONS IN ROTORDYNAMICS

presented by

Jinsiang Shaw

has been accepted towards fulfillment
of the requirements for

Ph.D degree in Mechanical Engineering

Steven W. Shaw
Major professor

Date September 29, 1989

NON-LINEAR INTERACTIONS IN ROTORDYNAMICS

By

Jinsiang Shaw

A DISSERTATION

Submitted to
Michigan State University
in partial fulfillment of the requirements
for the degree of

DOCTOR OF PHILOSOPHY

Department of Mechanical Engineering

1989

ABSTRACT

NON-LINEAR INTERACTIONS IN ROTORDYNAMICS

By

Jinsiang Shaw

The non-linear dynamic behavior of symmetric rotors is investigated using methods from dynamical systems and bifurcation theories. Rotordynamic instabilities and resonances caused by internal hysteresis, fluid film bearing forces and mass unbalance are analyzed. Two types of models have been proposed to study these effects on rotordynamics: a slender, flexible shaft made of a viscoelastic material and rotating at a constant rate about its longitudinal axis is used to study the effects of internal hysteresis and mass unbalance on rotordynamics, and an unbalanced disk mounted midway between two supporting fluid film journal bearings on a rigid shaft is used to examine the effects of fluid bearing forces and mass unbalance.

For the perfectly balanced flexible shaft model it is well known that internal damping can cause an instability at a certain critical speed. The instabilities are predicted using the linearized shaft model and the post-critical behaviors are determined by applying the center manifold theory to the full non-linear equations of motion. Bifurcations of the trivial shaft configuration (the undeformed, straight position) caused by internal damping include: simple Hopf, double Hopf, and double zero eigenvalues. It is determined that synchronous whirl, non-synchronous whirl, and competing-mode types of

behaviors are possible for various ranges of the parameter values. The results obtained prove that the modal truncations typically used when analyzing instabilities of a continuous shaft are mathematically justifiable.

The first vibrational mode of the shaft is then used to determine the effect of unbalance on system behavior. Special attention is paid to the interaction between the primary resonance caused by mass unbalance and the destabilizing influence of internal damping. Global behavior in terms of the existence and stability of synchronous steady state motions is examined and is followed by an investigation of local behavior near bifurcation points by applying the center manifold theorem. It is shown that the non-linear resonance for a rotating shaft is much more complicated than a simple Duffing-type resonance when any amount of internal damping is present. It includes saddle-node, Hopf, saddle connection, and saddle-node saddle connection bifurcations. The corresponding shaft responses include synchronous constant amplitude motions and amplitude modulated solutions.

For the second model the non-linear oscillations of a rotor supported in fluid film journal bearings is analyzed. The long-bearing approximation with π-film model for cavitation is adopted. With the introduction of periodic forcing due to rotor unbalance, the results show that the limit cycle arising from the whirl instability (a Hopf bifurcation) in the neighborhood of the threshold speed is perturbed and a rich variety of response types is observed when certain resonant conditions occur. These include harmonic, subharmonic, as well as amplitude modulated responses.

In both models, mass unbalance introduces a periodic forcing term which allows the response of the system to be analyzed in terms of a periodically perturbed Hopf bifurcation. Complete bifurcation diagrams in parameter space and results from simulation studies are presented to illustrate the dynamics of the system as system parameters are varied.

To my parents

ACKNOWLEDGMENTS

I would like to take this opportunity to express my sincere gratitude to my adviser, Steven W. Shaw, for his inspiring guidance and encouragement during the course of this research. His valuable insights and suggestions have considerably enriched this research, and are deeply appreciated.

I am also grateful to the other committee members, Ronald Rosenberg, David Yen, and Alan Haddow for their discussion and comments of this dissertation.

Finally, I thank my parents for their love and support throughout my graduate study and research.

TABLE OF CONTENTS

LIST OF FIGURES

CHAPTER I

INTRODUCTION

1.1 Problem Under Investigation

It is a necessary task in the design of rotating machinery to accurately predict the dynamic behavior of rotors over a range of operating conditions. One property of such rotors is high rotational speeds relative to other types of machines of the same physical size. Along with high speeds come the potential problems of shaft whirl, transverse vibration, and rotordynamic instability which greatly limit the designed performance, and can even lead to failure.

Many of the destabilizing forces which cause rotordynamic instability in a rotor system have been identified. Internal friction in rotating parts, hydrodynamic bearings, aerodynamic forces, magnetic and electrodynamic forces, gyroscopic forces, trapped fluids inside of a hollow shaft or rotor, dry friction, and labyrinth seals provide some examples (see Vance, 1987). These destabilizing forces coupled with high rotor speeds provide mechanisms by which some part of the energy of rotation can be transferred into whirl motion of the rotor. Non-linear analysis is often required to investigate the whirl motions in terms of amplitudes as well as stabilities, enabling one to judge how dangerous these vibrations are to the system and decide what measures can be taken to reduce them to acceptable levels.

Internal hysteresis in the material of the shaft and hydrodynamic bearing forces are among the most cited causes for rotordynamic instability, and these have drawn attention from many researchers.

Previous work on the interaction between these destabilizing forces and forces due to mass unbalance has been, to date, confined to linear systems. In this dissertation, the competing effects of rotordynamic instability and resonance will be thoroughly examined by applying dynamical systems and bifurcation theories to the governing non-linear differential equations. In addition, the instability of a continuous shaft is analyzed using these methods, and it is rigorously shown that the modal truncations typically used in the engineering literature are valid.

1.2 Literature Survey

Analysis of the whirling motion of a rotor can be dated back as far as 1919 when Jeffcott proposed a linear model (now widely known as the Jeffcott rotor) in order to analyze the response of high speed rotating machines to rotor unbalance. His analysis shows that the amplitude of synchronous whirl initially increases as the rotor speed is increased and reaches a maximum value at a critical resonant speed, and then decreases and approaches the value of static unbalance at super-critical speeds. In the early 1920's the General Electric Company experienced instability problems with some of their turbo compressors which had been developed for blast furnaces. The turbocompressor displayed a tendency to undergo self-excited tranverse vibrations at speeds other than the critical. These oscillations, which exhibited a lower frequency than the rotational speed, are certainly not associated with the mass unbalance and occur only when the rotational speed is beyond the critical speed of rotation. Among the engineers assigned to this problem, Kimball (1924) was able to show that the cause of their instability was internal hysteresis. In the course of another investigation at General Electric, Newkirk and Taylor (1925) also identified oil film journal bearings as another source of instability.

After the work carried out by Kimball the theoretical aspects of the problem with internal friction were investigated by many researchers (see for example Smith, 1933, Robertson, 1935, Dimentberg, 1951). Pozniak (1958) has compiled a critical summary of the literature on this subject up to 1956. The book by Bolotin (1963) extensively covers the response of a rotor modelled by linear and non-linear, finite and infinite dimensional differential equations under the action of internal friction, with a goal of determining the amplitudes of oscillations beyond the critical speeds; this analysis requires the solution of non-linear equations. Smith (1933) and Ehrich (1964) studied the instability in rotating systems induced by internal damping in the rotor and gave a stability boundary defined in terms of the ratio of external damping of the system to the internal damping in the shaft. It is shown that for various damping conditions one particular whirl mode is induced and that the whirl mode observed is generally the one whose natural frequency is closest to one half of the rotational speed. This is because the whirl motion is likely to occur when the rotational speed is approximately twice the natural frequency of the mode in whirl. Genin and Maybee (1970) have used energy methods and presented results in the form of boundedness and growth theorems for the problem of whirl motions of a linear viscoelastic continuous shaft. They also established conditions for the asymptotic stability of solutions and found lower bounds on the rate of growth of unbounded solutions. Other important treatments in this aspect include works by Tondl (1965), Gunter and Trumpler (1969), Muszynska (1974), Thomson, Younger and Gordon (1977), Torby (1979), Crandall (1980), Bucciarell (1982), Hendricks (1986), and

Zhang and Ling (1986). Crandall (1980) gives detailed physical explanations of the destabilizing effects of damping in rotating parts while Muszynska (1974) presents results for a variety of non-linear damping and structural behavior. Some of the references listed above have predicted post-critical behavior by studying a system of non-linear ordinary equations obtained by a finite dimensional modelling or by modal truncation of partial differential equations. In this dissertation, we will investigate the post-critical behavior by studying the full non-linear partial differential equations for a balanced shaft, thus capturing all the possible effects of each mode on the system response.

While many works (see for example Merkin, 1984, and Ishida et al., 1987) have been done on the dynamics of an unbalanced shaft without internal damping, the combined influence of these two effects, namely the internal damping and unbalance, has received little attention. To the author's knowledge, only the papers by Gunter and Trumpler (1969) and Hendricks (1986) included these effects in an analysis of a linearized rotor system and the works by Muszynska (1974) and Torby (1979) briefly described these effects on non-linear rotor systems. Ariaratnam and Namachchivaya (1986) have also considered the effects of periodic perturbations in rotating systems with non-linear characteristics, but did not consider the competing effects of internal damping and resonance. The competing effects and the resulting dynamics will be examined in this dissertation in both quantitative and qualitative terms for a single mode non-linear rotor system.

Ever since Newkirk and Taylor (1925) identified oil film journal bearing forces as one of the sources for rotordynamic instability, large research efforts have been put into this subject. Early work include those by Hagg (1946), Reddi and Trumpler (1962), Lund and Saibel (1967), and Badgley and Booker (1969). Worthy of mention is the work by Lund and Saibel in which they used method of averaging to solve the non-linear equations to obtain the whirl orbits in terms of their existence, position and amplitude. Badgley and Booker proposed three models for the journal bearing force due to the fluid film and investigated the corresponding rigid-body dynamics of rotors via numerical simulations. Representative recent works are those by Childs, Moes and van Leeuwen (1977), Barrett, Allaire and Gunter (1980), Taylor (1980), and Brindley, Elliott, and McKay (1983). Recently, more complete parameter studies for such systems have been carried out by Myers (1984) and Hollis and Taylor (1986) by applying the Hopf bifurcation theorem and by Gardner et al. (1985) by using the method of multiple scales.

The introduction of periodic forcing due to rotor unbalance has received less attention, mainly due to the lack of suitable methods. Barrett, Akers and Gunter (1976), Gunter, Humphris and Springer (1983) and Hollis and Taylor (1987) employed numerical integration to examine these perturbed motions. Here we present an analytical approach to periodically forced problem in the neighborhood of the threshold speed where self-excited oscillation exists for the balanced rotor. Numerical integrations are employed to support the findings.

1.3 Scope of the Investigation

In this dissertation, two simplified models for symmetric rotor systems with constant speed of rotation are proposed and detailed analyses are used to determine the qualitative features of their dynamics in the presence of internal damping, mass unbalance, and oil film journal bearing forces. An outline of the goals of these investigations is as follows:

(1). To determine the effect of internal damping on rotordynamic instability of a balanced, flexible, continuous rotating shaft. The instability boundary for the pure rotation of the shaft is obtained, above which whirl motions of the shaft are anticipated. The linearized model for this system also indicates which mode(s) is (are) eligible to whirl above the instability curve.

(2). To determine the post-critical speed behavior of the shaft when rotational speeds exceed the critical speed. The stabilities and whirl frequencies of the critical modes are determined. The center manifold theorem is applied to this infinite dimensional non-linear dynamical system (in the form of two coupled PDE's) in order to study the dynamics in the neighborhood of bifurcation points, thus ensuring that the necessary dynamics from all modes are included.

(3). To determine the response in the presence of the competing effects of internal damping and first mode resonance excited by mass unbalance. Here a single mode shaft model is employed. The amplitude and stability of steady state solutions representing synchronous whirling of the shaft are determined and presented in the form of frequency response curves for various levels of unbalance. The center manifold theorem is again applied in the neighborhood of the critical speed in order to deduce the shaft behavior near critical speeds. Special attention is placed on the occurrence of local and global bifurcations which result in a variety of transitions which can lead to sudden changes in the shaft motion. Response in terms of shaft motions are checked by computer simulations. The response is shown to generally be either synchronous whirl or a whirl which undergoes slow, but periodic, amplitude and phase modulations. The type of behavior observed depends on the system parameters and the initial conditions, and a quite complete account of these motions is presented.

(4). To determine the response of a rotor supported in fluid film journal bearings under the action of a constant load (due to gravity) and rotor unbalance. Due to the complex non-linear nature of the forces inherent in fluid film journal bearings, a variety of interesting motions are to be expected. The model we employ for these forces is originally proposed by Myers (1984) and employs the long-bearing assumption with π-film fluid to account for cavitation in the bearings. The center manifold theorem and normal form theorem are extensively employed in the analysis. Non-resonant and resonant responses with emphasis on the latter are studied and given in the form of bifurcation diagrams and associated phase portraits in terms of the system parameters. In particular, 1/1 and 1/2 resonances (here p/q is defined as the ratio of the frequency of the limit cycle arising from the Hopf bifurcation for the balanced case to the excitation frequency for the unbalanced case) are carefully investigated.

1.4 Methods of Analysis

Throughout this dissertation, methods of dynamical systems and bifurcation theories are frequently employed to investigate the non-linear dynamics of rotor systems. In this section we briefly review some of them. The books by Iooss (1979), Carr (1981), Guckenheimer and Holmes (1983), and Arnold (1987) should be referenced for more complete and in depth treatments of dynamical system theories and bifurcation theories.

In the following we confine our discussions to vector fields generated by differential equations. Analogous arguments (with some modifications) may be applied to discrete time maps. Changes in the qualitative structure of a system response may occur when the system parameter values are varied. These changes are called bifurcations and the corresponding parameter values are called bifurcation values. Bifurcations involved in the stability changes of individual equilibria and periodic orbits, as eigenvalues of the linearized system cross stability boundaries in the complex plane, are referred to as local bifurcations. That is, local bifurcations occur at parameter values which have neutral linear stability, in which case non-linear terms are important and small changes yield different behavior. Other bifurcations, which involve changes in the global structure of the phase space, are called global bifurcations. Examples of local bifurcations are transcritical, saddle-node, pitchfork, Hopf, and flip bifurcations. See Guckenheimer and Holmes (1983) for details of the above bifurcations and some more complicated local bifurcations which are not covered here, but do occur in the analysis described in this dissertation.

At a saddle-node bifurcation a pair of solutions (representing equilibria or periodic orbits) coalesce and annihilate one another as shown in Figure 1. A super- (sub-, resp.) critical pitchfork bifurcation is shown in Figure 2 in which a symmetric solution undergoes a stability change and an antisymmetric pair of stable (unstable, resp.) orbits bifurcate from that orbit at the bifurcation point. The Hopf bifurcation is responsible for the birth of limit cycles which exist above (below, resp.) the bifurcation point for the super- (sub-, resp.) critical Hopf bifurcation, as shown in Figure 3. Flip bifurcations, which are also referred to as period doubling bifurcations, involve the instability of a periodic solution and the birth of a new periodic

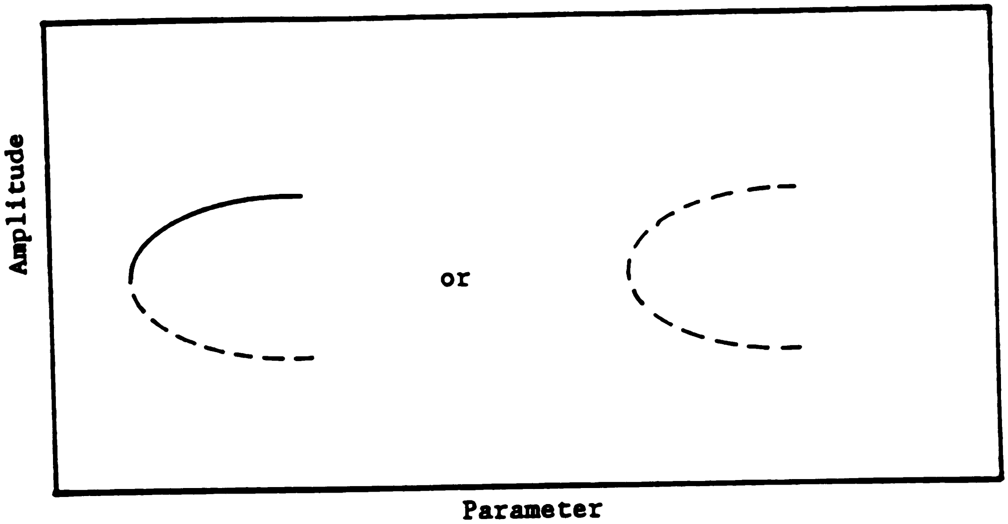

Figure 1. Saddle-node bifurcation.

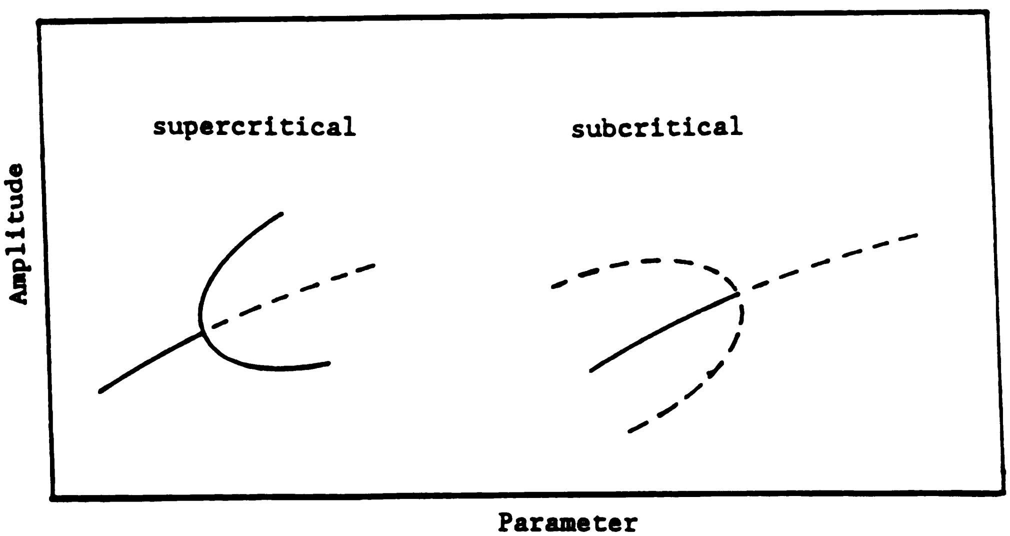

Figure 2. Pitchfork bifurcation.

motion with period double that of the original period. Figure 4 shows a super- (sub-,resp.) critical period doubling bifurcation in which a stable periodic orbit of period T loses its stability and becomes unstable with the appearance of a stable (unstable, resp.) periodic orbit with period 2T which exists above (below, resp.) the bifurcation point.

The global bifurcations which are encountered in this dissertation are saddle connections of homoclinic (and heteroclinic types, resp.) in which the stable manifold of a saddle type invariant set connects to its own (or another saddle set's, resp.) unstable manifold. Often a limit cycle appears or disappears at such a bifurcation point, although in systems with phase space of dimension greater than two, chaos and other exotic dynamics can occur near such bifurcations; see Wiggins (1988) for thorough treatment.

Two methods will be described here and used later to simplify equations of motion near certain critical points: they are the center manifold theory (dimensional reduction) and normal form theory (elimination of all non-essential non-linear terms by coordinate changes). For studying the <u>local</u> behavior near a bifurcation point, center manifold theory can be employed. A center manifold, denoted by W^c, is an invariant manifold (i.e., a surface) tangent to the center eigenspace E^c, i.e., the eigenspace associated with non-hyperbolic eigenvalues (an eigenvalue with zero real part is called non-hyperbolic). There are three essential theorems associated with center manifold theory. We start by considering the differential equations

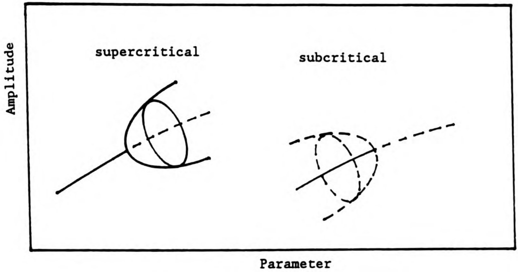

Figure 3. Hopf bifurcation.

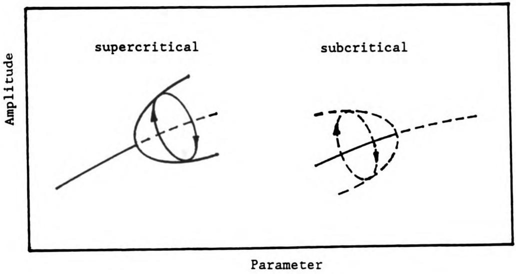

Figure 4. Flip bifurcation.

$$\dot{x} = Ax + f(x,y)$$

$$\dot{y} = By + g(x,y) \qquad , \ (x,y) \in R^c \times R^s \qquad (1.4.1)$$

with $f(0,0) = g(0,0) = Df(0,0) = Dg(0,0) = 0$. A is a $c \times c$ constant matrix having all eigenvalues with zero real parts while B is an $s \times s$ constant matrix having all eigenvalues with negative real parts. Proofs for the following three theorems can be found in the book by Carr (1981); only the theorems are stated here.

Theorem 1. (Existence and Reduction Theorem, Carr, 1981)

There exists a C^r center manifold for equation (1.4.1) for $r \geq 2$ which can be locally represented as follows (see also Figure 5)

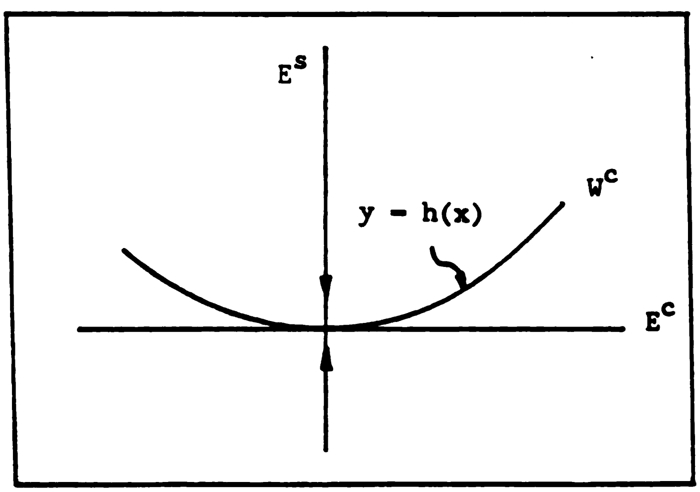

Figure 5. A center manifold.

$$W^c = \{ (x,y) \in R^c \times R^s \mid y = h(x),\ |x| < \delta,\ h(0) = Dh(0) \}$$

for δ sufficiently small. The dynamics of (1.4.1) on the center manifold is governed by the following c-dimensional vector field

$$\dot{u} = Au + f(u,h(u)) \qquad , u \in R^c \tag{1.4.2}$$

Theorem 2. (Stability of the Full system from the Reduced System, Carr, 1981)

(i) Stable (asymptotically stable, unstable, resp.) zero solution of equation (1.4.2) infers stable (asymptotically stable, unstable, resp.) zero solution of equation (1.4.1).

(ii) Suppose that the zero solution of equation (1.4.2) is stable. Then there is a solution u(t) of equation (1.4.2) such that the solution (x(t), y(t)) of equation (1.4.1) with (x(0), y(0)) sufficiently small approach (u(t), h(u(t))) exponentially fast as $t \to \infty$.

Theorems 1 and 2 guarantee the existence of a center manifold for equation (1.4.1) and provide the qualitative nature of the dynamics of equation (1.4.1). In the neighborhood of the zero solution these are well approximated by the dynamics of equation (1.4.2) on the center manifold, which has a lower dimension than the full system. This reduction of dimension makes the analyses of a dynamical system easier, while still capturing all the important recurrent dynamics (e.g. fixed points, periodic orbits, homoclinic orbits, etc.,). In practice, we need to compute the center manifold h(x) from equation (1.4.1). This can be done locally using Taylor series expansion as follows: take the derivative of y = h(x) with respect to time and use the chain rule to obtain:

$$\dot{y} = Dh(x)\dot{x} = Dh(x)\,[Ax + f(x,h(x))] = Bh(x) + g(x,h(x))$$

Now define N[h(x)] such that

$$N[h(x)] = Dh(x)\,[Ax + f(x,h(x))] - Bh(x) - g(x,h(x)) = 0 \qquad (1.4.3)$$

This equation for h(x) cannot be usually solved explicitly but can be approximated arbitrarily well by a Taylor series near the zero solution. This is stated in Theorem 3.

Theorem 3. (Approximation of Center Manifold, Carr, 1981)

Let $\phi(x) : R^c \to R^s$ be a C^1 mapping with $\phi(0) = D\phi(0) = 0$. Suppose that $N[\phi(x)] = O(|x|^p)$ as $|x| \to 0$ for some $p > 1$. Then

$$|h(x) - \phi(x)| = O(|x|^p) \text{ as } |x| \to 0 \qquad (1.4.4)$$

Hence we can approximate h(x) by $\phi(x)$ as closely as desired.

Another way of simplifying a dynamical system near critical points is by utilizing the normal form theorem. It is used to put a differential equation into the so-called normal form (defined below) by which the dynamics of the system are more easily derived. The normal form for a dynamical system depends only on the linear structure of the governing differential equations. Consider a C^r vector field described by

$$\dot{x} = Jx + F(x) \qquad x \in R^n \tag{1.4.5}$$

where J is in real Jordan canonical form (Bellman, 1970) and F(x) is non-linear. Expanding F(x) about zero by a Taylor series, equation (1.4.5) becomes

$$\dot{x} = Jx + F_2(x) + F_3(x) + \ldots + F_{r-1}(x) + 0\,(|x|^r) \tag{1.4.6}$$

Here we would like to ask the question, by changes of coordinates can one eliminate the 0(2) terms, then 0(3) terms, and so on, of equation (1.4.6) ? According to the normal form theorem (Arnold, 1987, chapter 5), one can eliminate 0(2) terms , then 0(3) terms, and so on by successive coordinate changes provided J has no eigenvalues with zero real parts (this is simply the Hartman-Grobman theorem, which says the dynamics of equation (1.4.5) in the neighborhood of the origin is dominated by the linear terms). If J has eigenvalues with zero real parts, one can still reduce large classes of equations to relatively simple nonlinear forms - normal forms.

The center manifold theorem combined with the normal form theorem give one a powerful tool to study the dynamics of dynamical systems governed by non-linear differential equations. We conclude this section with some remarks on extensions of the center manifold and normal form theorems:

(1). Center manifold and normal form theorems apply also to vector fields depending on parameters, for parameters close to critical values. This is done by employing the suspension trick.

(2). Center manifolds are not necessarily unique.

(3). Center manifold methods also apply to certain classes of infinite dimensional equations (i.e., PDE's)

(4). Center manifolds may be time dependent.

See Carr (1981) for more information on these extensions, which are vital to the studies here since the equations of motion (ODE' and/or PDE's) for the models considered depend on system parameters and are often time dependent.

1.5 Dissertation Arrangement

The dissertation is arranged as follows. Chapter II discusses the governing equations of motion and the stability and bifurcations of the undisturbed (pure rotation) solution of a balanced flexible shaft made of a viscoelastic material. This is followed by a non-linear analysis to examine the post-critical behavior of the shaft. Three types of bifurcation of the trivial solution are investigated and the results are interpreted in terms of physical dynamics of the shaft.

The competing effects of the destabilizing forces induced by internal friction and those due to the primary resonance excited by mass unbalance are investigated in Chapter III. Complete bifurcation diagrams, the associated phase portraits, and frequency response diagrams are presented in the neighborhood of the first critical speed. These provide a detailed description of the dynamic response of the shaft and clearly indicate the net effects of the two competing effects. Simulation results are also given to support the analytical findings. In Chapter IV we analyze the effects of the destabilizing forces of fluid film journal bearings on rotordynamic instability. Depending on system parameters, the equilibrium position of the perfectly balanced rotor may undergo either super- or sub-critical Hopf bifurcation. With the introduction of periodic forcing due to rotor unbalance, we then carefully examine the periodically perturbed Hopf bifurcation problem. In Chapter V we close the dissertation with some conclusions and directions for future work. In all cases descriptions of the physical dynamics of the rotor are provided along with the mathematical results.

CHAPTER II

INSTABILITIES AND BIFURCATIONS IN A PERFECTLY BALANCED ROTATING SHAFT

2.1 Mathematical Model

In this chapter we investigate the effects of internal damping on the dynamics of a rotor system. A relatively simple model is proposed to single out the role of internal friction arising from the assumption that the rotating shaft is made of a dissipative material. The model is as shown in Figure 6: a slender symmetric shaft of circular cross section, length ℓ, and rotating about its longitudinal axis at a fixed rate, Ω, undergoes motions which can be represented by transverse displacements in a rotating coordinate frame (x, y, z). The shaft will be assumed to be simply supported at both ends, other types of boundary condition can be considered and would give rise to different mode shapes for the shaft, but the method of analysis will be unchanged. The equations of motion will be generated using Hamilton's principle.

Employing the usual beam theory assumptions, the displacement of an arbitrary point in the cross-section is given by $\vec{r} = (u+x)\vec{i} + (v+y)\vec{j} + (w - xu' - yv')\vec{k}$ where $u(z,t)$, $v(z,t)$, $w(z,t)$ are the displacement components of a point on the neutral axis, a prime denotes differentiation with respect to z, and $(\vec{i},\vec{j},\vec{k})$ are the usual unit vectors. The velocity of this point is given by $\vec{V} = \dot{\vec{r}} + (\vec{\Omega} \times \vec{r})$ where $\vec{\Omega} = \Omega\vec{k}$. The kinetic energy of the shaft T can then be written as

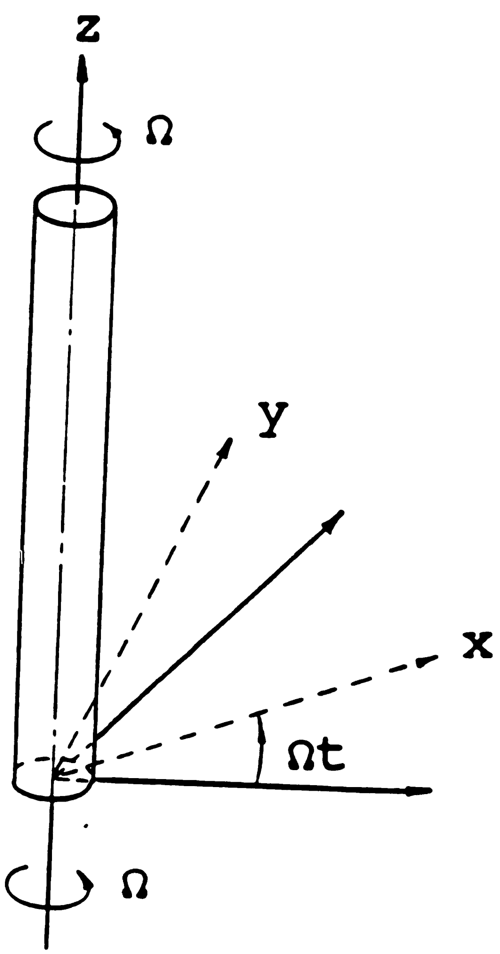

Figure 6. The physical system and associated coordinates.

$$T = \frac{1}{2} \int \vec{V} \cdot \vec{V} \, dm = \frac{1}{2} \int_0^{\ell} \int_A \rho \, V^2 \, dAdz \quad .$$

If the shaft is axially restrained and large deflections are permitted it can be shown (see Ho, Scott, and Eisley, 1975) that the only non-zero strain component is in the z direction, and it is given by

$$\epsilon = w' - xu'' - yv'' + \frac{1}{2} (u'^2 + v'^2)$$

from which the strain energy is given as

$$U = \frac{1}{2} \int_0^{\ell} \int_A E \, \epsilon^2 \, dAdz$$

The shaft is made of a Voight viscoelastic material with stress given by $\sigma = E(\epsilon + \mu_i \dot{\epsilon})$ where ϵ is the strain, E is Young's elastic modulus, and μ_i is a material viscosity parameter (representing internal damping). External damping is modeled by assuming that the resulting dissipative force on a beam element is proportional to its absolute velocity. The work W done by these non-conservative forces can readily be determined. The equations of motion are then obtained by applying Hamilton's principle

$$\int_{t_1}^{t_2} [\, \delta \, (T - U) + W \,] \, dt = 0$$

which have the following forms

$$-\rho A\ddot{w} + EAw'' + EA(u'u'' + v'v'') + EA\mu_i(\dot{w}' + u'\dot{u}' + v'\dot{v}')' = 0$$

$$-\rho A\ddot{u} - EIu'''' - \mu_e\dot{u} + 2\rho A\Omega\dot{v} + \rho A\Omega^2 u + \mu_e\Omega v - EI\mu_i\dot{u}''''$$

$$+ EA(w'u')' + EA[\, u''(u'^2 + v'^2) + u'(u'^2 + v'^2)'\,]/2 + EA\mu_i(u'\dot{w}')'$$

$$+EA\mu_i[\, u'(u'\dot{u}' + v'\dot{v}')\,]' = 0 \qquad (2.1.1)$$

$$-\rho A\ddot{v} - EIv'''' - \mu_e\dot{v} - 2\rho A\Omega\dot{u} + \rho A\Omega^2 v - \mu_e\Omega u - EI\mu_i\dot{v}''''$$

$$+ EA(w'v')' + EA[\, v''(u'^2 + v'^2) + v'(u'^2 + v'^2)'\,]/2 + EA\mu_i(v'\dot{w}')'$$

$$+EA\mu_i[\, v'(u'\dot{u}' + v'\dot{v}')\,]' = 0$$

The z component of these equations is simplified by neglecting the longitudinal inertial force which yields

$$[w' + \frac{1}{2}(u'^2 + v'^2) + \mu_i\dot{w}' + \mu_i(u'\dot{u}' + v'\dot{v}')]' = 0. \qquad (2.1.2)$$

Integrating this with respect to z and using the boundary conditions $w(0) = w(\ell) = 0$ yields

$$w' + \frac{1}{2}(u'^2 + v'^2) + \mu_i\dot{w}' + \mu_i(u'\dot{u}' + v'\dot{v}') =$$

$$\frac{1}{2\ell}\int_0^{\ell}(u'^2 + v'^2)\,ds + \mu_i\frac{1}{2\ell}\frac{d}{dt}\int_0^{\ell}(u'^2 + v'^2)\,ds \qquad (2.1.3)$$

The variable z can be eliminated by substituting equations (2.1.2) and (2.1.3) into the x and y components of (2.1.1) yielding

$$\rho A\ddot{u} + EIu'''' + \mu_e\dot{u} - 2\rho A\Omega\dot{v} - \rho A\Omega^2 u - \mu_e\Omega v + EI\mu_i\dot{u}''''$$

$$- \frac{EA}{2\ell}\left[\int_0^\ell (u'^2 + v'^2)\,ds + \mu_i \frac{d}{dt}\int_0^\ell (u'^2 + v'^2)\,ds\right] u'' = 0$$

$$\rho A\ddot{v} + EIv'''' + \mu_e\dot{v} + 2\rho A\Omega\dot{u} - \rho A\Omega^2 v + \mu_e\Omega u + EI\mu_i\dot{v}''''$$

$$- \frac{EA}{2\ell}\left[\int_0^\ell (u'^2 + v'^2)\,ds + \mu_i \frac{d}{dt}\int_0^\ell (u'^2 + v'^2)\,ds\right] v'' = 0 \qquad (2.1.4)$$

where ρ denotes mass density, A the cross-sectional area, I the second moment of area of the cross-section, and μ_e, μ_i are the external and internal damping constants, respectively.

In order to express (2.1.4) in dimensionless form, the following non-dimensional variables are introduced:

$$\bar{u} = u/\ell \ , \ \bar{v} = v/\ell \ , \ \bar{z} = z/\ell$$

$$\tau = \sqrt{EI/\rho A\ell^4}\, t = \gamma t \ , \ \bar{\mu}_e = \mu_e/\rho A\gamma$$

$$\bar{\mu}_i = \mu_i\gamma \ , \ \alpha = A\ell^2/2I \ , \ \bar{\Omega} = \Omega/\gamma$$

Under this rescaling equation (2.1.4) becomes, after dropping all overbars for convenience:

$$\ddot{u} + u'''' + \mu_e \dot{u} - 2\,\Omega \dot{v} - \Omega^2 u - \mu_e \Omega v + \mu_i \dot{u}'''' - \alpha \left[\int_0^1 (u'^2 + v'^2)\, ds \right.$$

$$\left. + \mu_i \frac{d}{d\tau} \int_0^1 (u'^2 + v'^2)\, ds \right] u'' = 0$$

$$\ddot{v} + v'''' + \mu_e \dot{v} + 2\Omega \dot{u} - \Omega^2 v + \mu_e \Omega u + \mu_i \dot{v}'''' - \alpha \left[\int_0^1 (u'^2 + v'^2)\, ds \right.$$

$$\left. + \mu_i \frac{d}{d\tau} \int_0^1 (u'^2 + v'^2)\, ds \right] v'' = 0 \qquad (2.1.5)$$

where $(\dot{\ }) = \frac{\partial(\ )}{\partial \tau}$ and $(\ )' = \frac{\partial(\ )}{\partial z}$.

Remarks:

i) This equation is described in a system of coordinates x-y-z rotating at the constant angular speed Ω with the shaft about the z axis.

ii) The effects of mass unbalance, transverse shear, rotary inertia, longitudinal inertia, externally applied forces and torques, and gravity are not included.

For simply supported ends the solution of equation (2.1.5) is assumed to have the form

$$u = \sum_{n=1}^{\infty} u_n(\tau)\, \phi_n(z)$$

$$v = \sum_{m=1}^{\infty} v_m(\tau)\, \phi_m(z) \tag{2.1.6}$$

where $u_n(\tau)$ and $v_m(\tau)$ are unknown functions of time, τ, and $\phi_n(z) = \sqrt{2}$ sin $(n\pi z)$ are the eigenfunctions of the linearized system. Substituting assumption (2.1.6) into equation (2.1.5) and using Galerkin's method gives the following set of non-linear ordinary differential equations in terms of the modal amplitudes:

$$\ddot{u}_n + \Omega_n^2 u_n + \mu_e \dot{u}_n - 2\Omega \dot{v}_n - \Omega^2 u_n - \mu_e \Omega v_n + \mu_i \Omega_n^2 \dot{u}_n$$

$$+ \alpha\, \Omega_n^2 \left\{ \left(1 + \mu_i \frac{d}{d\tau} \right) \left[\sum_{j=1}^{\infty} \left(u_j^2 + v_j^2 \right) \Omega_j^2 \right] \right\} u_n = 0$$

$$\ddot{v}_n + \Omega_n^2 v_n + \mu_e \dot{v}_n + 2\Omega \dot{u}_n - \Omega^2 v_n + \mu_e \Omega u_n + \mu_i \Omega_n^2 \dot{v}_n$$

$$+ \alpha\, \Omega_n^2 \left\{ \left(1 + \mu_i \frac{d}{d\tau} \right) \left[\sum_{j=1}^{\infty} \left(u_j^2 + v_j^2 \right) \Omega_j^2 \right] \right\} v_n = 0 \quad \forall n \in N \tag{2.1.7}$$

where $N = \{1, 2, 3, \ldots\}$ and $\Omega_n = (n\pi)^2$ is the flexural vibration frequency of small oscillations of mode n of the non-rotating shaft. Existence and stability of steady state solutions are discussed in the next section.

2.2 Steady State Solutions

A steady state synchronous motion corresponds to a constant solution of equation (2.1.7). It is easy to see that the trivial solution corresponding to the undeformed configuration of the shaft is always such a solution. A straightforward calculation shows that non-trivial steady state solutions exist only when $\Omega > \Omega_1$ and $\mu_e = 0$ (i.e., no external damping) and that these are given by

$$u_n^2 + v_n^2 = (\Omega^2 - \Omega_n^2)/\alpha\Omega_n^2 \ , \text{ for } n = \{1,2,\dots, n_{max}\} \text{ which satisfy}$$

$$\Omega_n < \Omega \text{ and } u_j = v_j = 0 \quad , \quad \forall\, j > n_{max} \tag{2.2.1}$$

These solutions are circles of equilibria which bifurcate from the trivial solution whenever the rotational speed exceeds an Ω_n. These equilibria represent buckling of the shaft and correspond to synchronous whirling, that is, the shaft position is fixed in the rotating frame (x,y,z). This indicates that for $\Omega_n < \Omega \leq \Omega_{n+1}$ only the first n modes are eligible to undergo synchronous whirl at rotational speed Ω. The determination of which modes are observable requires knowledge about the stability of these non-trivial solutions; this is discussed in Section 2.4. Note that these solutions exist only in the absence of external damping.

The stability of the trivial steady state solution may be determined by employing the substitution

$$u_n(\tau) = A_1 \exp(\lambda_n \tau)$$

$$v_n(\tau) = A_2 \exp(\lambda_n \tau) \tag{2.2.2}$$

in equation (2.1.7) and neglecting non-linear terms. The resulting characteristic equations have the following form

$$\lambda_n^4 + C_1\lambda_n^3 + C_2\lambda_n^2 + C_3\lambda_n + C_4 = 0 \ \forall\ n\epsilon N. \tag{2.2.3}$$

The Routh-Hurwitz criteria indicates that the $n^{\underline{th}}$ mode is stable if the condition $C_1C_2C_3 - C_3^2 - C_1^2 C_4 \geq 0$ holds, which can be expressed in terms of the system parameters as

$$\Omega \leq \Omega^*_n = \Omega_n + \frac{\mu_e}{\mu_i \Omega_n} \quad . \tag{2.2.4}$$

Bolotin (1963), Ehrich (1964), and Zhang and Ling (1986) give the same result. The frequency Ω^*_n is the angular velocity above which pure rotation is unstable and hence the $n^{\underline{th}}$ mode is expected to whirl (this will be examined for the full non-linear system by using center manifold methods). It is noted from equation (2.2.4) that the external resistance delays the instability of pure rotation and that depending on the ratio of external damping to internal damping, $\frac{\mu_e}{\mu_i}$, the mode undergoing whirl is not necessarily the first mode. In fact, the limiting stability condition is associated with the $n^{\underline{th}}$ mode over the range

$$n^2 (n-1)^2 < \frac{\mu_e}{\mu_i \Omega_1^2} < n^2 (n+1)^2 . \qquad (2.2.5)$$

from which it is seen that the first mode will undergo whirling if $0 < \mu_e/\mu_i\Omega_1^2 < 4$ is satisfied, i.e., the ratio of external damping to internal damping is not too large. See Ehrich (1964) for a complete description. In Figure 7 the neutral stability curves are presented, from which it is seen that there are three distinct ways in which the trivial shaft configuration can lose its stability according to the linear theory. These are referenced in Figure 7 as follows: a double zero eigenvalue structure at the points D_i where two zero eigenvalues

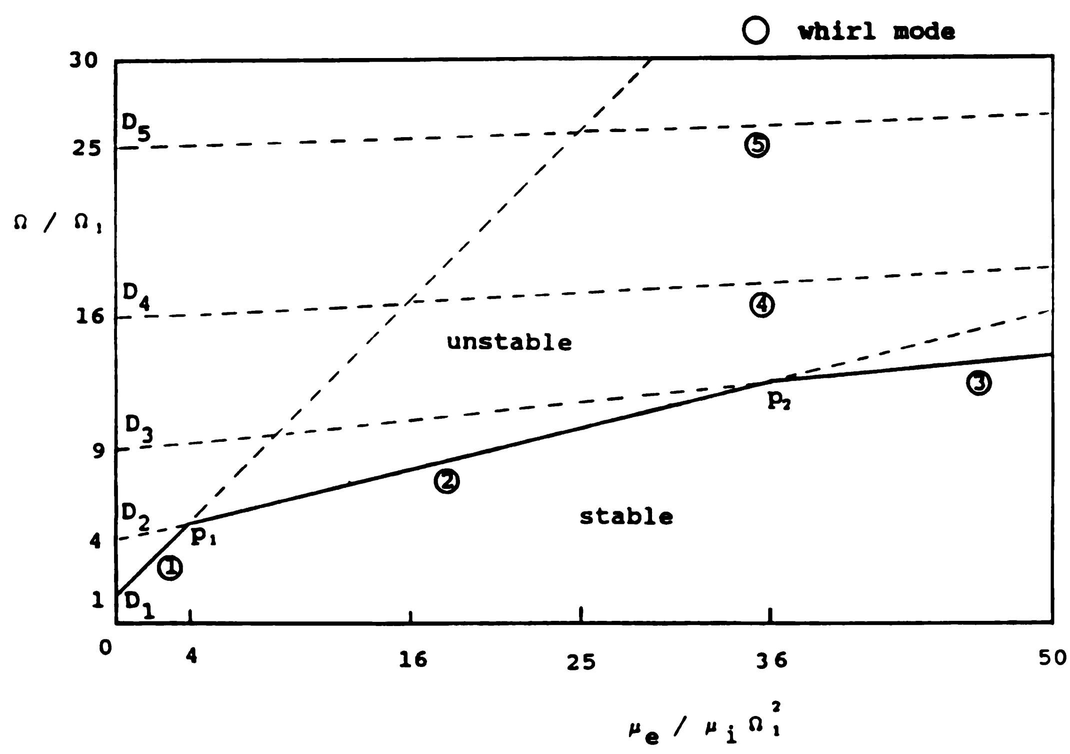

Figure 7. **Stability boundaries in** $(\Omega/\Omega_1,\ \mu_e/\mu_i\Omega_1^2)$ **space.**

associated with mode i exist; a pair of purely imaginery eigenvalues at all non-intersection points on the curves; and two pairs of purely imaginary eigenvalues (one pair from mode i and the other from mode i+1) at the points P_i. The corresponding bifurcations will be a simple double zero, a simple Hopf, and a non-resonant double Hopf, respectively.

The following three sections contain the main results. The procedure used to analyze the dynamics near the points of instability will be as follows. The partial differential equation is first written as an ordinary differential equation in a suitable space. At the points where stability changes occur, center manifold theory is used to construct a finite set of ordinary differential equations (ODE's) which completely and rigorously (Carr, 1981) capture the shaft dynamics near the instabilities. The dependent variables in these finite ODE's correspond to modal amplitudes and phases and the nature of the associated shaft dynamics can be readily interpreted from them. These equations take on the standard normal forms for the corresponding bifurcations and are easily analyzed using phase plane techniques. Conclusions are drawn about the behavior of the rotating shaft near the bifurcation points by investigating the coefficients of the normal forms.

By using center manifold theory one can be certain that the full effects of all modes are captured in the post-critical dynamics. It does turn out that in the cases considered in this chapter one could obtain exactly the same results by simple truncation, that is, by simply ignoring the dynamics of the modes which are not obviously involved in the instability. However, one cannot know this without tackling the full problem.

Equation (2.1.5) can be written as an ordinary differential equation (in infinite dimensions) as follows:

$$\dot{W} = CW + N(W) \tag{2.2.6}$$

where $W = (w_1, w_2, w_3, w_4)^T = (u, v, \dot{u}, \dot{v})^T$,

$$CW = \begin{bmatrix} w_3 \\ w_4 \\ \left(\Omega^2 - \dfrac{d^4}{dz^4}\right) w_1 + \mu_e \Omega\, w_2 - \left(\mu_e + \mu_i \dfrac{d^4}{dz^4}\right) w_3 + 2\Omega\, w_4 \\ -\mu_e \Omega\, w_1 + \left(\Omega^2 - \dfrac{d^4}{dz^4}\right) w_2 - 2\Omega\, w_3 - \left(\mu_e + \mu_i \dfrac{d^4}{dz^4}\right) w_4 \end{bmatrix} ,$$

$$N(W) = \begin{bmatrix} 0 \\ 0 \\ g_1\ (W) \\ g_2\ (W) \end{bmatrix} ,$$

$$g_1(W) = \left\{ \alpha \int_0^1 \left[w_1'\ (\theta)^2 + w_2'\ (\theta)^2 \right] d\theta + 2\alpha\, \mu_i \int_0^1 \left[w_1'\ (\theta)\ w_3'\ (\theta) + w_2'\ (\theta)\ w_4'\ (\theta) \right] d\theta \right\} w_1'' \quad , \text{ and}$$

$$g_2\ (W) = \left\{ \alpha \int_0^1 \left[w_1'\ (\theta)^2 + w_2'\ (\theta)^2 \right] d\theta + 2\alpha\, \mu_i \int_0^1 \left[w_1'\ (\theta)\ w_3'\ (\theta) + w_2'\ (\theta)\ w_4'\ (\theta) \right] d\theta \right\} w_2'' \ .$$

Note that C is linear operator associated with the linearized shaft dynamics which are given by $\dot{W} = CW$. Its spectrum will consist of distinct eigenvalues which are the roots of the characteristic equations (2.2.3). The term N(W) contains the nonlinearities.

In terms of mathematical formalism, W is an element in a Banach space, Z, with norm $||\cdot||$ where $Z = (H_0^2(0,1))^2 \times (L^2(0,1))^2$. H_0^2 (0,1) denotes the Sobolev space of twice differentiable functions which vanish at 0 and 1 and L^2 (0,1) is the usual Hilbert space of square integratable functions. The linear operator C generates a strongly continuous semigroup on Z and N is a C^∞ map from Z to Z with $N(0) = N'(0) = 0$ where N' is the Frechet derivative of N.

By varying the parameters μ_e and Ω equilibrium points and limit cycles of equation (2.2.6) can appear, disappear and change their stability types in bifurcations. The three different types of bifurcations encountered are now described in detail.

2.3 Bifurcation Analysis Near a Double Zero Eigenvalue

In the following the dynamics of the shaft model will be explored near the parameter values where C has a double zero eigenvalue, in particular, point D_1 in Figure 7 will be considered. Two small parameters are introduced which measure the parameter deviations from point D_1: $\epsilon_1 = \Omega - \Omega_1$ represents rotational speed variation from the natural and $\epsilon_2 = \mu_e$ is the external damping coefficient. The vector ϵ is defined by $(\epsilon_1, \epsilon_2)^T$.

It is the first mode of the shaft which becomes unstable at point D_1. The fact that a double zero eigenvalue structure exists at D_1

implies that the behavior of the shaft near D_1 will be dominated by a pair of ordinary differential equations which represent the "slow" dynamics associated with those eigenvalues. The remaining eigenvalues all have negative real parts and represent rapidly decaying dynamics. The nonlinear coupling between modes prevents one from immediately ignoring these "fast" dynamics; the center manifold and normal form methods provide one way to determine which of the nonlinear terms are essential to the dynamics.

To begin the analysis, consider that part of C which corresponds to the first mode, that is, restricted to the first mode subspace = $\{r \sin(\pi z): r = (r_1, r_2, r_3, r_4)^T \epsilon \mathbf{R}^4\}$. It is denoted by C_1 and can be written as:

$$C_1 = \begin{bmatrix} 0 & 0 & 1 & 0 \\ 0 & 0 & 0 & 1 \\ \Omega^2-\Omega_1^2 & -\mu_e\Omega & -\mu_i\Omega_1^2-\mu_e & 2\Omega \\ -\mu_e\Omega & \Omega^2-\Omega_1^2 & -2\Omega & -\mu_i\Omega_1^2-\mu_e \end{bmatrix} = \begin{bmatrix} 0 & 0 & 1 & 0 \\ 0 & 0 & 0 & 1 \\ 0 & 0 & -\mu_i\Omega_1{}^2 & 2\Omega_1 \\ 0 & 0 & -2\Omega_1 & -\mu_i\Omega_1{}^2 \end{bmatrix}$$

$$+ \begin{bmatrix} 0 & 0 & 0 & 0 \\ 0 & 0 & 0 & 0 \\ \epsilon_1(\epsilon_1 + 2\Omega_1) & \epsilon_2(\epsilon_1 + \Omega_1) & -\epsilon_2 & 2\epsilon_1 \\ -\epsilon_2(\epsilon_1 + \Omega_1) & \epsilon_1(\epsilon_1+2\Omega_1) & -2\epsilon_1 & -\epsilon_2 \end{bmatrix} = C_{1,0} + C_{1,\epsilon}$$

where $C_{1,0}$ represents C_1 evaluated at D_1 and $C_{1,\epsilon}$ represents the change in C_1 as ϵ is varied, i.e., as one changes parameters away from point

D_1. The matrix $C_{1,0}$ has two zero eigenvalues and a pair of complex conjugate eigenvalues with negative real parts. It is convenient to work with the equations of motion written in terms of the eigencoordinates associated with the eigenvalues $(0, 0, -\sigma \pm \lambda j)$, σ, $\lambda > 0$ where $j^2 = -1$. To this end, let the matrix $Q = (q_1, q_2, q_3, q_4)$ where q_i is the eigenvector corresponding to the $i^{\underline{th}}$ eigenvalue of $C_{1,0}$. Using Q in a similarity transformation, $W = QZ$, the quation of motion (2.2.6) is written in terms of the eigencoordinates Z:

$$\dot{Z} = Q^{-1} CQZ + Q^{-1}N(QZ). \qquad (2.3.1)$$

It is desired to split Z into its two essential parts: one part corresponding to the slow dynamics associated with the zero eigenvalues and the other part containing the remaining fast dynamics. This is accomplished by defining two subspaces, X and Y, such that $Z = X \oplus Y$, where $X = (s_1, s_2, 0, 0)^T \psi(z)$ with $\psi(z) = \sin(\pi z)$ and $(s_1, s_2) \in \mathbf{R}^2$ represents the slow dynamic coordinates and Y is the complement of X. Y is given by $V \oplus [X \oplus V]^{\perp}$ where $[\ ]^{\perp}$ is the complement space of $[\ ]$, $V = (0, 0, s_3, s_4)^T \psi(z)$ with $(s_3, s_4) \in \mathbf{R}^2$ is the subspace of the fast dynamics of the first mode (associated with the $-\sigma \pm \lambda j$ eigenvalues) and $[X \oplus V]^{\perp}$ represents the coordinates corresponding to the second and higher shaft vibrational modes. Elements in Y will be denoted by y and those in X are uniquely determined by $S = (s_1, s_2)^T$.

The full dynamics given by equation (2.3.1) are now projected onto the slow subspace X using the projection operator $P = Z \rightarrow X$ defined by

$$P \begin{bmatrix} z_1 \\ z_2 \\ z_3 \\ z_4 \end{bmatrix} = \begin{bmatrix} \bar{z}_1 \\ \bar{z}_2 \\ 0 \\ 0 \end{bmatrix} \psi \, , \quad \bar{z}_i = 2 \int_0^1 z_i(\theta) \sin(\pi\theta) \, d\theta .$$

(Note that P is much like a modal projection except that it shifts out <u>all</u> of the fast dynamics, not just the higher modes). P and (I - P) ((I - P) is the complement of P and is the projection onto the space Y) are applied to equation (2.3.1) (see Carr, 1981) to yield the dynamics separated into slow, S, and fast, y, components:

$$\dot{S} = \begin{bmatrix} 0 & 0 \\ 0 & 0 \end{bmatrix} S + \langle PQ^{-1} C_{1,\epsilon} Q \begin{bmatrix} S \\ 0 \end{bmatrix} \psi, \beta \rangle + \langle PQ^{-1} C_{1,\epsilon} Qy, \beta \rangle \qquad (2.3.2a)$$

$$+ \langle P Q^{-1} N(S, y), \beta \rangle$$

$$\dot{y} = By + (I-P) Q^{-1} C_{1,\epsilon} Q \begin{bmatrix} S \\ 0 \end{bmatrix} \psi + (I-P) Q^{-1} C_{1,\epsilon} Qy \qquad (2.3.2b)$$

$$+ (I-P) Q^{-1} N(S,y)$$

$$\dot{\epsilon} = 0 \qquad (2.3.2c)$$

where the matrix $B = (I - P) Q^{-1} C_{1,0} Q$, the vector $\beta = (1, 1, 0, 0)^T$ $\psi(z)$, $\langle \, , \, \rangle$ is the inner product defined as $\langle \Phi, \Psi \rangle = (e_1, e_2, e_3, e_4)^T$, where

$$e_i = 2 \int_0^1 \phi_i \psi_i d\theta$$

and where $\epsilon = (\epsilon_1, \epsilon_2)^T$ is being treated as a state variable (the suspension trick, see Carr, 1981). This inclusion of ϵ in the dynamics allows one to apply the center manifold theorem at parameter values near to, as well as at, D_1. Note that the eigenvalues of B have negative real parts.

The center manifold theorem states that there exists an invariant manifold near $(S, y, \epsilon) = (0, 0, 0)$ which can be written as $y = h(S, \epsilon)$ with $|S|<\delta$ and $|\epsilon|<\delta$. This manifold contains the slow dynamics, which in turn dominate the full equation of motion. The dynamics on $h(S, \epsilon)$ can be obtained by substituting $h(S,\epsilon)$ for y in equation (2.3.2a) and noting that the ϵ dynamics are trivial. A functional equation for $h(S,\epsilon)$ can be obtained by substituting $h(S,\epsilon)$ into equation (2.3.2) (see Carr):

$$M[h] = \frac{\partial h}{\partial S}\left[< PQ^{-1} C_{1,\epsilon} Q \begin{bmatrix} S \\ 0 \end{bmatrix} \psi, \beta > + < PQ^{-1} C_{1,\epsilon} Qh, \beta > \right.$$

$$\left. + < PQ^{-1} N(S,h), \beta > \right] - Bh - (I-P)Q^{-1} C_{1,\epsilon} Q \begin{bmatrix} S \\ 0 \end{bmatrix} \psi - (I-P) Q^{-1} C_{1,\epsilon} Qh$$

$$- (I-P) Q^{-1} N(S, h) = 0 \qquad (2.3.3)$$

This partial differential equation for h cannot be solved explicitly but can be approximated arbitrarily well by a Taylor series near $(S, \epsilon) = (0,0)$, provided its Taylor series exists. Henry (1981) and Carr (1981) show that if a function $\phi(S,\epsilon)$, with $\phi(0) = D\phi(0) = 0$ can be found such that $M\,[\phi(S,\ \epsilon)] = O(|S,\ \epsilon|^{p})$ for some $p>1$ as $|S,\epsilon| \to 0$, then it follows that

$$h(S,\epsilon) = \phi(S,\epsilon) + O(|S,\epsilon|^{p}) \text{ as } |S,\epsilon| \to 0\ . \tag{2.3.4}$$

Hence we can approximate h as closely as desired by seeking series solution of equation (2.3.3).

By choosing $\phi(S,\epsilon) = O(|S,\epsilon|^{2})$ such that

$$B\phi(S,\epsilon) + (I-P)Q^{-1}C_{1,\epsilon}\ Q\begin{bmatrix} S \\ 0 \end{bmatrix} \psi = 0 \tag{2.3.5}$$

$h = \phi(S,\epsilon) + O(|S,\epsilon|^{3})$ by equation (2.3.4). Calculating $\phi(S,\epsilon)$ in equation (2.3.5) up to order two and substituting the result into the first component of equation (2.3.2) yields the quations which govern the slow dynamics and which include all essential components of the coupling to the fast dynamics:

$$\begin{bmatrix} \dot{s}_1 \\ \\ \dot{s}_2 \end{bmatrix} = \begin{bmatrix} \frac{2\Omega_1\sigma}{d}\epsilon_1 - \frac{\lambda\ \Omega_1}{d}\epsilon_2 + f_1(\epsilon_1,\epsilon_2), & \frac{2\Omega_1\lambda}{d}\epsilon_1 + \frac{\Omega_1\sigma}{d}\epsilon_2 + f_2(\epsilon_1,\epsilon_2) \\ \\ -\frac{2\Omega_1\lambda}{d}\epsilon_1 - \frac{\Omega_1\sigma}{d}\epsilon_2 - f_2(\epsilon_1,\epsilon_2), & \frac{2\Omega_1\sigma}{d}\epsilon_1 - \frac{\lambda\Omega_1}{d}\epsilon_2 + f_1(\epsilon_1,\epsilon_2) \end{bmatrix} \begin{bmatrix} s_1 \\ \\ s_2 \end{bmatrix}$$

$$- \frac{\alpha\Omega_1^2}{2} \begin{bmatrix} \frac{\sigma}{d}\left(s_1^2 + s_2^2\right) s_1 + \frac{\lambda}{d}\left(s_1^2 + s_2^2\right) s_2 \\ -\frac{\lambda}{d}\left(s_1^2 + s_2^2\right) s_1 + \frac{\sigma}{d}\left(s_1^2 + s_2^2\right) s_2 \end{bmatrix} + O(|S,\epsilon|^{4}) \tag{2.3.6}$$

where $d = \sigma^2 + \lambda^2$ and f_1, f_2 are quadratic functions in ϵ_1, ϵ_2. Finally, if one writes $s_1^2 + s_2^2 = r^2$ and $\tan\theta = s_2/s_1$ equation (2.3.6) becomes

$$\dot{r} = \left[\left(\frac{2\Omega_1\sigma}{d}\epsilon_1 - \frac{\lambda\Omega_1}{d}\epsilon_2\right) - \frac{\alpha\sigma\Omega_1^2}{2d}r^2\right] r$$

$$\dot{\theta} = \left[-\left(\frac{2\Omega_1\lambda}{d}\epsilon_1 + \frac{\Omega_1\sigma}{d}\epsilon_2\right) + \frac{\alpha\lambda\Omega_1^2}{2d}r^2\right] \qquad (2.3.7)$$

where f_1, f_2, and higher order terms have been neglected. This equation describes a codimension two bifurcation of double zero type with unfolding parameters ϵ_1 and ϵ_2.

The variable r simply represents the amplitude of the first mode of the shaft and θ represents the phase difference between the shaft and the frame of reference rotating at Ω. Solutions of constant r with $\dot{\theta} = 0$ represent synchronous whirling of the shaft in its first mode. Such solutions arise as a circle of equilibria as a consequence of the symmetry of the shaft, i.e., it has no preferred orientation when buckled. Solutions of constant r with $\dot{\theta} \neq 0$ represent nonsynchronous whirling of the first mode, these arise as limit cycles in equation (2.3.7). The $r = 0$ solution corresponds to the trivial shaft configuration.

The structure of equation (2.3.7) is also worthy of note. The linear part of the equations is dominated by the ϵ variables and is zero when $\epsilon = 0$; this recovers the fact that a double zero eigenvalue occurs for $\epsilon = 0$. The nonlinear terms originate from the nonlinear structural effects, α, and contain the net effect of these effects at the bifurcation point. (If, in such an analysis, one obtains zero for the coefficient of the leading nonlinear terms, the next order nonlinear terms must be computed to determine the dynamics. Here the coeffecients of the cubic terms are strictly nonzero.)

The dynamics of equation (2.3.7) are summarized here; recall that $\mu_e = \epsilon_2$ and $\Omega = \Omega_1 + \epsilon_1$:

(1) For $\epsilon_2=0$, corresponding to zero external resistance: the zero amplitude solution is asymptotically stable (unstable) when $\epsilon_1 < 0$ ($\epsilon_1 > 0$). A non-trivial circle of equilibria bifurcates from the trivial solution at $\epsilon_1=0$, these exist and are stable for $\epsilon_1 > 0$ and are given by

$$r^2 = \frac{4}{\alpha\Omega_1}\,\epsilon_1,\ \dot{\theta} = 0$$

which indicates that the first mode is whirling synchronously.

(2) $\epsilon_2 > 0$: A supercritical Hopf bifurcation occurs at $\epsilon_1 = \frac{\lambda}{2\sigma}\epsilon_2$ where nontrivial constant r solutions appear. The zero solution loses its stability and bifurcates into a stable limit cycle for $\epsilon_1 > \frac{\lambda}{2\sigma}\epsilon_2$. Non-synchronous, but nearly synchronous, whirling of the first mode arises in this case since $\dot{\theta}$ is nonzero but small. In fact $\dot{\theta} = -\frac{\Omega_1}{\sigma}\,\epsilon_2$ for the nontrivial r solutions, indicating that subsynchronous whirling of the shaft always occurs since the absolute rotational speed is given by $\Omega_1 + \epsilon_1 + \dot{\theta} = \Omega_1 + \epsilon_1 - \Omega_1\,\epsilon_2\,/\,\sigma$ which is greater than Ω_1 (since $\epsilon_1 > \lambda\epsilon_2\,/\,2\sigma$ ($= \Omega_1\epsilon_2/\sigma$) holds in the parameter region where the limit cycle exists). The whirling speed at the stability boundaries will be

discussed more thoroughly in next section in which Hopf bifurcations of the zero solution are considered.

Figure 8 shows the bifurcation set and associated phase portraits for equation (2.3.7).

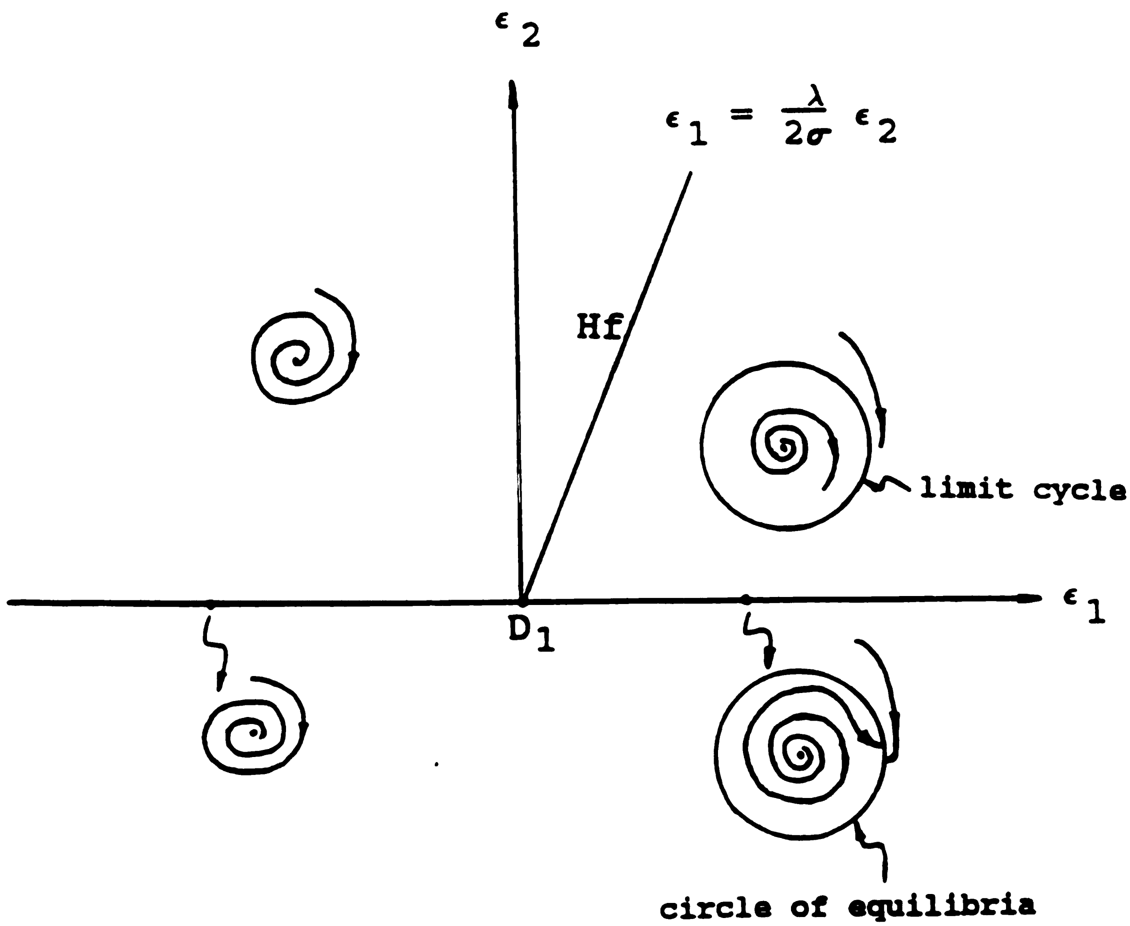

Figure 8. Bifurcation diagram and associated phase portraits of equation (2.3.7). Hf: Hopf bifurcation. D_1: double zero bifurcation

It must be stated that equation (2.3.7) can be obtained by simply ignoring all vibrational modes except the first. Effects from the nonlinear coupling of the modes appear only in the coefficient of r^4 terms and higher. However, this cannot be determined without including the higher modes in the analysis in some manner.

Similar analyses can be applied to points D_2, D_3, . . . in Figure 7 which all correspond to the same type of bifurcation. However, the circles of equilibria and limit cycles for modes 2, 3, . . . (for $\Omega >$ Ω_2, Ω_3, . . .) are stable only <u>in the center manifold</u> which itself is not attracting. The unstable nature of the first mode dominates the response near these bifurcation points.

For other examples of codimension two bifurcations of the double zero type with zero linear part, the reader is referred to Golubitsky and Schaeffer (1978, 1979).

2.4 The Hopf Bifurcation

For damping ratios lying in the range of equation (2.2.5), but not equal to the values at points D_i or P_i, it is seen that one pair of complex conjugate eigenvalues of the trivial solution, associated with the $n^{\underline{th}}$ mode, cross the imaginary axis in the complex plane when the rotational speed exceeds Ω_n^*. Bifurcation of a limit cycle from the zero solution is thus expected. Using the same procedure as given in Section 2.3, phase and amplitude equations similar to equation (2.3.7) are obtained representing the response of the $n^{\underline{th}}$ mode for parameters near the bifurcation point. The relation between the whirling speed and the rotational speed (as a function of the damping ratio) can be determined by examining the phase equation.

In this case only one parameter variation is required. The variation in the rotational speed from critical is denoted by $\epsilon = \Omega - \Omega_n^*$. The procedure for obtaining the essential dynamics near the instability is exactly the same in this case. The resulting differential equations will again be two in number and will specify the $n^{\underline{th}}$ mode dynamics near the instability.

The linear operator C restricted to the $n^{\underline{th}}$ modal subspace $\{r \sin(n\pi z):\ r = (r_1, r_2, r_3, r_4)^T \in \mathbf{R}^4\}$ can be represented by the matrix

$$C_n = \begin{bmatrix} 0 & 0 & 1 & 0 \\ 0 & 0 & 0 & 1 \\ \lambda\omega & \sigma\omega & -\sigma & \lambda+\omega \\ -\sigma\omega & \lambda\omega & -(\lambda+\omega) & -\sigma \end{bmatrix} + \begin{bmatrix} 0 & 0 & 0 & 0 \\ 0 & 0 & 0 & 0 \\ 2\Omega_n^*\epsilon+\epsilon^2 & \mu_e\epsilon & 0 & 2\epsilon \\ -\mu_e\epsilon & 2\Omega_n^*\epsilon+\epsilon^2 & -2\epsilon & 0 \end{bmatrix}$$

$$= C_{n,0} + C_{n,\epsilon}$$

where $\omega = \mu_e/\mu_i\Omega_n$, $\sigma = \mu_i\Omega_n^2 + \mu_e$, and $\lambda = 2\Omega_n + \mu_e/\mu_i\Omega_n$. The eigenvalues of $C_{n,0}$ are $\pm\ \omega j$, $-\sigma \pm \lambda j$ and the eigenvalues of C_k, $k \neq n$, all have negative real parts when $\epsilon = 0$ for those cases on the stability boundary of Figure 7. Hence, center manifold theory can be used to reduce the analysis of the bifurcation to the study of a two-dimensional differential equation.

Using the same symbols and procedures introduced in Section 2.3, and replacing $\sin(\pi z)$ by $\sin(n\pi z)$ (that is, mode 1 by mode n), one obtains the "split" dynamics:

$$\begin{bmatrix}\dot{s}_1\\ \\ \dot{s}_2\end{bmatrix} = \begin{bmatrix}0 & -\omega\\ \\ \omega & 0\end{bmatrix}\begin{bmatrix}s_1\\ \\ s_2\end{bmatrix} + \langle PQ_n^{-1}C_{n,\epsilon}\,Q_n\begin{bmatrix}S\\0\end{bmatrix}\psi,\ \beta\rangle + \langle P\,Q_n^{-1}\,C_{n,\epsilon}\,Q_n y,\ \beta\rangle$$

$$+ \langle P\,Q_n^{-1}\,N(S,y),\ \beta\rangle$$

$$\dot{y} = By + (I-P)\,Q_n^{-1}\,C_{n,\epsilon}\,Q_n\begin{bmatrix}S\\0\end{bmatrix}\psi + (I-P)\,Q_n^{-1}\,C_{n,\epsilon}\,Q_n y$$

$$+ (I-P)\,Q_n^{-1}\,N\,(S,\ y) = 0 \qquad (2.4.1)$$

$$\dot{\epsilon} = 0$$

where Q_n is the similarity transformation matrix which puts $C_{n,0}$ into canonical form. A center manifold $h(S,\epsilon)$ exists for the above equation and can be approximated up to order two if

$$\frac{\partial\phi(S,\epsilon)}{\partial S}\begin{bmatrix}0 & -\omega\\ \omega & 0\end{bmatrix}\begin{bmatrix}s_1\\ s_2\end{bmatrix} - B\,\phi(S,\epsilon) - (I-P)\,Q_n^{-1}\,C_{n,\epsilon}\,Q_n\begin{bmatrix}S\\0\end{bmatrix} = 0 \qquad (2.4.2)$$

such that $h(S,\epsilon) = \phi(S,\epsilon) + 0\left(|S,\epsilon|^3\right)$. Substituting $h(S,\epsilon)$ into equation (2.4.1) yields, for the $\dot{S}$ equation,

$$\begin{bmatrix}\dot{s}_1\\ \dot{s}_2\end{bmatrix} = \begin{bmatrix}d_1(\epsilon,\epsilon^2) + d_2(\epsilon^2,\epsilon^3) & -(\omega + c_1(\epsilon,\epsilon^2) + c_2(\epsilon^2,\epsilon^3))\\ \\ \omega + c_1(\epsilon,\epsilon^2) + c_2(\epsilon^2,\epsilon^3) & d_1(\epsilon,\epsilon^2) + d_2(\epsilon^2,\epsilon^3)\end{bmatrix}\begin{bmatrix}s_1\\ s_2\end{bmatrix}$$

$$+ \begin{bmatrix}a(s_1^2 + s_2^2)\,s_1 + b(s_1^2 + s_2^2)\,s_2\\ \\ -b(s_1^2 + s_2^2)\,s_1 + a(s_1^2 + s_2^2)\,s_2\end{bmatrix} + O(|S,\epsilon|^5 \qquad (2.4.3)$$

where d_1 and c_1 arise from the contribution of the second term of $\dot{S}$ in equation (2.4.1) and d_2 and c_2 arise from the third term of that equation. These terms are zero when $\epsilon = 0$. Also, the constants a and b are given by

$$a = -\frac{1}{2}\,\alpha\Omega_n^2\,\sigma/[\sigma^2 + (\lambda-\omega^2)] < 0,\ b = \frac{1}{2}\,\alpha\Omega_n{}^2(\lambda-\omega)/[\sigma^2 + (\lambda-\omega)^2] > 0 \quad .$$

Equation (2.4.3) is in the normal form for a Hopf bifurcation. The occurence of a supercritical Hopf bifurcation is thus concluded by the sign of a. Transforming equation (2.4.3) back to the original modal variables by the relation $W = QZ$ and writing them in polar coordinates one obtains an equation which describes the shaft dynamics near the Hopf bifurcation:

$$\begin{aligned} \dot{r} &= [(d_1 + d_2) + ar^2]\ r \\ \dot{\theta} &= [-\ (\omega + c_1 + c_2) + br^2] \end{aligned} \qquad (2.4.4)$$

where r and θ are the physical amplitude and relative phase for the $n^{\underline{th}}$ mode in the (x, y, z) frame.

Again, the $r = 0$ solution corresponds to the trivial shaft configuration. It is stable for $\epsilon < 0$ and unstable for $\epsilon > 0$. A nonzero constant r solution appears for $\epsilon > 0$; its amplitude is given by $r^2 = -\ (d_1 + d_2)/a$ (recall $a < 0$) and corresponds to a limit cycle with frequency $\dot{\theta} = -\ (\omega_1 + c_1 + c_2 + b\ (d_1 + d_2)\ /\ a)$. Figure 9 depicts the bahavior of solutions of equation (2.4.4) for $\epsilon > 0$.

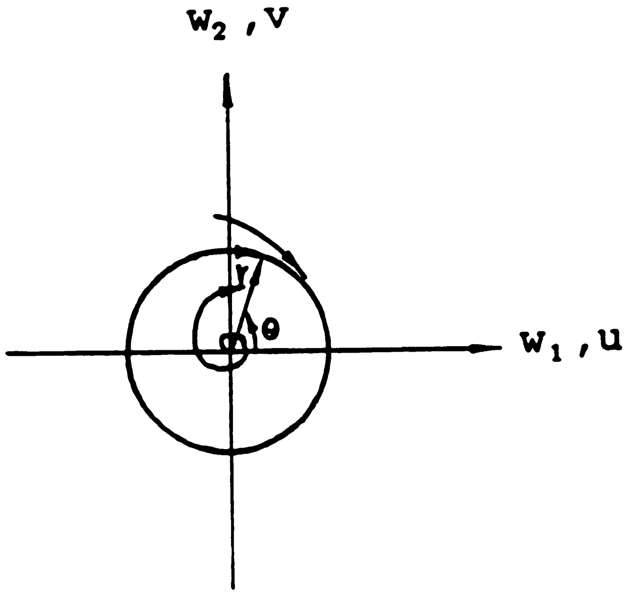

Figure 9. Phase portrait of equation (2.4.4).

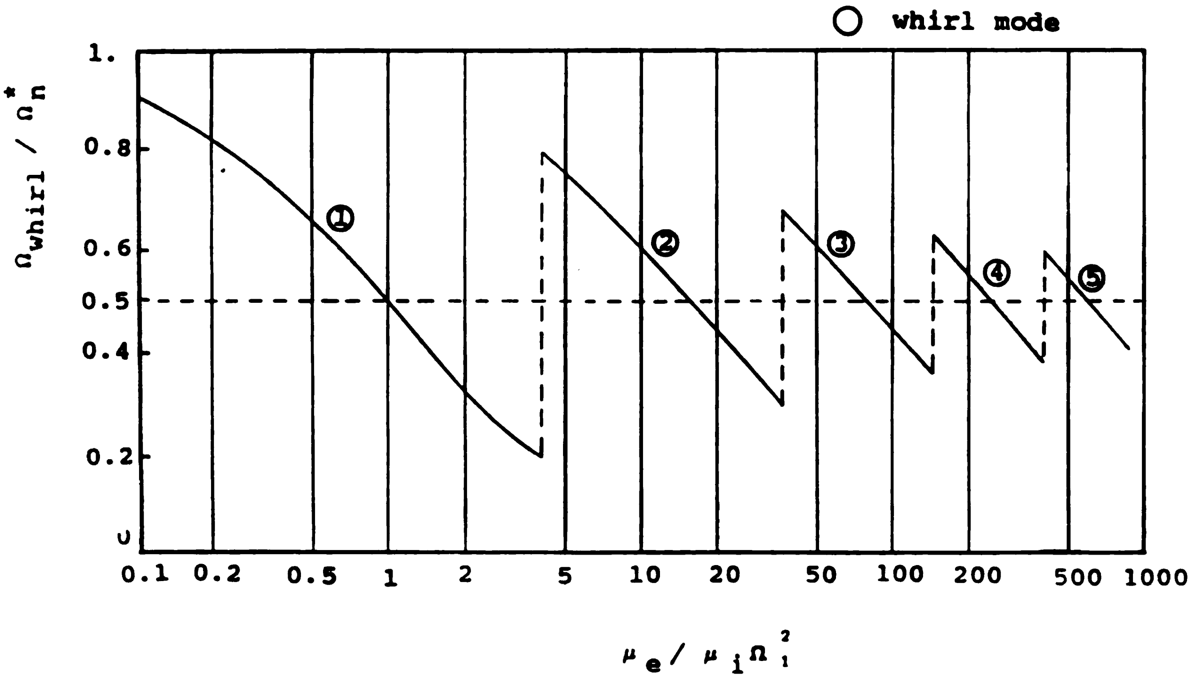

Figure 10. Ratio of whirl speed to rotational speed versus damping ratio.

Note that near $\epsilon = 0$ the frequency of the limit cycle is dominated by the $- \omega$ term since the c_i's and d_1's are of order ϵ. This indicates that the whirling speed of the shaft when pure rotation is unstable can be approximated by

$$\Omega_{whirl} = \Omega + \dot{\theta} \simeq \Omega_n^* - \omega = \Omega_n$$

i.e., the center line of the shaft will precess at a rate approximately equal to the n^{th} natural frequency. This phenomenon was observed in Newkirk's experiment (1924) and was used by Ehrich (1964) to determine the stability boundary.

The relation between the whirling speed and the rotational speed is shown in Figure 10. Note that the whirling speed approaches one-half of the rotational speed as μ_e/μ_i becomes large; this was observed in both Newkirk's and Ehrich's experiments.

This analysis indicates that stable limit cycles are born at the stability boundaries. These limit cycles arise as the speed is raised beyond any of the lines (except at points D_i and P_i) in Figure 7. However, the limit cycles arising at boundaries anywhere in the region marked "unstable" are stable only in the center manifold, which is itself not attracting. Again, the unstable nature of the previously bifurcated mode(s) will dominate the dynamics. Only those limit cycles arising along the heavy line in Figure 7, i.e., the stability boundary for the trivial solution, correspond to observable dynamics.

Also, as in the previous case, the dynamics obtained from a simple truncation of all modes except the n^{th} mode will be identical to those obtained by the present method. Thus, this analysis proves the validity of modal trucation in this situation.

2.5 The Double Hopf Bifurcation

At points P_n in Figure 7 two pairs of purely imaginary eigenvalues, one pair from the C_n matrix and another from C_{n+1}, are found to coexist, suggesting the existence of a double Hopf bifurcation. Center manifold theory is applied to study the qualitative behavior of the two mode interactions near these points.

For this analysis the full partial differential equation (2.2.6) is reduced to an m-mode approximate system by Galerkin's method. This reduced system has a phase space of $\mathbf{R}^{4m}$ and is of the following form (here $W \epsilon \mathbf{R}^{4m}$ and is not to be confused with the W in equation (2.2.6):

$$\dot{W} = C^m W + N(W) \qquad (2.5.1)$$

where C^m is the 4m x 4m matrix given by

$$C^m = \begin{bmatrix} C_1 & & & 0 \\ & C_2 & & \\ & & \ddots & \\ 0 & & & C_m \end{bmatrix}$$

where

$$C_n = \begin{bmatrix} 0 & 0 & 1 & 0 \\ 0 & 0 & 0 & 1 \\ \Omega^2-\Omega_n^2 & -\mu_e\Omega & -\mu_i\Omega_n^2-\mu_e & 2\Omega \\ -\mu_e\Omega & \Omega^2-\Omega_n^2 & -2\Omega & -\mu_i\Omega_n^2-\mu_e \end{bmatrix}, \quad n = 1, 2, \ldots m.$$

$$W = \begin{bmatrix} u_1 \\ v_1 \\ \dot{u}_1 \\ \dot{v}_1 \\ \vdots \\ u_m \\ v_m \\ \dot{u}_m \\ \dot{v}_m \end{bmatrix}, \text{ and } N(W) = \begin{bmatrix} 0 \\ 0 \\ -\alpha\Omega_1{}^2\left\{\left(1 + \mu_i \frac{d}{d\tau}\right)\left[\sum_{j=1}^{m} (u_j{}^2 + v_j{}^2)\Omega_j{}^2\right]\right\} u_1 \\ -\alpha\Omega_1{}^2\left\{\left(1 + \mu_i \frac{d}{d\tau}\right)\left[\sum_{j=1}^{m} (u_j{}^2 + v_j{}^2)\Omega_j{}^2\right]\right\} v_1 \\ \vdots \\ 0 \\ 0 \\ -\alpha\Omega_m{}^2\left\{\left(1 + \mu_i \frac{d}{d\tau}\right)\left[\sum_{j=1}^{m} (u_j{}^2 + v_j{}^2)\Omega_j{}^2\right]\right\} u_m \\ -\alpha\Omega_m{}^2\left\{\left(1 + \mu_i \frac{d}{d\tau}\right)\left[\sum_{j=1}^{m} (u_j{}^2 + v_j{}^2)\Omega_j{}^2\right]\right\} v_m \end{bmatrix}.$$

The solution of the m-mode truncated system converges to the 'true' solution as $m \to \infty$ (see Holmes and Marsden, 1978, for a proof for a similar system).

At point P_n, $\bar{\mu}_e = \mu_i \Omega_1^2 n^2 (n + 1)^2$ and $\bar{\Omega} = \Omega_n^* = \Omega_n + \Omega_1 (n + 1)^2$, and matrices C_n and C_{n+1} have eigenvalues of ($\pm\, \omega_1 j$, $-\,\sigma_1 \pm \lambda_1 j$) and ($\pm\, \omega_2 j$, $-\,\sigma_2 \pm \lambda_2 j$), respectively, while the other C_j's have eigenvalues with strictly nonzero real parts. Therefore a double Hopf bifurcation occurs for equation (2.5.1). This bifurcation does not involve any special resonance conditions since $\omega_2/\omega_1 = (n+1)^2/n^2$ and only the cases $\omega_2/\omega_1 = p/q$, $q \le 3$ and $p < q$ are special (see Arnold, 1987). The bifurcation of the finite dimensional system (2.5.1) does not differ from that of the full system (2.2.6) near the point P_n. It is then justifiable to study the two-mode system with the $n^{\underline{th}}$ and $(n+1)^{\underline{th}}$ modes, i.e., simple model truncation is employed here. Based on the two mode model, equation (2.5.1) becomes

$$\dot{W} = \begin{bmatrix} C_n & 0 \\ 0 & C_{n+1} \end{bmatrix} W + N(w) \quad . \tag{2.5.2}$$

Let $\epsilon = (\epsilon_1, \epsilon_2)^T$ where $\epsilon_1 = \Omega - \bar{\Omega}$ and $\epsilon_2 = \mu_e - \bar{\mu}_e$. As before, C_n is decomposed into $C_{n,0} + C_{n,\epsilon}$ with the knowledge that $(\pm\, \omega_1 j,\ -\sigma_1 \pm \lambda_1 j)$ are the eigenvalues of $C_{n,0}$. A similar decomposition may be done for C_{n+1}. In order to put equation (2.5.2) into canonical form the transformation matrix $Q = \text{diag}\,(Q_1, Q_2)$ is constructed such that $Q_1^{-1}\, C_n Q_1$ and $Q_2^{-1}\, C_{n+1}\, Q_2$ are in Jordan normal form. Let $W = QZ$, equation (2.5.2) then becomes

$$\dot{Z} = \begin{bmatrix} Q_1^{-1}\, C_{n,0}\, Q_1 & 0 \\ 0 & Q_2^{-1} C_{n+1,0} Q_2 \end{bmatrix} Z + \begin{bmatrix} Q_1^{-1} C_{n,\epsilon} Q_1 & 0 \\ 0 & Q_2^{-1} Q_{n+1,\epsilon} Q_2 \end{bmatrix} Z$$

$$+ Q^{-1}\, N\,(Q\, Z) \tag{2.5.3}$$

where $Q_1^{-1} C_{n,0} Q_1 = \begin{bmatrix} 0 & -\omega_1 & 0 & 0 \\ \omega_1 & 0 & 0 & 0 \\ 0 & 0 & -\sigma_1 & -\lambda_1 \\ 0 & 0 & \lambda_1 & -\sigma_1 \end{bmatrix}$ and $Q_2^{-1} C_{n+1,0} Q_2 = \begin{bmatrix} 0 & -\omega_2 & 0 & 0 \\ \omega_2 & 0 & 0 & 0 \\ 0 & 0 & -\sigma_2 & -\lambda_2 \\ 0 & 0 & \lambda_2 & -\sigma_2 \end{bmatrix}$.

Rearranging the above equation by letting $X = (z_1,\ z_2,\ z_5,\ z_6)^T$, and $Y = (z_3,\ z_4,\ z_7,\ z_8)^T$ yields the "split" dynamics:

$$\begin{aligned} \dot{X} &= AX + E_1 X + E_2 Y + F_1(X,Y) \\ \dot{Y} &= BY + E_3 X + E_4 Y + F_2(X,Y) \end{aligned} \tag{2.5.4}$$

$$\dot{\epsilon} = 0$$

where $A = \begin{bmatrix} 0 & -\omega_1 & 0 & 0 \\ \omega_1 & 0 & 0 & 0 \\ 0 & 0 & 0 & -\omega_2 \\ 0 & 0 & \omega_2 & 0 \end{bmatrix}$ and $B = \begin{bmatrix} -\sigma_1 & -\lambda_1 & 0 & 0 \\ \lambda_1 & -\sigma_1 & 0 & 0 \\ 0 & 0 & -\sigma_2 & -\lambda_2 \\ 0 & 0 & \lambda_2 & -\sigma_2 \end{bmatrix}$.

Elements of E_i are functions of (ϵ_1, ϵ_2) and elements of F_i are cubic functions of its arguments. By the center manifold theorem there exists a center manifold $Y=h(X,\epsilon)$ such that

$$\left[\frac{\partial h}{\partial x}, \frac{\partial h}{\partial \epsilon}\right] \begin{pmatrix} AX + E_1X + E_2h + F_1(X,h) \\ 0 \end{pmatrix} - Bh - E_3X - E_4h - F_2(X,h) = 0. \quad (2.5.5)$$

Approximating $h(X,\epsilon)$ up to order two and substituting this into the $\dot{X}$ equation in (2.5.4) yields the equations governing the slow dynamics

$$\dot{X} = \begin{bmatrix} \alpha_1 & -(\omega_1+\beta_1) & 0 & 0 \\ \omega_1+\beta_1 & \alpha_1 & 0 & 0 \\ 0 & 0 & \alpha_2 & -(\omega_2+\beta_2) \\ 0 & 0 & (\omega_2+\beta_2) & \alpha_2 \end{bmatrix} X +$$

$$\begin{bmatrix} (a_1x_1 + b_1x_2)(x_1^2 + x_2^2) + (c_1x_1 + d_1x_2)(x_3^2 + x_4^2) \\ (-b_1x_1 + a_1x_2)(x_1^2 + x_2^2) + (-d_1x_1 + c_1x_2)(x_3^2 + x_4^2) \\ (c_2x_3 + d_2x_4)(x_1^2 + x_2^2) + (a_2x_3 + b_2x_4)(x_3^2 + x_4^2) \\ (-d_2x_3 + c_2x_4)(x_1^2 + x_2^2) + (-b_2x_3 + a_2x_4)(x_3^2 + x_4^2) \end{bmatrix} + 0(|X,\epsilon|^4)$$

(2.5.6)

where α_i and β_i are functions of (ϵ_1, ϵ_2) up to order two and a_i, b_i, c_i, and d_i depend only on the system parameters. Equation (2.5.6) is transformed to polar coordinates with $r_1^2 = x_1^2 + x_2^2$ and $r_2^2 = x_3^2 + x_4^2$ to yield

$$
\begin{aligned}
\dot{r}_1 &= \alpha_1 r_1 + a_1 r_1^3 + c_1 r_1 r_2^2 + O(|r|^5) \\
\dot{r}_2 &= \alpha_2 r_2 + c_2 r_1^2 r_2 + a_2 r_2^3 + O(|r|^5) \\
\dot{\theta}_1 &= \omega_1 + \beta_1 + O(|r|^2) \\
\dot{\theta}_2 &= \omega_2 + \beta_2 + O(|r|^2) \quad .
\end{aligned}
\tag{2.5.7}
$$

The coefficients a_i and c_i are crucial to determine the bifurcation diagram for the above equation; they are given as follows

$$a_1 = -\alpha\Omega_n^2\sigma_1/[\sigma_1^2 + (\lambda_1-\omega_1)^2] < 0, \quad a_2 = -\alpha\Omega_{n+1}^2\,\sigma_2/[\sigma_2^2 + (\lambda_2-\omega_2)^2] < 0$$

$$c_1 = -\alpha\Omega_n\Omega_{n+1}\sigma_1/[\sigma_1^2 + (\lambda_1-\omega_1)^2] < 0, \quad c_2 = -\alpha\Omega_n\,\Omega_{n+1}\sigma_2/[\sigma_2^2+(\lambda_2-\omega_2)^2] < 0.$$

Equation (2.5.7) is in the standard normal form for a non-resonant, double Hopf bifurcation (Takens, 1974). However, the equations do have a special symmetry which is discussed below. The parameters α_1 and α_2 are the unfolding parameters, they are functions of (ϵ_1,ϵ_2) and $\alpha_1 = \alpha_2 = 0$ corresponds to the point P_n. The amplitude and phase components of equation (2.5.7) are uncoupled so that the bifurcations and asymptotic behavior of solutions of this system can be studied via the two dimensional amplitude equations

$$\dot{r}_1 = \alpha_1 r_1 + a_1 r_1^{\ 3} + c_1 r_1 r_2^{\ 2}$$

$$\dot{r}_2 = \alpha_2 r_2 + c_2 r_1^{\ 2} r_2 + a_2 r_2^{\ 3} \quad . \tag{2.5.8}$$

The $\dot{\theta}$ equations can be used to determine the whirling speeds. In order to reduce the number of coefficients one can rescale equation (2.5.8) by letting $\bar{r}_1 = r_1 \sqrt{|a_1|}$ and $\bar{r}_2 = r_2 \sqrt{|a_2|}$ which results in, after dropping the over-bars,

$$\dot{r}_1 = \alpha_1 r_1 - r_1^{\ 3} + b r_1 r_2^{\ 2}$$

$$\dot{r}_2 = \alpha_2 r_2 + c\, r_1^{\ 2} r_2 - r_2^{\ 3} \tag{2.5.9}$$

where $b = c_1/|a_1|$ and $c = c_2/|a_1|$. (For a more complete description of unfolding equation (2.5.9) with different combinations of constants b and c, the reader is referred to Guckenheimer and Holmes, 1983, Chapter 7). Here the constants b and c can be shown to take the value of -1 after substituting a_1, a_2, c_1 and c_2. Hence equation (2.5.9) becomes

$$\dot{r}_1 = \alpha_1 r_1 - r_1^{\ 3} - r_1 r_2^{\ 2}$$

$$\dot{r}_2 = \alpha_2 r_2 - r_1^{\ 2} r_2 - r_2^{\ 3} \tag{2.5.10}$$

The variables r_1 and r_2 represent the amplitudes of mode n and n+1, respectively, and θ_1 and θ_2 in equation (2.5.7) are the corresponding phases.

Equation (2.5.10) has a special symmetry between the modes. The equations are unchanged if (r_1, α_1) is switched with (r_2, α_2). This arises from the symmetry of the shaft and implies certain restrictions on the solutions. In some cases such symmetries lead to a variety of exotic dynamics; see Knoblock (1986), for example. In the present case it affects the behavior in a straightforward manner.

It is desired to determine the dynamics for all parameter values near the P_n points. This is accomplished by studying the dynamics given by equation (2.5.10) for (α_1, α_2) varying in a neighborhood of (0, 0). This is equivalent to varying (μ_e, Ω) near $(\bar{\mu}_e, \bar{\Omega})$. It is carried out using phase plane methods: locating the equilibrium points, analyzing their stabilities, and checking for the possible existence of limit cycles and global bifurcations. The resulting bifurcation sets and associated phase portraits are sketched in Figure 11.

The dynamics resulting from Equation (2.5.10) are summarized here:

(1) (0, 0) is always an equilibrium, corresponding to the trivial configuration of the shaft. It is stable if $\alpha_1, \alpha_2 < 0$, unstable otherwise.

(2) $(r_1, r_2) = (\sqrt{\alpha_1}, 0)$ is an equilibrium if $\alpha_1 > 0$, it corresponds to mode n whirling. If, in addition, $\alpha_1 > \alpha_2$, it is stable. Otherwise, it is unstable.

(3) $(r_1, r_2) = (0, \sqrt{\alpha_2})$ is an equilibrium if $\alpha_2 > 0$, it corresponds to mode n+1 whirling. If, in addition, $\alpha_2 > \alpha_1$, it is stable. Otherwise, it is unstable.

(4) If $\alpha_1 = \alpha_2$ $(=\alpha)$, a circle of equilibria is found at $r_1^2 + r_2^2 = \alpha$. It is locally attractive, as determined by the non-linear cubic terms. Any non-zero fixed point in the interior of the positive quadrant indicates the existence of mixed mode whirling for the system. Here mixed mode whirling corresponds to a solution composed of two distinct modes whirling at different speeds, whereas single mode whirling corresponds to a single frequency component solution. (However, higher-order terms or symmetry considerations need to be included to obtain structurally stable bifurcation diagrams near $\alpha_1 = \alpha_2$. It is expected that the circle of equilibria will persist to all orders due to the inherent symmetry of the model.)

(5) In Figure 11 two straight lines (one solid, one dashed), traversed in the direction shown, indicate two different successions of phase portraits as the rotational speed is increased. The solid line represents the case for $\mu_e > \bar{\mu}_e$, the dashed one $\mu_e < \bar{\mu}_e$. If $\mu_e < \bar{\mu}_e$, the trivial pure rotation loses stability to the steady state mode n whirling as the rotational speed increases. This whirling solution remains stable as Ω is increased further, mode n + 1 whirling is introduced, but it is unstable. For $\mu_e > \bar{\mu}_e$, in contrast to the previous case, the trivial rotation loses stability

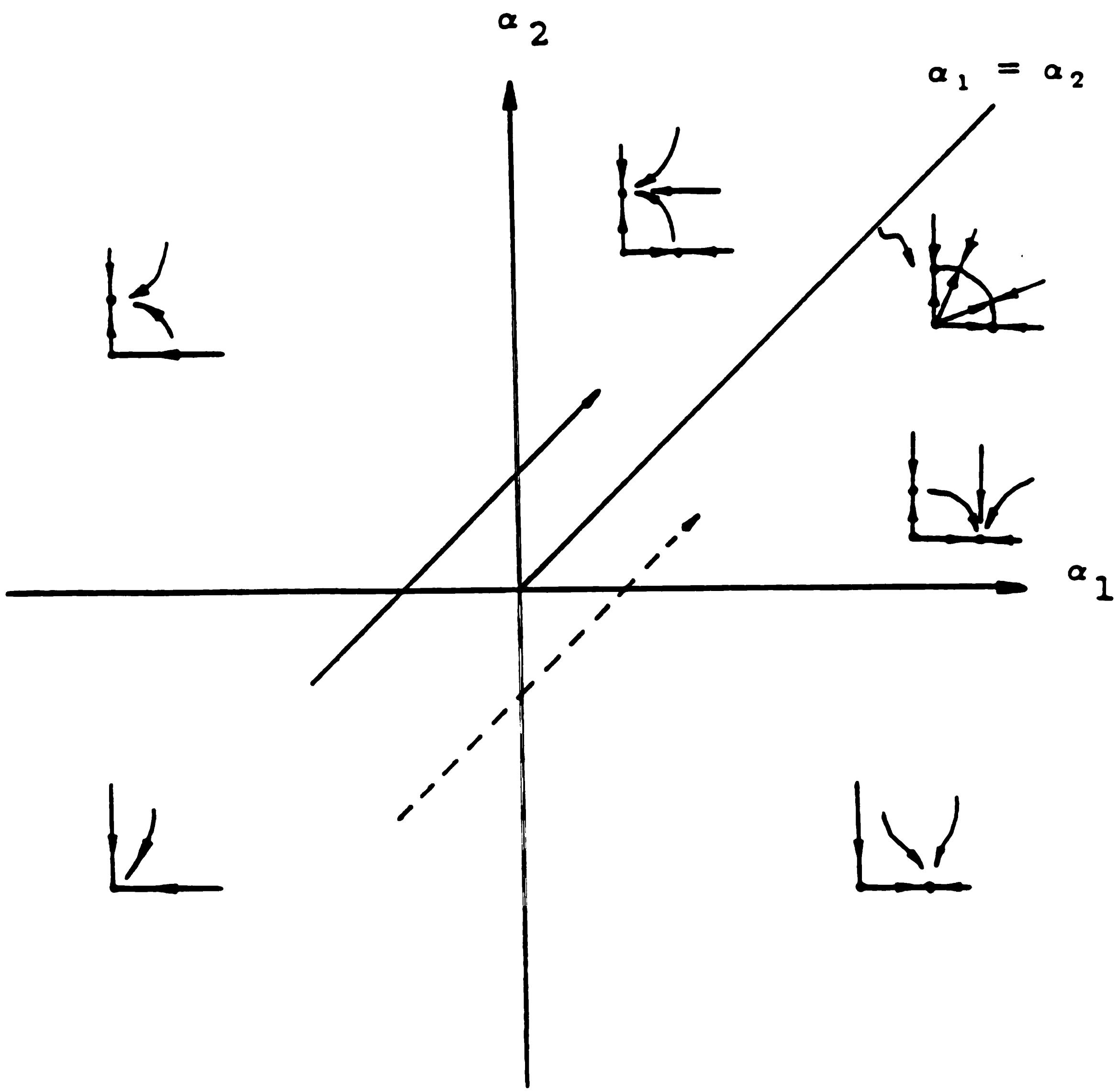

Figure 11. Bifurcation diagram for the normal form (equation (2.5.10)) of the double Hopf bifurcation.

to mode n + 1 whirling as the rotational speed increases and this whirling remains stable. Mode n whirling is introduced, but is unstable in this case. For $\mu_e = \bar{\mu}_e$, i.e., $\alpha_1 = \alpha_2$, the response is more complicated. The pure rotation loses stability simultaneously to both modes, n and n + 1. This mixed mode solution is stable. In practice, other effects, such as small asymmetries, etc., will determine the dynamics in this case.

Modal interactions occuring near a double Hopf bifurcation have been analyzed for a number of physical systems; the papers by Knobloch and Guckenheimer (1983) and Moroz and Holmes (1985) provide examples.

2.6 Conclusions

We have rigorously shown by the use of center manifold and normal form theories the existence of synchronous and non-synchronous post-critical-speed whirling of a rotating shaft. These results are in accord with intuition and physical experiments (Newkirk, 1924 and Ehrich, 1964) and provide a formal justification for the modal trucations widely used in studies of shaft dynamics.

Although the model studied here is a highly idealized one, the approach can be applied to more sophisticated models which incorporate other effects which may include, for example, non-symmetric stiffness, applied axial loads and torques, etc., or even non-linear rheological models of the shaft material (Muszynska, 1974). The bifurcation diagrams may be more complicated and computation of the non-linear coefficients will be a more formidable task.

The interaction between the instabilities described in this work and the resonance effects which arise from eccentricity and/or unbalance in the shaft will be studied in next chapter using similar methods.

CHAPTER III

EFFECTS OF MASS UNBALANCE ON THE DYNAMICS OF A ROTATING SHAFT WITH INTERNAL DAMPING

3.1 Equations of Motion

In this chapter, the dynamic response of an unbalanced rotating shaft with internal damping is considered. As shown in Chapter II, the internal damping can have a destabilizing effect on a rotating shaft : the straight, undeformed configuration of a perfectly balanced shaft loses stability when the impressed rotational speed exceeds the first critical speed Ω_1^*, assuming $0 < \mu_e/\mu_i\Omega_1^2 < 4$, i.e., that the external damping is not too large. Figure 12 shows the corresponding Hopf bifurcation diagram for this case. In the post stable region nonlinear effects limit the amplitude and a stable limit cycle exists, corresponding to nonsynchronous (actually, subsynchronous) whirling at a constant amplitude. The inclusion of mass unbalance to the system gives rise to a periodic disturbance which, by itself, leads to simple synchronous whirling and a nonlinear resonance near the first flexural vibration frequency Ω_1 of the shaft. As is shown in this chapter, the combined effects can result in synchronous whirling and/or amplitude modulated whirling depending on the level of unbalance, the rotational speed, and other parameters.

Near the primary resonance of the shaft the first mode dynamics dominate the shaft response. Hence, we will present and analyze equations of motion for the first mode. These can be obtained from equations (2.1.7) by neglecting higher modes and including the effect of

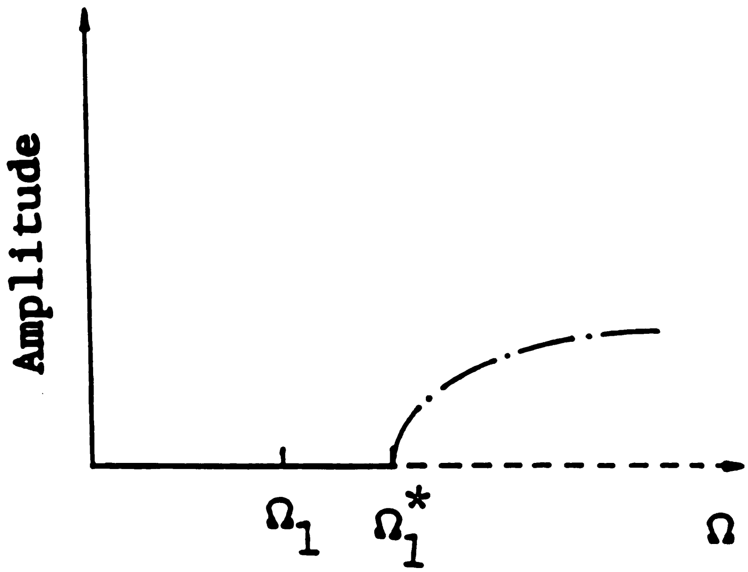

12. **Bifurcation diagram of a balanced shaft.**
Ω_1: first natural frequency, Ω_1^*: first critical frequency
trivial solution: ——— stable, ------- unstable
stable periodic subsynchronous whirl: -.-.-.-

mass unbalance :

$$\ddot{u} + (\mu_e + \mu_i\Omega_1^2)\,\dot{u} - 2\Omega\dot{v} + (\Omega_1^2 - \Omega^2)\,u - \mu_e\Omega v + \alpha\Omega_1^2\,(u^2 + v^2)\,u$$

$$+ 2\alpha\mu_i\Omega_1^2\,(u\dot{u} + v\dot{v})\,u = e\Omega^2$$

$$\ddot{v} + (\mu_e + \mu_i\Omega_1^2)\,\dot{v} + 2\Omega\dot{u} + (\Omega_1^2 - \Omega^2)\,v + \mu_e\Omega u + \alpha\Omega_1^2\,(u^2 + v^2)\,v$$

$$+ 2\alpha\mu_i\Omega_1^2\,(u\dot{u} + v\dot{v})\,v = 0 \qquad (3.1.1)$$

where u and v are the transverse displacements of the first mode in the x and y directions, respectively, Ω_1, μ_e, μ_i, Ω and α have the same meanings as those of Chapter II, and $e = 2\sqrt{2}c/\pi\ell$ is the parameter representing the effect of unbalance (where c is the distance from center of gravity to the geometric center of the shaft). The equations of motion (3.1.1) are presented in terms of a coordinate frame X-Y-Z which is rotating at the rotational speed Ω about the Z axis; hence the force due to unbalance appears as a constant. A nonzero equilibrium point in these coordinates represents a synchronous whirling of the shaft. In this case the rotating coordinate system provides an autonomous set of governing equations, much like the averaging process used in periodically forced systems. The absence of explicitly time-dependent terms facilitates the analysis considerably.

When $e = 0$ the response diagram of equation (3.1.1) is as shown in Figure 12 where

$$\Omega_1^* = \Omega_1 + \frac{\mu_e}{\mu_i \Omega_1} \tag{3.1.2}$$

is the first critical speed at which the trivial solution loses its stability and bifurcates into a stable periodic solution which whirls at a speed different from the rotational speed. However, for $e \neq 0$ and small, the trivial configuration is no longer a solution of equation (3.1.1) and the resulting steady state synchronous whirling solutions are obtained by setting all time derivatives equal to zero. Due to symmetry, synchronous motions of constant amplitude of equation (3.1.1) exist in the form

$$\bar{u} = R \cos \theta$$

$$\bar{v} = R \sin \theta \tag{3.1.3}$$

where R is the amplitude and θ is the relative phase (both constant) of a steady state solution. Substituting equation (3.1.3) into equation (3.1.1) and some rearrangement yields two algebraic equations relating R and θ to the system parameters:

$$[\alpha\Omega_1^2 R^3 + (\Omega_1^2 - \Omega^2)R]^2 + (\mu_e \Omega R)^2 = e^2\Omega^4 \tag{3.1.4}$$

$$\tan(\theta) = -\mu_e\Omega \Big/ \left[\alpha\Omega_1^2 R^2 + (\Omega_1^2 - \Omega^2)\, R\right] \tag{3.1.5}$$

Though the equations of motion (3.1.1) are nonlinear, the steady state solutions (3.1.3) obtained by solving equations (3.1.4) and (3.1.5) are exact (that is, no approximations have been used) and can be solved for the synchronous response of the shaft.

3.2 Synchronous Steady State Solutions

Equation (3.1.4) is a quadratic equation in Ω^2 in terms of system parameters and R, hence two solutions of Ω^2 are obtained for every value of R. The requirements that Ω^2 be greater than zero and real lead to the three distinct cases, depending on the level of external damping; these distinguish three types of possible synchronous response. The stability of the solutions is discussed subsequently; the three cases are:

(I) $0 \leq \mu_e^2 \leq \alpha\, e^2\, \Omega_1^2$

Figure 13(a) depicts the frequency response curve for this case. It is a typical nonlinear response curve for a hardening nonlinearity (provided here by the midline stretching of the shaft). For $\Omega < \Omega_{SN1}$ a single stable synchronous steady state exists. At $\Omega = \Omega_{SN1}$ a vertical tangency, or in bifurcation terminology a saddle-node bifurcation, occurs which introduces two new constant amplitude solutions. One of these is unstable (of saddle type) and increases in amplitude as Ω increases, and asymtotically approaches the uppermost stable solution as $\Omega \rightarrow \infty$. The lower solution branch is initially stable but undergoes a flutter instability, i.e., a Hopf bifurcation, at Ω_H and remains unstable as Ω is increased further.

(II) $\alpha\, e^2\, \Omega_1^2 < \mu_e^2 < 2\, \Omega_1^2\, (\alpha e^2 + 1)$

The frequency response in this case is shown in Figure 13(b). It is very similar to case (I) above except that the two upper solution branches merge and annihilate each other in another vertical tangency at $\Omega = \Omega_{SN2}$, leaving only the lower branch, which approaches the magnitude of unbalance e as Ω is increased.

(III) $\mu_e^2 \geq 2\Omega_1^2\, (\alpha e^2 + 1)$

Unlike the two previous cases, due to the large external damping no multiple solutions of R exist. The amplitude increases asymptotically to e as Ω increases as shown in Figure 13(c), and the response undergoes a Hopf bifurcation at Ω_H.

The multiple response boundaries can be determined by computing the locations of the vertical tangencies of the response curves. This can be accomplished here by locating the degenerate double roots of the

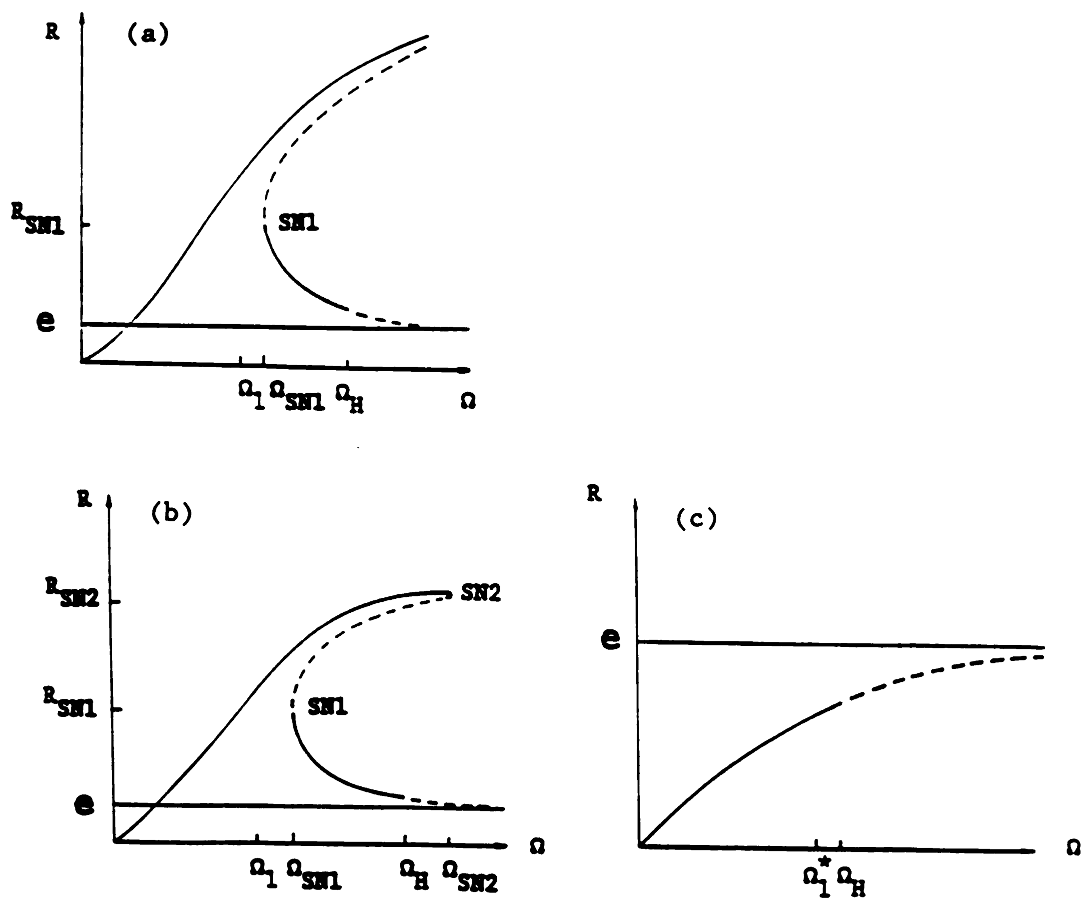

Figure 13. Amplitude - frequency curves of equation (3.1.4).
SN1: first saddle node, SN2: second saddle node, H: Hopf bifurcation

(a) $0 \le \mu_e^2 \le \alpha\ e^2\ \Omega_1^2$, **(b)** $\alpha\ e^2\ \Omega_1^2 < \mu_e^2 < 2\ \Omega_1^2\ (\alpha\ e^2 + 1)$

(c) $2\ \Omega_1^2\ (\alpha\ e^2 + 1) \le \mu_e^2$, ——— stable, ------ unstable cubic equation in R^2, equation (3.1.4). Equation (3.1.4) is a cubic function of R^2, i.e., $f(R^2) = 0$. Figure 14 shows the function f as R^2 varies while Ω is fixed at Ω_{SN1}. At R_{SN1} and Ω_{SN1}, it is required that $f'\left(R^2_{SN1}\right) = 0$ and $f\left(R^2_{SN1}\right) = 0$ where ()' denotes d() /dR^2. These two conditions lead to conditions for R_{SN1} and Ω_{SN1} which are given as

$$\frac{2}{27}\left(\Omega^2_{SN1} - \Omega^2_1\right)^3 + \frac{2}{3}\left(\Omega^2_{SN1} - \Omega^2_1\right)\mu_e^2\,\Omega^2_{SN1} - e^2\,\alpha\,\Omega^2_1\Omega^4_{SN1} + \left[\frac{2}{27}\left(\Omega^2_{SN1} - \Omega^2_1\right)^2 - \frac{2}{9}\,\mu_e^2\,\Omega^2_{SN1}\right]\left[\left(\Omega^2_{SN1} - \Omega^2_1\right)^2 - 3\mu_e^2\,\Omega^2_{SN1}\right]^{1/2} = 0$$

$$R^2{}_{SN1} = \frac{2\left(\Omega^2_{SN1} - \Omega^2_1\right) - \sqrt{\left(\Omega^2_{SN1} - \Omega^2_1\right)^2 - 3\,\mu_e^2\,\Omega^2_{SN1}}}{3\,\alpha\,\Omega^2_1} \qquad (3.2.1a)$$

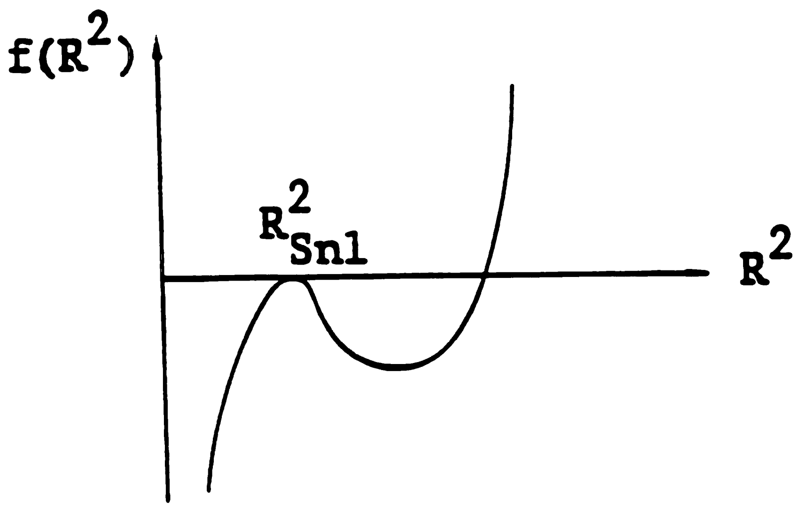

Figure 14. The function f at $\Omega = \Omega_{SN1}$.

Similar results can be obtained for the values of R_{SN2} and Ω_{SN2} in Figure 13(b):

$$\frac{2}{27}\left(\Omega_{SN2}^2 - \Omega_1^2\right)^3 + \frac{2}{3}\left(\Omega_{SN2}^2 - \Omega_1^2\right)\mu_e^2\,\Omega_{SN2}^2 - e^2\,\alpha\,\Omega_1^2\Omega_{SN2}^4 + \left[-\frac{2}{27}\left(\Omega_{SN2}^2 - \Omega_1^2\right)^2 - \frac{2}{9}\mu_e^2\,\Omega_{SN2}^2\right]\left[\left(\Omega_{SN2}^2 - \Omega_1^2\right)^2 - 3\mu_e^2\,\Omega_{SN2}^2\right]^{1/2} = 0$$

$$R^2_{\;SN2} = \frac{2\left(\Omega_{SN2}^2 - \Omega_1^2\right) + \sqrt{\left(\Omega_{SN2}^2 - \Omega_1^2\right)^2 - 3\,\mu_e^2\,\Omega_{SN2}^2}}{3\,\alpha\,\Omega_1^2} \tag{3.2.1b}$$

In order to determine the stability of the synchronous steady states, linearization is used. Small perturbations $(\tilde{u},\tilde{v})$ of the steady state $(\bar{u},\bar{v})$ are introduced as follows: $u = \bar{u} + \tilde{u}$ and $v = \bar{v} + \tilde{v}$. These are substituted into equation (3.1.1) which are then expanded in Taylor series in terms of $(\tilde{u},\tilde{v})$. Retaining only those terms which are linear in $(\tilde{u},\tilde{v})$ and their time derivatives yields the following linear equations which govern the dynamics of the perturbations, and thus the local stability of $(\bar{u},\bar{v})$:

$$\ddot{\tilde{u}} + g_1\,\dot{\tilde{u}} + g_2\,\dot{\tilde{v}} + g_3\,\tilde{u} + g_4\,\tilde{v} = 0$$

$$\ddot{\tilde{v}} + g_5\,\dot{\tilde{v}} + g_6\,\dot{\tilde{u}} + g_7\,\tilde{v} + g_8\,\tilde{u} = 0 \tag{3.2.2}$$

where $\quad g_1 = (\mu_e + \mu_i\Omega_1^2) + 2\alpha\mu_i\Omega_1^2R^2\cos^2\theta$

$$g_2 = -2\Omega + 2\alpha\mu_i\Omega_1^2R^2\sin\theta\cos\theta$$

$$g_3 = (\Omega_1^2 - \Omega^2) + \alpha\Omega_1^2R^2(1 + 2\cos^2\theta)$$

$$g_4 = -\mu_e\Omega + 2\alpha\Omega_1^2R^2\sin\theta\cos\theta$$

$$g_5 = (\mu_e + \mu_i\Omega_1^2) + 2\alpha\mu_i\Omega_1^2R^2\sin^2\theta$$

$$g_6 = 2\Omega + 2\alpha\mu_i\Omega_1^2R^2\sin\theta\cos\theta$$

$$g_7 = (\Omega_1^2 - \Omega^2) + \alpha\Omega_1^2R^2(1 + 2\sin^2\theta)$$

$$g_8 = \mu_e\Omega + 2\alpha\Omega_1^2R^2\sin\theta\cos\theta$$

The eigenvalues of equation (3.2.2) determine the stability characteristics of $(\bar{u},\bar{v})$. A tedious calculation yields the following quartic equation for the eigenvalues, λ:

$$\lambda^4 + C_1\lambda^3 + C_2\lambda^2 + C_3\lambda + C_4 = 0 \qquad (3.2.3)$$

where

$$C_1 = 2\left(\mu_e + \mu_i\Omega_1^2 + \alpha\mu_i\Omega_1^2 R^2\right)$$

$$C_2 = 2\left(\Omega_1^2 + \Omega^2 + 2\alpha\Omega_1^2 R^2\right) + \left(\mu_e + \mu_i\Omega_i^2\right)\left(\mu_e + \mu_i\Omega_1^2 + 2\alpha\mu_i \Omega_1^2 R^2\right)$$

$$C_3 = 2\mu_e\left(\Omega_1^2 + \Omega^2 + 2\alpha\Omega_1^2 R^2\right) + 2\mu_i\Omega_1^2\left[\Omega_1^2 - \Omega^2 + \alpha R^2\left(3\Omega_1^2 - \Omega^2 + \alpha\Omega_1^2R^2\right)\right]$$

$$C_4 = \left(\Omega_1^2 - \Omega^2\right)\left(\Omega_1^2 - \Omega^2 + 4\alpha\Omega_1^2 R^2\right) + 3\alpha^2\Omega_1^4 R^4 + \mu_e^2\Omega^2.$$

and where Ω is varied and R is evaluated at the roots of equation (3.1.4), i.e., at the steady state amplitudes (recall that $\bar{u} = R\cos\theta$ and $\bar{v} = R\sin\theta$). In the following discussion the term "branch" will be used in reference to the frequency response diagrams. Equation (3.2.3) is solved numerically for the system's linearized eigenvalues along these response branches as Ω is varied.

For cases represented by Figure 13(a,b) it is found that the upper branch is always stable, the middle branch is always unstable (in fact, of saddle type) and that the lower branch may or may not change stability type depending on the values of μ_i and μ_e. For the lower branch there exists one pair of complex conjugate eigenvalues with negative real part which move further into the left half of the complex plane as Ω increases; hence we will ignore them as we search for further instabilities.

It is known that at least one eigenvalue is zero at point SN1 (since a saddle-node bifurcation occurs), which is readily verified by noting that $C_4(R_{SN1}) = 0$. As one starts from point SN1 and follows the lower branch as Ω increases, three cases must be considered:

(i) $\mu_i = 0$, the zero eigenvalue becomes negative, merging with the other negative (real) one, and splits into a pair of complex conjugate eigenvalues which move further into the left half of the complex plane. This is the case for a simple Duffing-type resonance in which the lower branch is stable for all Ω values for which it exists.

(ii) $0 < \mu_i < \mu_i^*$ (μ_i^* given below), the zero eigenvalue first moves into the left half of the complex plane, then meets the other negative eigenvalue and splits into a pair of complex conjugates with negative real part. The pair of complex conjugate eigenvalues travel rightward as Ω increases and eventually cross the imaginary axis at a point designated by Ω_H (determined below). Hence the stable lower branch becomes unstable in a Hopf bifurcation at point Ω_H as shown in Figures 13(a,b).

(iii) $\mu_i \geq \mu_i^*$, there are either two zero eigenvalues $\left(\mu_i = \mu_i^*\right)$ or one zero and one positive and real $\left(\mu_i > \mu_i^*\right)$ eigenvalues at point SN1 which will combine and become complex conjugates with <u>positive</u> real part, and move continually rightward in the complex plane as Ω increases, i.e., the lower branch is unstable at its origin (point SN1) and remains unstable as Ω increases.

For the case of Figure 13(c), the unique branch becomes unstable in a Hopf bifurcation at point Ω_H for $\mu_i \neq 0$. In case of $\mu_i = 0$, this branch is stable for all Ω values.

An expression for μ_i^* can be obtained as follows: for $\mu_i = \mu_i^*$ there are two zero eigenvalues at point SN1, this implies $C_3 = 0$ in addition to $C_4 = 0$ in equation (3.2.3). Setting $C_3 = 0$ and utilizing $C_4 = 0$ to compute R_{SN1} and Ω_{SN1} yields

$$\mu_i^* = \frac{\mu_e\left(\Omega_1^2 + \Omega_{SN1}^2 + 2\alpha\Omega_1^2 R_{SN1}^2\right)}{\Omega_1^2\left[\Omega_{SN1}^2 - \Omega_1^2 + \alpha R_{SN1}^2\left(\Omega_{SN1}^2 - 3\Omega_1^2 - \alpha\Omega_1^2 R_{SN1}^2\right)\right]} \qquad (3.2.4)$$

In order to obtain an expression for Ω_H one can apply the Routh-Hurwitz criterion to equation (3.2.3). At $\Omega = \Omega_H$ the following condition must hold (to have one pair of purely imaginary eigenvalues):

$$C_1 C_2 C_3 - C_3^2 - C_1^2 C_4 = 0. \qquad (3.2.5)$$

Equation (3.2.5) (with C_i from equation (3.2.3)) and equation (3.1.4) can be combined to solve for Ω_H implicitly. (An explicit expression is not obtainable.)

3.3 Application of the Center Manifold Theorem

The above analysis is quite general but is not able to determine post-critical dynamics or the manner in which the synchronous solutions and the bifurcating solutions, which turn out to be amplitude moduated, that is, quasi-periodic, interact. In order to obtain a more complete picture of the overall dynamics one would need to determine all of the steady state solutions of equation (3.1.1), whether they be periodic, quasi-periodic, etc., a formidable task. However, a quite complete description of the overall dynamics can, in a restricted parameter region, be obtained using tools from the qualitative theory of dynamical systems, in particular, the center manifold method. The parameter range to be considered is as follows: (i) $\mu_e/\mu_i\Omega_1$, the ratio of external to internal damping, is small; (ii) rotational speeds remain close to the first critical speed Ω_1^*; and (iii) the unbalance, e, is small. Condition (i) implies that the first critical speed is near the first resonance (recall equation (3.1.2)); condition (ii) restricts attention to rotational speeds near critical (and resonance), the region of interest; and condition (iii) simply states that the effects of a slight unbalance on the instability are considered. In this case the first mode dynamics are dominated by the behavior associated with the two eigenvalues which have, in this parameter region, nearly zero real parts. The dynamics associated with the remaining two eigenvalues, which lie well into the left half of the complex plane, will rapidly decay. Due to nonlinear coupling effects, the dynamics associated with these latter eigenvalues cannot simply be ignored in general, and the center manifold technique provides a constructive tool by which the "reduced" slow dynamics can correctly account for such effects. The treatment begins by splitting the linearlized dynamics into the slow and fast components; the center manifold is then constructed, and finally the dynamic equations on the center manifold, i.e., the "reduced" dynamic equations are derived. The analysis of the "reduced" equations is then carried out and the inferred shaft responses can be described.

In the following the center manifold theorem will be applied to equation (3.1.1) in the neighborhood of the first critical speed to deduce the "reduced" dynamic equations. From this stage on we will treat e and ϵ as dependent variables (i.e., the unfolding parameters) where e represents the small perturbation of unbalance and ϵ measures the deviation of speed Ω from Ω_1^*. We also introduce new coordinates $X = (x_1, x_2, x_3, x_4, e)^T = (u, v, \dot{u}, \dot{v}, e)^T$. By treating e and ϵ as dependent dynamic variables, terms such as ϵx_1, ϵe, etc., are rendered as nonlinear in the coordinates $(X,\epsilon) \in \mathbf{R}^6$ (this seemingly trivial step is known as the suspension trick, see Carr , 1981, and it permits application of the center manifold theorem for parameter values away from, but near to, the critical case). Though here we treat both e and ϵ as unfolding parameters, they come into play at different stages; e is regarded as a dependent variable first in equation (3.3.1) below so that no constant terms appear in equation (3.3.1), which is then in the same form as equation (1.4.1), to which the center manifold theorem may be directly applied. ϵ is then introduced into the equation as another dependent variable exactly the same way as in the previous chapter, so as to be consistent. The system of equations (3.1.1) can be written in first order form as follows:

$$\dot{X} = \begin{bmatrix} \dot{x}_1 \\ \dot{x}_2 \\ \dot{x}_3 \\ \dot{x}_4 \\ \dot{e} \end{bmatrix} = \begin{bmatrix} 0 & 0 & 1 & 0 & 0 \\ 0 & 0 & 0 & 1 & 0 \\ \Omega^2-\Omega_1^2 & \mu_e\Omega & -\mu_e-\mu_i\Omega_1^2 & 2\Omega & \Omega^2 \\ -\mu_e\Omega & \Omega^2-\Omega_1^2 & -2\Omega & -\mu_e-\mu_i\Omega_1^2 & 0 \\ 0 & 0 & 0 & 0 & 0 \end{bmatrix} \begin{bmatrix} x_1 \\ x_2 \\ x_3 \\ x_4 \\ e \end{bmatrix} +$$

$$\begin{bmatrix} 0 \\ 0 \\ -\alpha\Omega_1^2 \left(x_1^2+x_2^2\right) x_1 - 2\alpha\mu_i\Omega_1^2 \, (x_1x_3+x_2x_4)x_1 \\ -\alpha\Omega_1^2 \left(x_1^2+x_2^2\right) x_2 - 2\alpha\mu_i\Omega_1^2 \, (x_1x_3+x_2x_4)x_2 \\ 0 \end{bmatrix} = BX + F(X) \quad (3.3.1)$$

The term BX represents the linearized shaft dynamics, F(X) the structural nonlinear terms. At $\Omega = \Omega_1^*$, the eigenvalues of B are : $\pm j\omega_1$, $-\sigma_2 \pm j\omega_2$ and 0 where $\omega_1 = \mu_e/\mu_i\Omega_1$, $\sigma_2 = \mu_e + \mu_i\Omega_1^2$, $\omega_2 = 2\Omega_1 + \mu_e/\mu_i\Omega_1$, and $j^2 = -1$. Letting $\Omega = \Omega_1^* + \epsilon$ where ϵ measures the deviation of speed Ω from Ω_1^* and decomposing B into $B_o + B_\epsilon$, equation (3.3.1) becomes

$$\dot{X} = B_oX + B_\epsilon X + F\,(X) \qquad (3.3.2)$$

$$\dot{\epsilon} = 0$$

where B_o has the same eigenvalues as B at $\Omega = \Omega_1^*$ and B_ϵ is identically the zero matrix when $\epsilon = 0$.

Employing the change of coordinates X=QZ, where Q contains the eigenvectors of B_o in cooorespondence to the eigenvalues $-\sigma_2 \pm j\omega_2$, $\pm j\omega_1$, and 0, and is given below:

$$Q = \begin{bmatrix} 1 & 0 & 1 & 0 & -\omega_2\Omega_1^{*2} \\ 0 & -1 & 0 & -1 & -\sigma_2\Omega_1^{*2} \\ -\sigma_2 & -\omega_2 & 0 & -\omega_1 & 0 \\ -\omega_2 & \sigma_2 & -\omega_1 & 0 & 0 \\ 0 & 0 & 0 & 0 & \omega_1(\omega_2^2+\sigma_2^2) \end{bmatrix}$$

equation (3.3.2) is transformed into the standard form in order to apply the center manifold theorem:

$$\begin{bmatrix} \dot{Z}_1 \\ \dot{Z}_2 \\ \dot{Z}_3 \\ \dot{Z}_4 \\ \dot{Z}_5 \end{bmatrix} = \begin{bmatrix} -\sigma_2 & -\omega_2 & 0 & 0 & 0 \\ \omega_2 & -\sigma_2 & 0 & 0 & 0 \\ 0 & 0 & 0 & -\omega_1 & 0 \\ 0 & 0 & \omega_1 & 0 & 0 \\ 0 & 0 & 0 & 0 & 0 \end{bmatrix} \begin{bmatrix} Z_1 \\ Z_2 \\ Z_3 \\ Z_4 \\ Z_5 \end{bmatrix} + \left\{ Q^{-1}B_\epsilon QZ + Q^{-1}F\ (QZ) \right\} \quad (3.3.3)$$

$$\dot{\epsilon} = 0$$

Note that (Z_1, Z_2) are the coordinates associated with the "fast" dynamics, while (Z_3, Z_4, Z_5, ϵ) are the coordinates associated with the "slow" dynamics. The last two non-linear terms of equation (3.3.3) can be written in explicit matrix/vector forms as:

$$Q^{-1}B_\epsilon QZ = \begin{bmatrix} D_1 & D_2 \\ & \\ D_3 & D_4 \end{bmatrix} \begin{bmatrix} Z_1 \\ Z_2 \\ Z_3 \\ Z_4 \\ Z_5 \end{bmatrix} \quad ; \quad Q^{-1}F\,(QZ) = \begin{bmatrix} f_1 \\ f_2 \\ f_3 \\ f_4 \\ 0 \end{bmatrix}$$

where D_i are matrix functions of ϵ and ϵ^2: D_1 is 2 x 2, D_2 is 2 x 3, D_3 is 3 x 2 and D_4 is 3 x 3. The center manifold, given by $(Z_1, Z_2) = h$ $(Z_3, Z_4, Z_5, \epsilon)$, may be approximated as a power series in its variables. It satisfies equation (1.4.3) which, for the present case, is :

$$N[h] = Dh \left(\begin{bmatrix} 0 & -\omega_1 & 0 \\ \omega_1 & 0 & 0 \\ 0 & 0 & 0 \end{bmatrix} \begin{bmatrix} Z_3 \\ Z_4 \\ Z_5 \end{bmatrix} + D_3 h + D_4 \begin{bmatrix} Z_3 \\ Z_4 \\ Z_5 \end{bmatrix} + \begin{bmatrix} f_3 \\ f_4 \\ 0 \end{bmatrix} \right)$$

$$- \begin{bmatrix} -\sigma_2 & -\omega_2 \\ & \\ \omega_2 & -\sigma_2 \end{bmatrix} h - D_1 h - D_2 \begin{bmatrix} Z_3 \\ Z_4 \\ Z_5 \end{bmatrix} - \begin{bmatrix} f_1 \\ \\ f_2 \end{bmatrix} = 0 \qquad (3.3.4)$$

The center manifold $h(Z_3, Z_4, Z_5, \epsilon)$ can be approximated up to order two if

$$Dh \begin{bmatrix} 0 & -\omega_1 & 0 \\ \omega_1 & 0 & 0 \\ 0 & 0 & 0 \end{bmatrix} \begin{bmatrix} Z_3 \\ Z_4 \\ Z_5 \end{bmatrix} - \begin{bmatrix} -\sigma_2 & -\omega_2 \\ & \\ \omega_2 & -\sigma_2 \end{bmatrix} h - D_2 \begin{bmatrix} Z_3 \\ Z_4 \\ Z_5 \end{bmatrix} = 0 \qquad (3.3.5)$$

is satisfied. Solving (3.3.5) for h and substituing h for (Z_1, Z_2) in the last four equations of (3.3.3), the resulting "reduced" dynamics on the center manifold are given by

$$\begin{bmatrix}\dot{Z}_3\\ \dot{Z}_4\end{bmatrix} = \begin{bmatrix}\mu(\epsilon) & -\omega_1-\beta(\epsilon)\\ \omega_1+\beta(\epsilon) & \mu(\epsilon)\end{bmatrix}\begin{bmatrix}Z_3\\ Z_4\end{bmatrix} + \begin{Bmatrix} a\left(Z_3^2+Z_4^2\right)Z_3 + b\left(Z_3^2+Z_4^2\right)Z_4\\ -b\left(Z_3^2+Z_4^2\right)Z_3 + a\left(Z_3^2+Z_4^2\right)Z_4\end{Bmatrix}$$

$$+\begin{Bmatrix} d_1(\epsilon)\,q + d_2q^3 + (d_3Z_3+d_4Z_4)\,q^2 + \left(d_5Z_3^2 + d_6Z_3Z_4 + d_7Z_4^2\right)q\\ d_8(\epsilon)\,q + d_9q^3 + (d_{10}Z_3+d_{11}Z_4)\,q^2 + \left(d_{12}Z_3^2 + d_{13}Z_3Z_4 + d_{14}Z_4^2\right)q\end{Bmatrix}$$

$$\dot{q} = 0$$

$$\dot{\epsilon} = 0, \tag{3.3.6}$$

where $q = Z_5 = e / \omega_1\left(\omega_2^2 + \sigma_2^2\right)$ has replaced e for convenience. The constants μ, β, d_1 and d_8 depend on ϵ and other system parameters and vanish when ϵ vanishes. The remaining constants depend on the system parameters only and not on ϵ. The terms in the last bracket of equation (3.3.6) represent the perturbations to the perfectly balanced shaft since when $q = 0$ these terms vanish. The remaining terms describe the Hopf bifurcation of a balanced shaft. A supercritical Hopf bifurcation, corresponding to the birth of a stable limit cycle from the trivial solution, as depicted in figure 12 is thus concluded since $a = -\alpha\,\Omega_1^2\,\sigma_2 / \left[\sigma_2^2 + (\omega_2 - \omega_1)^2\right]$ is negative. (This is expected since the unbalance cannot affect the sign of a.) The dynamics of the full system (equation (3.1.1)) with small unbalance and Ω near Ω_1^* are fully captured by the dynamics of equation (3.3.6), the "reduced" equations.

Here the benefits of the center manifold method are evident. Instead of analyzing the full system of four first order nonlinear differential equations, we can carry out the investigation by studying only two first order equations. This provides a method for predicting and describing the response without the use of the extensive simulations which would be required in a numerical study, due to the number of parameters. The analysis utilizes standard phase plane techniques; it involves locating the equilibrium points, determining their stabilities, and checking for the possible occurrence of limit cycles and global bifurcations, such as saddle connections.

In order to interpret the shaft motions from the dynamics on the center manifold, the facts and correspondences given here should be kept in mind. First, the center manifold is a two dimensional surface embedded in the full four dimensinoal phase space. It is invariant - that is, solutions on the center manifold remain on it. It is also locally attractive - that is, solutions started near it tend towards it asymptotically, since the dynamics away from the center manifold will be dominated by the linear terms corresponding to the two eigenvalues which have negative real parts. Equilibrium points in the center manifold correspond to constant amplitude and phase synchronous shaft motions, such as those determined in the previous section, and the stability types correspond. A limit cycle in the center manifold corresponds to a shaft motion which undergoes amplitude and phase oscillations about a synchronous motion. In terms of the rotating coordinates the shaft will oscillate in a periodic manner in both amplitude and phase, with a frequency which is approximately equal to that associated with the Hopf bifurcation, i.e., ω_1 (recall that $\pm j\omega_1$, are the eigenvalues associated with the instability). In terms of fixed, laboratory coordinates, the shaft will be observed to undergo a quasiperiodic motion consisting of two frequencies (plus combinations and harmonics); these frequencies correspond to Ω_1 (free oscillation) and Ω (forced vibration). This is not unexpected since, for $\mu_e/\mu_i\Omega_1 - \omega_1$ small, the internal damping drives the shaft towards nearly synchronous whirling while the unbalance drives it towards exactly synchronous whirling. Thus, when combinations of these two motions occur, the result is composed of two oscillations of nearly equal frequency, and a beating type motion, (that is, amplitude modulated motion) with a long period envelope occurs.

The equilibrium points are obtained by setting $\dot{Z}_3 = \dot{Z}_4 = 0$ in equation (3.3.6). The two resulting algebraic equations are cubic in Z_3 and Z_4 and one, two, or three real solutions are possible for each set of (e, ϵ) (Though, mathematically, there are up to 9 solutions possible for two cubic equations). The stability of the equilibria is determined via linearization. Since the balanced shaft $(e = 0)$ undergoes a Hopf bifurcation at $\Omega = \Omega_1^*$ $(\epsilon = 0)$, it is expected that at least one equilibrium solution will undergo a Hopf bifurcation at some point with $\epsilon > 0$. Once the Hopf bifurcation is found, its type (sub- or super-critical) is known to be supercritical from the unperturbed system, since small perturbations ($e << 1$ in this case) cannot affect the order one coefficient, a, in the normal form for the Hopf bifurcation. Thus a stable limit cycle will arise.

Due to the complexity of the equations in (3.3.6), numerical root solving methods and simulations were employed. Figure 15 depicts a series of numerically calculated phase portraits obtained by fixing e and increasing ϵ from below zero; these clearly show the occurrences of a saddle-node bifurcation (portrait 2), a Hopf bifurcation (portraits 3-4), a saddle connection (portrait 5), and the birth of a limit cycle immediately after the second saddle-node bifurcation (portrait 8) (in fact, a saddle-node, saddle connection bifurcation occurs here ,Schecter, 1988). A complete bifurcation diagram with e and ϵ as the unfolding parameters is shown in Figure 16, with the regions of the associated phase portraits from Figure 15 indicated (Portraits 6 and 7, and 4 and 10 are are grouped together since they are qualitatively the same in terms of topological structure.) Bifurcation diagrams for

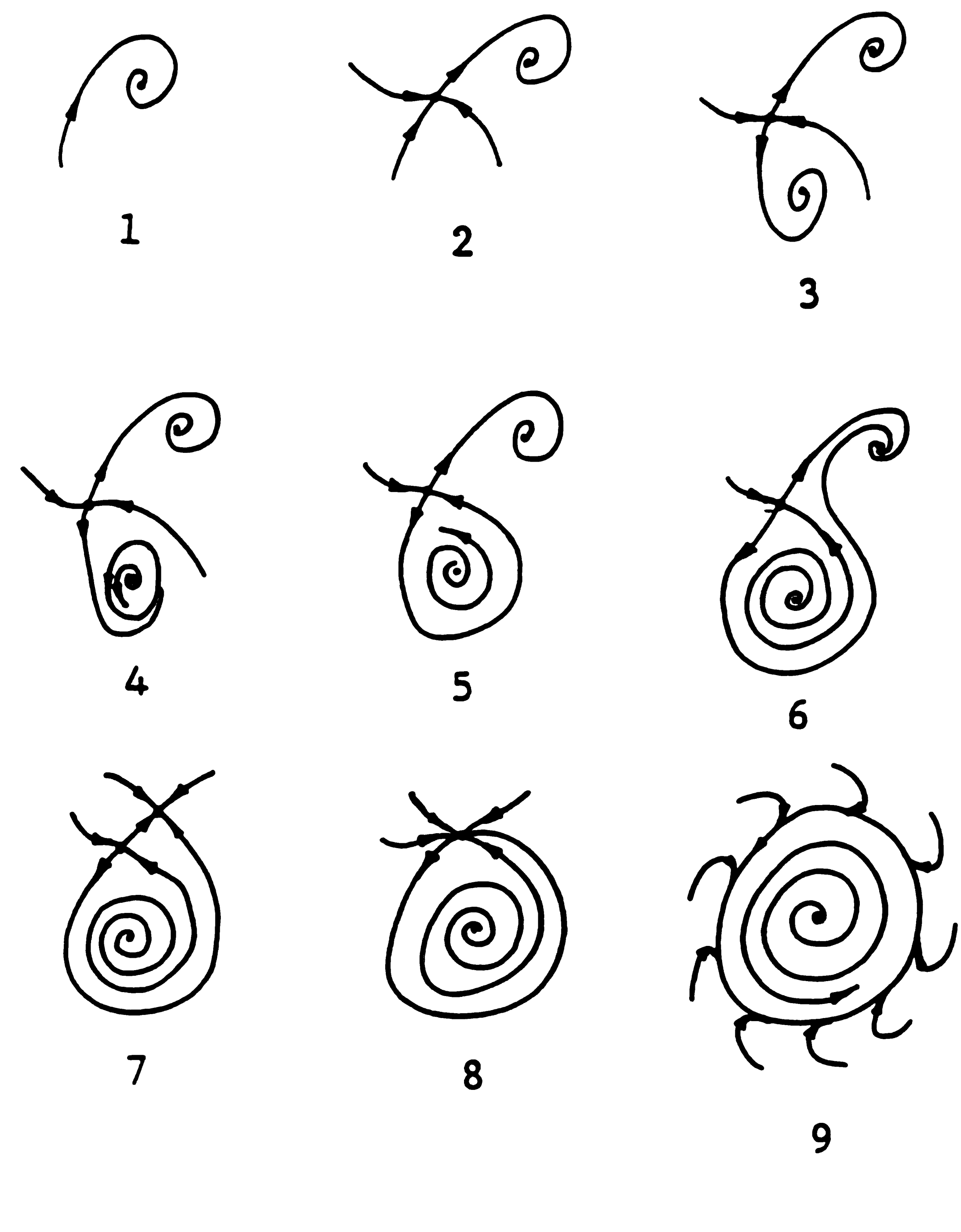

Figure 15. Phase portraits of eqution (3.3.6) as ϵ is increased.
$\mu_e = 0.08$, $\mu_i = 4.5 / \Omega_1^2$, $\alpha = 10$, $e = 0.001$

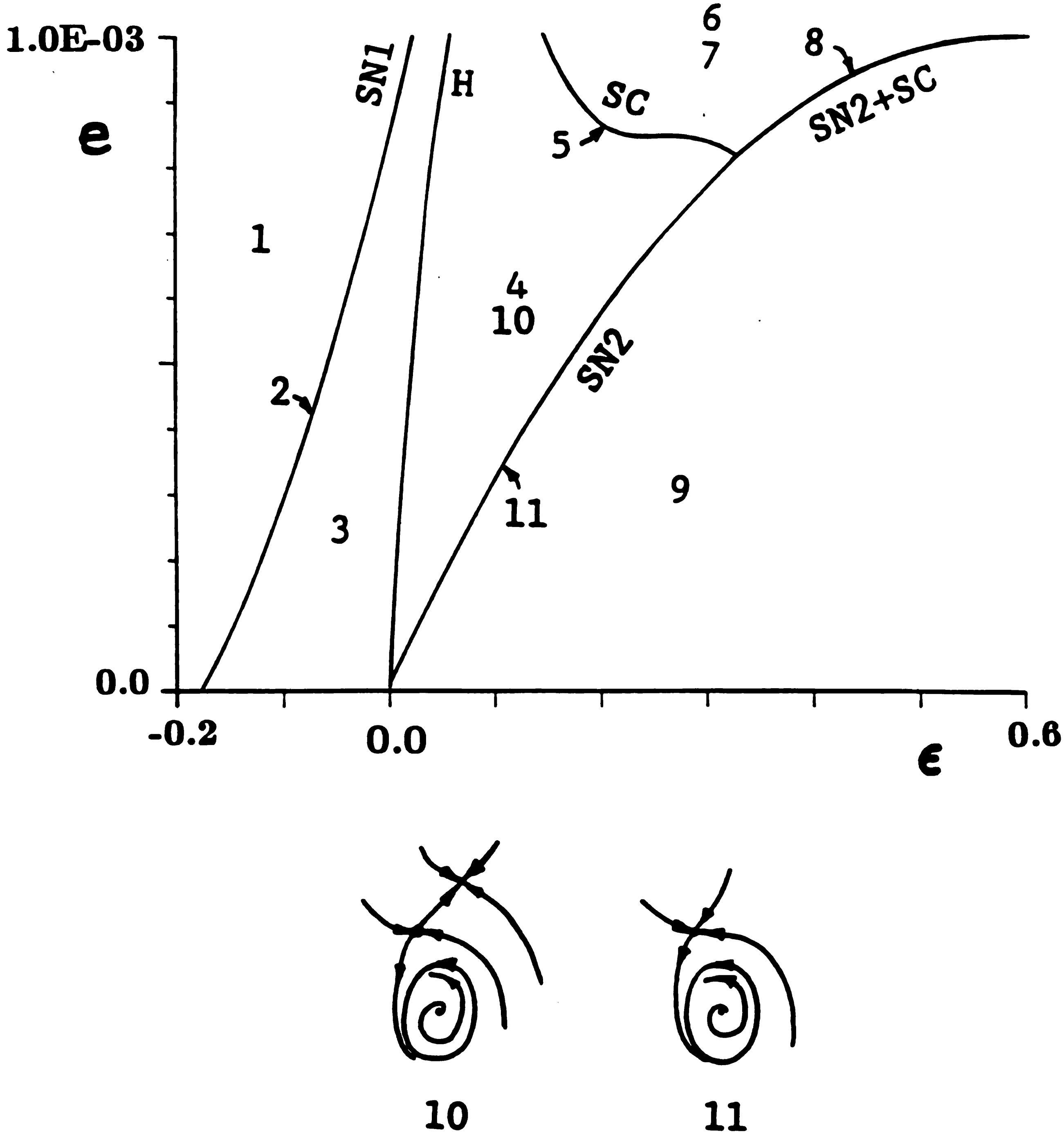

Figure 16. Bifurcation diagram and phase portraits of equation (3.3.6). SC: saddle connection, $r = \sqrt{Z_3^2 + Z_4^2}$, $\mu_e = 0.08$, $\mu_i = 4.5 / \Omega_1^2$ $\alpha = 10$. See Figure 6 for phase portraits 1,2, ...9.

equation (3.1.1) based on the dynamic equivalence to equation (3.3.6) and on the properties derived in Section 3.2 are shown in Figure 17. A discussion of the main results follows.

3.4 Results

Figure 17 depicts the bifurcation curves for the shaft response; each point in the (e,Ω) space corresponds to a specific unbalance magnitude and rotational speed. The present discussion will focus on frequency response diagrams for the shaft, which display a measure of the shaft's vibrational amplitude versus rotational speed. By including the unbalance as a parameter in Figure 17, the response curves for various levels of unbalance can be obtained. In Figure 17 stable synchronous response amplitudes are indicated by solid lines, unstable synchronous amplitudes are indicated by dashed lines, and quasiperiodic response amplitudes are shown as broken lines. The amplitudes and stability types for synchronous motions are determined from the analysis in Section 3.2. The existence and stability of the quasiperiodic motions, as well as the interaction of these with synchronous motions, is derived from the results presented in Section 3.3.

In Figure 17 the curves marked SN1 are associated with the conditions for the first saddle-node bifurcation (equation (3.2.1)) in which the lower two branches of the synchronous response diagram are born as Ω increases. The curves SN2 and SN2 + SC correspond to the saddle-node bifurcation in which the upper and middle synchronous response branches merge and disappear. Note that this curve is asymptotic to a finite value of e (e such that $\mu_e^2 = \alpha e^2\Omega_1^2$) as Ω increases, indicating that for sufficiently large unbalance this bifurcation will not occur. The SN2 corresponds to a simple saddle-node whereas the SN2 + SC corresponds to a more complicated bifurcation in which the saddle-node bifurcation interacts with a saddle connection, resulting in the appearance of a limit cycle corresponding to an amplitude modulated motion (this is depicted in Figure 15, portraits 7-9, with 8 showing the condition at SN2 + SC). Schecter (1988), gives a complete account of this bifurcation. The curve H corresponds to the point at which the lowest synchronous response branch becomes unstable in a Hopf bifurcation, at which point the quasiperiodic response is born. The curve marked SC corresponds to the condition in which the limit cycle amplitude has grown to the point where it touches the saddle point corresponding to the unstable middle branch of the synchronous response curve, forming a simple saddle connection (portrait 5 in Figure 15). This bifurcation annihilates the limit cycle. The points where these curves meet correspond to more complicated, codimension two bifurcations which are, in themselves, of interest. This is not pursued here since the required information is obtained in a direct fashion using simulations; the interested reader is referred to Guckenheimer and Holmes (1983) for background on this topic.

The various curves fit together in a consistent manner, providing a complete description of the shaft response near resonance. Figure 17(a) (17(b), resp.) is a bifurcation diagram for the case in which the Hopf bifurcation disappears before (after, resp.) the second saddle-node bifurcation disappears as the magnitude of unbalance is increased, i.e. the two cases are distinguished by the relative magnitudes of unbalance e which correspond to the conditions $\mu_e^2 = \alpha e^2 \Omega_1^2$ and $\mu_i = \mu_i^*$. These two cases result in minor qualitative differences in the frequency response of the shaft for different levels of unbalance; this is described in detail below. The repsonse of the unbalanced shaft as its rotational speed is increased (from below Ω_1) can be inferred from these bifurcation diagrams; these responses are indicated in the corresponding frequency response diagrams.

The response curves corresponding to the bifurcation diagrams of Figures 17(a,b) are described here. There are four distinct frequency respones possible in Figure 17(a), depending on the level of unbalance. These correspond to cases marked by unbalance levels labeled I, III, IV, and V. Case II represents a special situation which lies on a boundary separating two generic cases. The stable, that is, observable, motions are described below.

For very small levels of unbalance, Case I, the shaft response consists of a region of a single possible synchronous whirl amplitude for $\Omega < \Omega_{SN1}$; two possible synchronous whirl amplitudes, one large and one small, (the actual steady state depending on initial conditions) for $\Omega_{SN1} < \Omega < \Omega_H$; a large amplitude synchronous whirl and a lower magnitude amplitude modulated whirl for $\Omega_H < \Omega < \Omega_{SN2}$; and only the amplitude modulated whirl for $\Omega_{SN2} < \Omega$. In Case I the amplitude modulated whirl never interacts with the synchronous whirl. Case II represents the level of unbalance for which this interaction begins; here the amplitude modulated whirl is just tangent to the synchronous whirl at the second saddle-node point, Ω_{SN2}.

Case III is very similar to Case I except that the amplitude modulated whirl is destroyed in a collision with the middle synchronous whirl branch. This results in the following regions: $\Omega_{SN1} < \Omega < \Omega_H$, in which two stable synchronous whirl solutions exist; $\Omega_{SC} < \Omega < \Omega_{SN2}$, in which only one stable synchronous whirl solution exists; and $\Omega_H < \Omega < \Omega_{SC}$, in which synchronous and amplitude modulated whirl are possible. The ranges $\Omega < \Omega_{SN1}$ and $\Omega > \Omega_{SN2}$ are the same as in Case I.

Case IV, and the borderline level of unbalance given by $\mu_i = \mu_i^*$ between Cases III and IV at which the Hopf bifurcation occurs exactly at the first saddle-node point, are dynamically similar. In this case, and for all larger values of unbalance, i.e. Case V, the lowest synchronous response branch is nowhere stable. In Case IV the synchronous response grows and becomes amplitude modulated for $\Omega \geq \Omega_{SN2}$; at each Ω there is a unique stable response. In Case V there exists a unique stable synchronous response for all values of Ω. Here the unbalance dominates the response, the instability merely renders the lowest synchronous response branch unstable and no amplitude modulated motions occur.

For Figure 17(b) Cases I, II, III, and V are the same as those in Figure 17(a). The difference between the two Figures is in case IV. In order to describe the difference the following notation is introduced: let e_1 correspond to the e value such that $\mu_i = \mu_i^*$, above which in terms of e the lowest synchronous response branch is unstable for all Ω above Ω_{SN1}, and let e_2 denote the value corresponding to $\mu_e^2 = \alpha e^2 \Omega_1^2$, above which the uppermost synchronous response branches do not merge, with all other parameters fixed except the rotational speed. In Figure 17(a) $e_2 > e_1$; in this case e_1, that is, the e value above which the lowest response branch is "completely unstable" (i.e., unstable over $\Omega_{SN1} < \Omega < \infty$), is below the large Ω asymptote of the SN2+SC curve, e_2. In this situation, for $e_1 < e < e_2$, the response curves exhibit a completely unstable lower branch, and the upper two branches merge at SN2+SC (see Case IV in Figure 17(a)). In Figure 17(b) $e_2 < e_1$; here Case IV is different in that, while the lowest response branch is completely unstable, the upper two branches do not merge as Ω is increased.

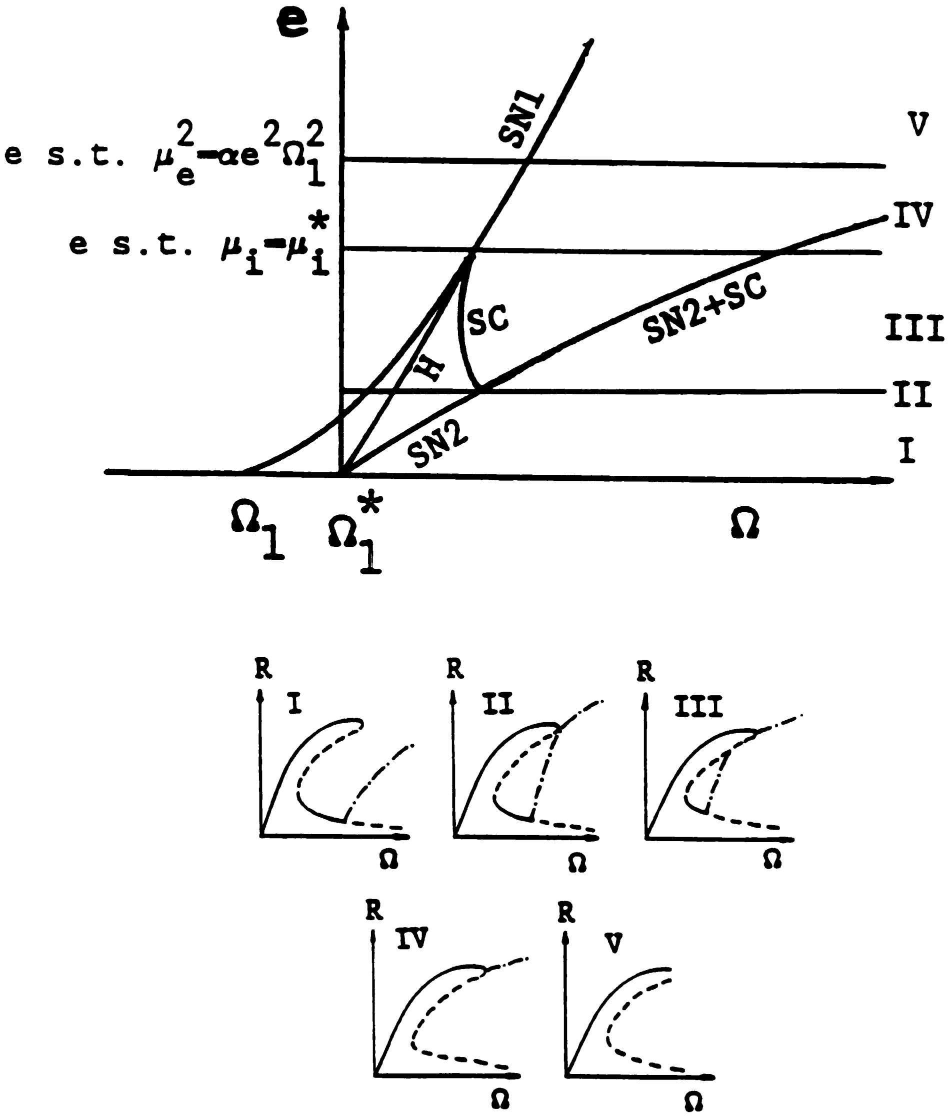

17 (a). **Bifurcation diagram and amplitude-frequency curves for the full system (3.1.1).**

——— (-------) stable (unstable) equilibria (stable (unstable) steady state 2π/Ω periodic motions of the shaft), -.-.-.- stable limit cycle (stable two-frequency component response of the shaft)

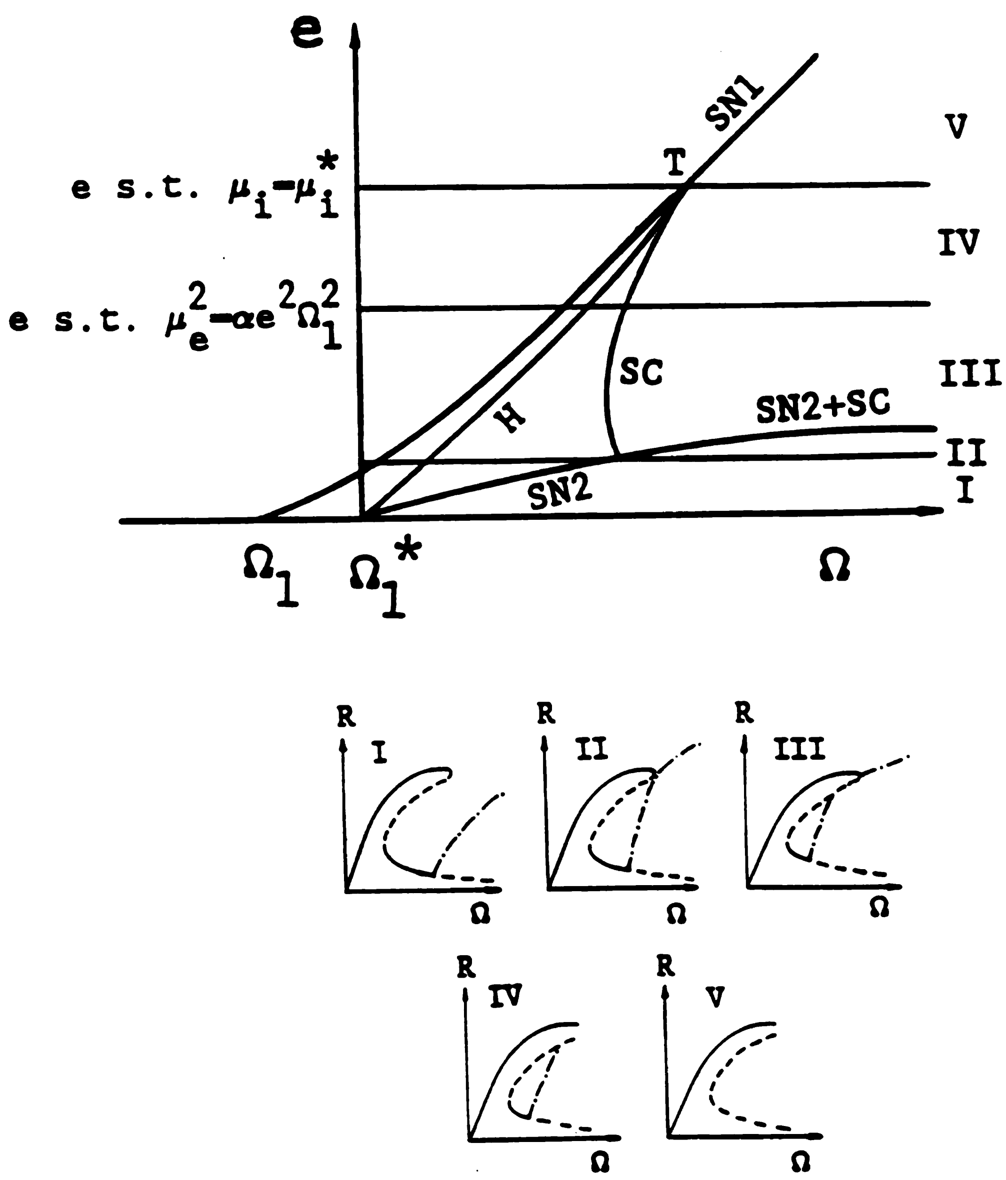

17 (b). **Bifurcation diagram and amplitude-frequency curves for the full system (3.1.1).**

——— (-------) stable (unstable) equilibria (stable (unstable) steady state $2\pi/\Omega$ periodic motions of the shaft), -.-.-.- stable limit cycle (stable two-frequency component

3.5 Computer Simulations and Discussion

Simulations of the full first mode shaft dynamics equations (3.1.1) verify the bifurcation diagrams of Figure 17. Here we present only simulation results for Case III of Figure 17. These simulation results are presented in terms of nonrotating, i.e., fixed coordinates in order to aid with visualization of the shaft response. Figure 18(a) shows a unique stable synchronous whirl for a value of Ω below Ω_{SN1}. Two possible synchronous whirling motions, one large and one small, are shown in Figure 18(b) for $\Omega_{SN1} < \Omega < \Omega_H$. Figure 18(c) shows a large synchronous response and an amplitude modulated whirl for $\Omega_H < \Omega < \Omega_{SC}$.

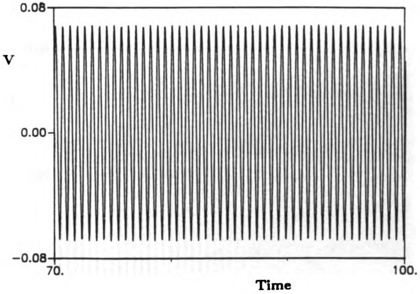

18 (a). **Responses of the shaft depicted in a fixed coordinates.**

$\Omega = 10.04$, $\mu_e = 0.08$, $\mu_i = 4.5 / \Omega_1^2$, $\alpha = 10$, $e = 0.001$

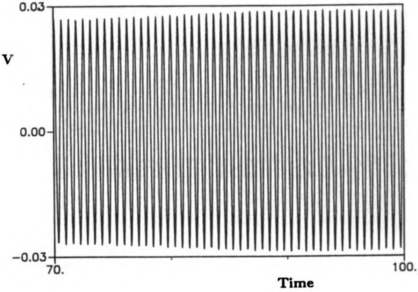

18 (b). **Responses of the shaft depicted in a fixed coordinates.**

$\Omega = 10.085,\ \mu_e = 0.08,\ \mu_i = 4.5 / \Omega_1^2,\ \alpha = 10,\ e = 0.001$

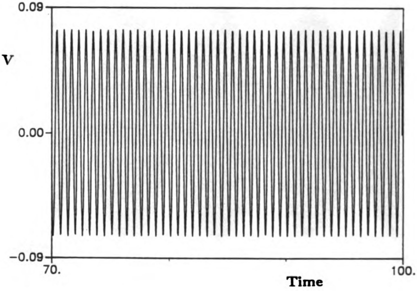

18 (b). **Responses of the shaft depicted in a fixed coordinates.**

$\Omega = 10.085,\ \mu_e = 0.08,\ \mu_i = 4.5 / \Omega_1^2,\ \alpha = 10,\ e = 0.001$

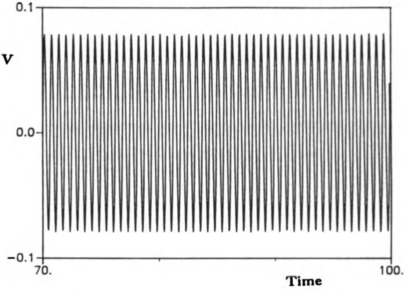

18 (c). Responses of the shaft depicted in a fixed coordinates.

$\Omega = 10.125$, $\mu_e = 0.08$, $\mu_i = 4.5 / \Omega_1^2$, $\alpha = 10$, $e = 0.001$

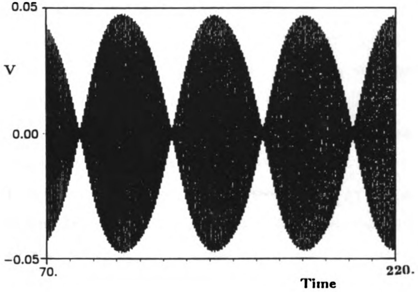

18 (c). Responses of the shaft depicted in a fixed coordinates.

$\Omega = 10.125$, $\mu_e = 0.08$, $\mu_i = 4.5 / \Omega_1^2$, $\alpha = 10$, $e = 0.001$

The actual steady state solution of Figure 18(b,c) depends on initial conditions. Figure 18(d) shows the unique stable large synchronous whirl for $\Omega_{SC} < \Omega < \Omega_{SN2 + SC}$ (the amplitude modulated whirl has been annihilated through a saddle-connnection). The unique stable amplitude modulated whirl is depicted in Figure 18(e) for $\Omega > \Omega_{SN2 + SC}$.

The long period envelope is evident in Figures 18(c,e). For $\mu_e/\mu_i\Omega_1$ small (i.e., Ω_1^* close to Ω_1), all amplitude modulated motions which exist near Ω_1^* are expected to have long period envelopes since the forcing frequency Ω is near to the free vibration frequency. However, if the ratio $\mu_e/\mu_i\Omega_1$ is not small, it is known that the rotordynamic instability may occur at a much higher value of Ω than the first resonance considered here (see Ehrich, 1964 or Chapter 2 of this dissertation). Between resonances, interactions of the type discussed here will be much less complicated and probably simply result in amplitude modulated motion. In these cases the envelope may not have so long a period, since the whirl frequency may not be near to synchronous. However, situations may arise in which the instability interacts with the nonlinear resonance of a higher mode, or with a subharmonic resonance. These topics remain open for future research.

Finally, it may well occur that <u>irregular</u> (that is, nonperiodic or chaotic) amplitude modulations of the motion are observed in simulation studies of equation (3.1.1) or similar models. These can arise from <u>chaotic</u> motions in the full four dimensional phase space which cannot be captured by the center manifold dynamics (since they are two dimensional). These would most likely occur near the saddle-connection bifurcations since saddle connections (that is, homoclinic motions) in a four dimensional phase space can give rise to chaos in quite general circumstances. The book by Wiggins (1988) describes many of these possibilities in mathematical detail. Chaotic amplitude modulations

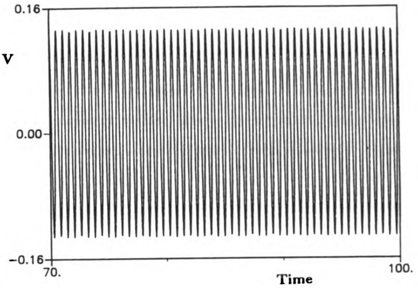

18 (d). Responses of the shaft depicted in a fixed coordinates.

$\Omega = 10.7$, $\mu_e = 0.08$, $\mu_i = 4.5 / \Omega_1^2$, $\alpha = 10$, $e = 0.001$

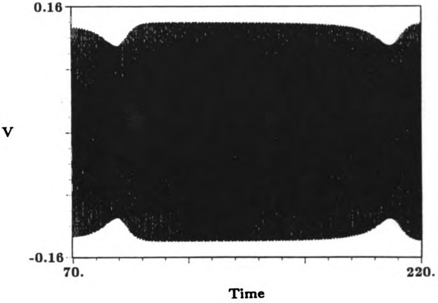

18 (e). Responses of the shaft depicted in a fixed coordinates.

$\Omega = 10.8$, $\mu_e = 0.08$, $\mu_i = 4.5 / \Omega_1^2$, $\alpha = 10$, $e = 0.001$

have been found to occur in the vibrations of systems with internal resonances; the paper by Johnson and Bajaj (1989) provides an example of this and gives several references.

In the previous two chapters, internal damping resulting from the dissipative property of the shaft material is the cause of rotordynamic instability. Another common cause of rotordynamic instability is non-linear bearing forces; this is investigated in the following chapter.

CHAPTER IV

INSTABILITIES AND RESONANCES DUE TO FLUID FILM JOURNAL BEARINGS

4.1 The Journal Bearing Equations and Hopf Bifurcations

In this chapter methods similar to those used in the previous chapters will be employed to investigate the effects of fluid film forces in journal bearings and mass unbalance on the dynamics of a rotor. The model consists of an unbalanced disk mounted midway between two supporting fluid film journal bearings on a rigid shaft. Studies on this problem have been carried out by other researchers, see for example Barrett, Akers and Gunter (1976), Gunter, Humphris and Springer (1983) and Hollis and Taylor (1987), but are restricted to numerical investigations. In this chapter we present an analytical approach to this problem so as to obtain a more complete understanding in terms of response bifurcation diagrams and associated phase portraits.

It is well known that such systems, under the action of a constant load due to gravity and without mass unbalance, may exhibit a self-excited vibration known as "oil whip" as the rotor speed is increased beyond a certain threshold speed, above which the static equilibrium positions are unstable. These stable (unstable, resp.) whirl orbits, which arise above (below, resp.) the threshold speed, are consequences of the non-linear bearing hydrodynamical film forces which are capable of transferring energy from the rotation of the rotor into a whirl motion. Fairly complete parameter studies for such system are given by Myers (1984), Gardner et al. (1985), and Hollis and Taylor (1986).

The effects of rotor unbalance on these instabilities will be examined by using the center manifold theorem and the normal form theorem. Special attention is given to the resonant cases in which the frequency of the bifurcating cycle and the frequency of the excitation due to unbalance are commensurate, i.e., the ratio of the two frequencies is close to a rational number, p/q, where p and q are relatively prime, especially for strongly resonant cases, $q = 1, 2, 3$, which correspond to primary resonance, subharmonic resonances of order two and three, respectively. The dynamics in the nonresonant case are quite straightforward; the responses are mainly dominated by the forcing of period T due to the unbalance excitation, which become unstable (due to the action of bearing forces) when the rotational speed is increased beyond a certain value, beyond which the responses consist of two components, one from the excitation and the other from the oil whip with frequencies approximately equal to those of the rotation and the oil whirl, respectively; these are simple quasi-periodic responses. For the weakly resonant cases ($q \geq 4$), in addition to the phenomena mentioned above, there exists a resonant "horn" in parameter space (see Gambaudo, 1985) in which periodic motions with period qT exist. The dynamics for the strongly resonant cases are much more complicated than those mentioned above, as will be seen in the sequel.

The model for the fluid film forces considered here was originally proposed by Myers (1984); it consists of a rigid, symmetric disk with mass unbalance mounted midway between two identical, plain cylindrical journal bearings on a rigid shaft. The investigation is confined to cylindrical whirling in which the two ends of the rotor remain in phase so that it is sufficient to consider only one bearing (Figure 19), which then supports a load equal to one half of the applied load F on the rotor. Note that the rotor has mass 2M and unbalance e and the journal center has horizontal and vertical displacements Y and X, respectively, measured from the center of the bearing. Other system parameters are the bearing length in the axial direction L, the bearing radius R, the angular rotor speed ω, the radial clearance c, and the lubricant viscosity ν. The equations of motion are derived by assuming the long-bearing approximation with π-film model for cavitation and are, in nondimensionalized form:

$$
\begin{aligned}
\dot{x}_1 &= x_2 \\
\dot{x}_2 &= S(1/S\bar{\omega} + f_r\cos\phi - f_\phi\sin\phi)/\bar{\omega} + \rho^2\cos t \\
\dot{x}_3 &= x_4 \\
\dot{x}_4 &= S(f_r\sin\phi + f_\phi\cos\phi)/\bar{\omega} + \rho^2\sin t
\end{aligned}
\tag{4.1.1}
$$

where

$$x_1 = x = X/c, \quad x_2 = \dot{x}, \quad x_3 = y = Y/c, \quad x_4 = \dot{y}, \quad (\dot{\ }) = d(\ )/dt$$

$$t = \omega\tau, \ \bar{\omega} = (Mc/F)^{1/2}\omega, \ \rho^2 = e/c, \ S = LR^3\nu/(FMc)^{1/2}c^2$$

and where the radial and tangential fluid forces are expressed as

$$f_r = F_r/S\bar{\omega}F = -6\left[\frac{2\epsilon^2(1-2\dot{\phi})}{(2+\epsilon^2)(1-\epsilon^2)} + \frac{[\pi^2(2+\epsilon^2)-16]\dot{\epsilon}}{\pi(2+\epsilon^2)(1-\epsilon^2)^{3/2}}\right]$$

$$f_\phi = F_\phi/S\bar{\omega}F = 6\left[\frac{\pi\epsilon(1-2\dot{\phi})}{(2+\epsilon^2)(1-\epsilon^2)^{1/2}} + \frac{4\epsilon\dot{\epsilon}}{(2+\dot{\epsilon}\ )(1-\epsilon^2)}\right] \tag{4.1.2}$$

where (ϵ, ϕ) are the polar coordinates for (x, y), given by

$x = \epsilon \cos\phi, \qquad y = \epsilon \sin\phi$

These fluid forces are obtained by solving the Reynold equation for a journal bearing (see the Appendix in Myers, 1984) for an expression for the pressure distribution around the journal with the assumption of a long bearing approximation and suitable boundary conditions (that is, the oil film occupies the converging half of the bearing and a cavity exists in the diverging region). The hydrodynamic fluid forces are then calculated by integrating the pressure distribution in the radial and tangential directions.

The parameters to be varied are the nondimensionalized running speed $\bar{\omega}$ and the system parameter S which is defined above; it is independent of the rotor speed ω and is constant for a given rotor system. For a perfectly balanced rotor, ρ, which measures the unbalance, is zero and the static equilibrium position (ϵ_0, ϕ_0) is obtained by setting all time derivatives in equation (4.1.1) to zero. It is a function of $\bar{\omega}$, and it is easily shown that (ϵ_0, ϕ_0) must satisfy the following conditions

$$S\bar{\omega} = (2 + \epsilon_0^2)(1 - \epsilon_0^2) \,/\, 6\epsilon_0\left[\pi^2(1 - \epsilon_0^2) + 4\epsilon_0^2\right]^{1/2}$$

$$\tan \phi_0 = \pi(1 - \epsilon_0^2)^{1/2} \,/\, 2\epsilon_0 \qquad (4.1.3)$$

the solution of which is shown in Figure 20 for various values of $\bar{\omega}$. The stability of this static equilibrium position can be determined by the eigenvalues of the system linearized at (ϵ_0, ϕ_0). It is found that the stable static equilibrium position becomes unstable when $\bar{\omega}$ exceeds

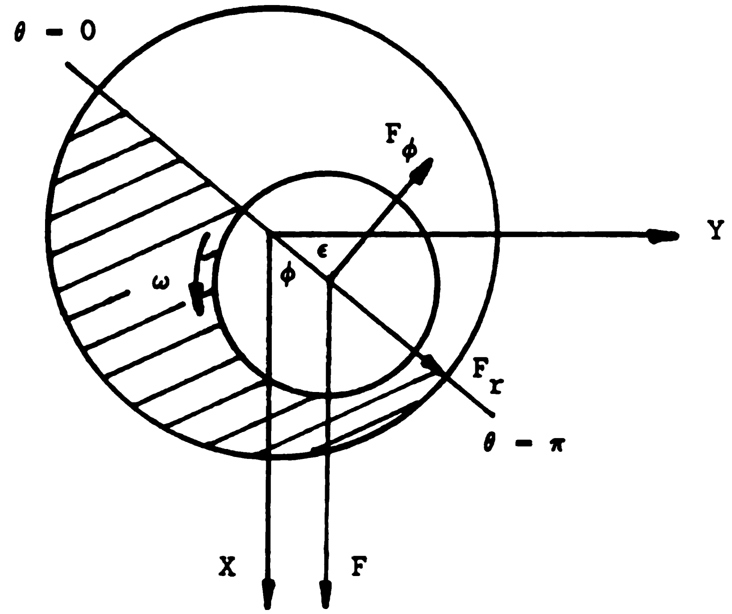

Figure 19. The Journal Bearing.

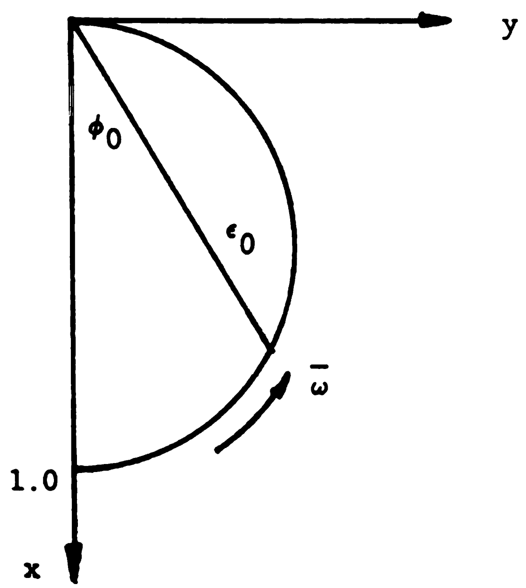

Figure 20. Locus of static equilibrium positions.

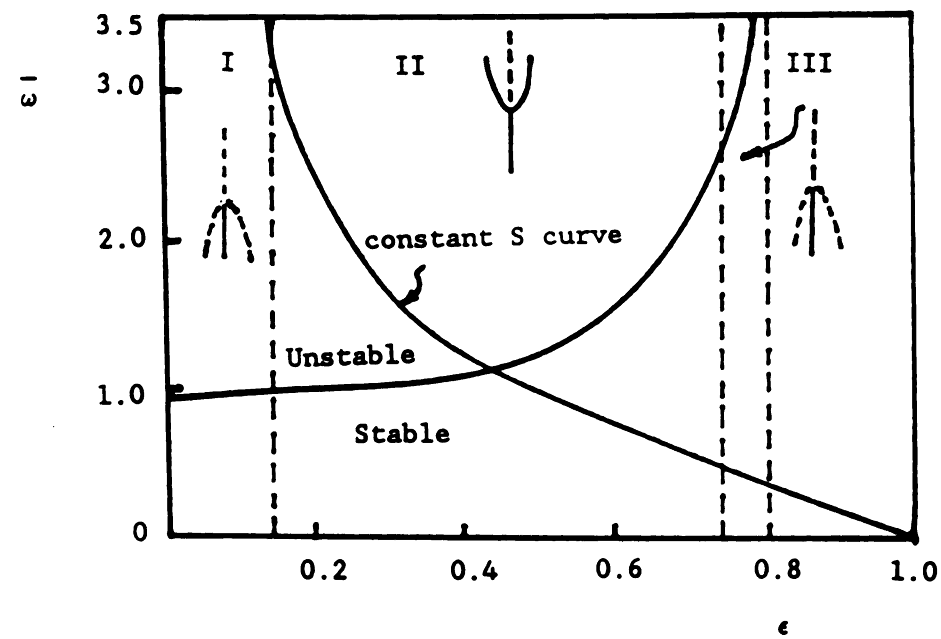

Figure 21. The stability boundary and bifurcation diagrams.

the critical speed $\bar{\omega}_0$ (which depends on S) at which point a pair of complex conjugate eigenvalues of the linearized system passes through the imaginary axis of the complex plane into the right hand side and a Hopf bifurcation occurs.

Myers (1984) used the Hopf bifurcation theory to examine the bifurcating limit cycles and obtained the resulting stability boundary and bifurcation diagrams shown in Figure 21. In regions I and III unstable small-amplitude limit cycles which exist below the critical speed $\bar{\omega}_0$ are predicted (subcritical bifurcation), while stable limit cycles existing above the critical speed are predicted in region II (supercritical bifurcation). Our present purpose is to investigate the behavior of the overall dynamics when $\rho \neq 0$, in which case the static equilibrium position is perturbed to a motion of period 2π (due to the excitation terms, $\rho^2\cos t$ and $\rho^2\sin t$) and the limit cycle is perturbed to a periodic or quasi-periodic motion depending on the delicate issue of whether these multiple frequencies are commensurate, close to commensurate, or far from commensurate. Other more exotic responses may also exist, as is shown below.

4.2 The Center Manifold Theorem and the Poincare Map

We shall first shift the origin of the coordinates to the static equilibrium position and perform a Taylor series expansion of equation (4.1.1) about the steady state position (x_0, y_0) out to third order. To this end, letting

$$y_1 = x - x_0, \quad y_2 = \dot{y}_1, \quad y_3 = y - y_0, \quad y_4 = \dot{y}_3$$

equation (4.1.1) becomes

$$\dot{y}_1 = y_2$$

$$\dot{y}_2 = \frac{S}{\bar{\omega}} (a_1 y_1 + a_3 y_2 + a_2 y_3 + a_4 y_4) + \frac{S}{\bar{\omega}} f_1(y_1, y_2, y_3, y_4) + \rho^2 \cos t$$

$$\dot{y}_3 = y_4 \tag{4.2.1}$$

$$\dot{y}_4 = \frac{S}{\bar{\omega}} (b_1 y_1 + b_3 y_2 + b_2 y_3 + b_4 y_4) + \frac{S}{\bar{\omega}} f_2(y_1, y_2, y_3, y_4) + \rho^2 \sin t$$

where $$a_1 = -\frac{1}{S\bar{\omega}} \frac{2[8\epsilon_0^2(2 + \epsilon_0^4) + \pi^2(1 - \epsilon_0^2)(2 - \epsilon_0^2 + 2\epsilon_0^4)]}{(2 + \epsilon_0^2)(1 - \epsilon_0^2)[\pi^2(1 - \epsilon_0^2) + 4\epsilon_0^2]^{3/2}}$$

$$a_2 = \frac{\pi(1 - \epsilon_0^2)^{1/2}}{2\epsilon_0} a_1$$

$$a_3 = -\frac{1}{S\bar{\omega}} \frac{2\{2\epsilon_0^2[\pi^2(2 + \epsilon_0^2) - 16] + \pi^2(1 - \epsilon_0^2)[\pi^2(1 + \epsilon^2) + 8\epsilon^2]\}}{\pi\epsilon_0(1 - \epsilon_0^2)^{1/2}[\pi^2(1 - \epsilon_0^2) + 4\epsilon_0^2]^{3/2}}$$

$$a_4 = b_3 = -\frac{1}{S\bar{\omega}} \frac{2(\pi^2 - 8)(2 + \epsilon_0^2)}{[\pi^2(1 - \epsilon_0^2) + 4\epsilon_0^2]^{3/2}}$$

$$b_1 = -\frac{1}{S\bar{\omega}} \frac{\pi[4\epsilon_0^4 - \pi^2(1 - \epsilon_0^2)^2]}{\epsilon_0(1 - \epsilon_0^2)^{1/2}[\pi^2(1 - \epsilon_0^2) + 4\epsilon_0^2]^{3/2}}$$

$$b_2 = -\frac{1}{S\bar{\omega}} \frac{2[4\epsilon_0^2 + \pi^2(2 - \epsilon_0^2)]}{[\pi^2(1 - \epsilon_0^2) + 4\epsilon^2]^{3/2}}$$

$$b_4 = \frac{\pi(1 - \epsilon_0^2)^{1/2}}{2\epsilon_0} a_4$$

and where the expressions for the coefficients of the quadratic and cubic terms of f_1 and f_2 are functions of (ϵ_0, ϕ_0) and can be found in Myers (1981). The stability boundary in Figure 21 is determined by examining the eigenvalues of equation (4.2.1) linearized about (0, 0, 0, 0) with $\rho = 0$. The boundary occurs when a pair of purely imaginary eigenvalues, $\pm \bar{\Omega} j$, and two eigenvalues (these may be complex conjugates) with negative real parts exist. For a specific rotor system, represented by the constant S curves of Figure 21, the static equilibrium position is stable when $\bar{\omega} < \bar{\omega}_0$ and unstable when $\bar{\omega} > \bar{\omega}_0$. The bifurcating limit cycle arising at $\bar{\omega} = \bar{\omega}_0$ has a natural frequency $\bar{\Omega}$, which may be close to (in a precise sense, see Arnold, 1987 or Gambaudo, 1985) a rational number p/q depending on the S value, in which case resonant phenomenon may occur for the system with unbalance ρ.

Application of the Center Manifold Theorem

Again the center manifold theorem will be applied to equation (4.2.1) in the neighborhood of $\bar{\omega}_0$ where ρ is assumed to be a small perturbation. The four dimensional equations of (4.2.1) are to be reduced to the "essential" two dimensional equations which govern the dynamics on the center manifold. This reduction of dimension simplifies the analysis of the response and captures the dynamics of the full system near the bifurcation points.

Introducing $\mu = \bar{\omega} - \bar{\omega}_0$ as a small parameter (which measures the deviation of $\bar{\omega}$ away from the threshold speed $\bar{\omega}_0$), equation (4.2.1) can be written in matrix form as

$$\dot{\bar{y}} = A_0\bar{y} + A_1\mu\bar{y} + (S/\bar{\omega}_0 - S/\bar{\omega}_0^2\mu)\begin{bmatrix} 0 \\ f_1 \\ 0 \\ f_2 \end{bmatrix} + \rho^2\begin{bmatrix} 0 \\ \cos t \\ 0 \\ \sin t \end{bmatrix} \tag{4.2.2}$$

where $\bar{y} = (y_1, y_2, y_3, y_4)^T$, $1/\bar{\omega}$ has been approximated by $1/\bar{\omega}_0 - \mu/\bar{\omega}_0^2$ and

$$A_0 = S \begin{bmatrix} 0 & \bar{\omega}_0/S & 0 & 0 \\ a_1 & a_3 & a_2 & a_4 \\ 0 & 0 & 0 & \bar{\omega}_0/S \\ b_1 & b_3 & b_2 & b_4 \end{bmatrix} / \bar{\omega}_0 \quad , \text{ and}$$

$$A_1 = - S \begin{bmatrix} 0 & 0 & 0 & 0 \\ a_1 & a_3 & a_2 & a_4 \\ 0 & 0 & 0 & 0 \\ b_1 & b_3 & b_2 & b_4 \end{bmatrix} / \bar{\omega}_0^2 \quad .$$

Note that A_0 has eigenvalues of $\pm \bar{\Omega}$ j and two others with negative real parts. Introducing the coordinate transformation $\bar{y} = Qv$ where Q contains the corresponding eigenvectors of the eigenvalues of A_0, equation (4.2.2) yields

$$\dot{v} = Q^{-1}A_0Qv + Q^{-1}A_1Q\mu v + Q^{-1}(S/\omega_0 - S/\omega_0^2\mu) \begin{bmatrix} 0 \\ f_1 \\ 0 \\ f_2 \end{bmatrix} + Q^{-1}\rho^2 \begin{bmatrix} 0 \\ \cos t \\ 0 \\ \sin t \end{bmatrix} \qquad (4.2.3)$$

Splitting equation (4.2.3) into two 2-dimensional equations, defining $\theta = t(\bmod 2\pi)$ and treating θ, ρ and μ as dependent variables such that μv, $\rho^2\cos\theta$ and $\rho^2\sin\theta$. etc., are nonlinear terms (the suspension trick again, see Carr, 1981), one obtains

$$\dot{\theta} = 1$$

$$\dot{\mu} = 0$$

$$\dot{\rho} = 0$$

$$\begin{bmatrix} \dot{v}_1 \\ \dot{v}_2 \end{bmatrix} = B_0 \begin{bmatrix} v_1 \\ v_2 \end{bmatrix} + B_1\mu \begin{bmatrix} v_1 \\ v_2 \end{bmatrix} + B_2\mu \begin{bmatrix} v_3 \\ v_4 \end{bmatrix} + S(1/\bar{\omega}_0 - \mu/\bar{\omega}_0^2)B_3 \begin{bmatrix} f_1 \\ f_2 \end{bmatrix}$$

$$+ \rho^2 B_3 \begin{bmatrix} \cos\theta \\ \sin\theta \end{bmatrix}$$

$$\begin{bmatrix} \dot{v}_3 \\ \dot{v}_4 \end{bmatrix} = C_0 \begin{bmatrix} v_3 \\ v_4 \end{bmatrix} + C_1\mu \begin{bmatrix} v_1 \\ v_2 \end{bmatrix} + C_2\mu \begin{bmatrix} v_3 \\ v_4 \end{bmatrix} + S(1/\bar{\omega}_0 - \mu/\bar{\omega}_0^2)B_3 \begin{bmatrix} f_1 \\ f_2 \end{bmatrix}$$

$$+ \rho^2 C_3 \begin{bmatrix} \cos\theta \\ \sin\theta \end{bmatrix} \qquad (4.2.4)$$

where $Q^{-1}A_0Q$ and $Q^{-1}A_1Q$ have been decomposed as follows:

$$Q^{-1}A_0Q = \begin{bmatrix} B_0 & 0 \\ 0 & C_0 \end{bmatrix}, \qquad Q^{-1}A_1Q = \begin{bmatrix} B_1 & B_2 \\ C_1 & C_2 \end{bmatrix},$$

and where B_i and C_i are constant 2 x 2 matrices with B_0 and C_0 in real Jordan canonical form :

$$B_0 = \begin{bmatrix} 0 & -\bar{\Omega} \\ \bar{\Omega} & 0 \end{bmatrix}, \qquad C_0 = \begin{bmatrix} -S_1 & 0 \\ 0 & -S_2 \end{bmatrix} \text{ or } C_0 = \begin{bmatrix} -S_1 & -S_2 \\ S_2 & -S_1 \end{bmatrix},$$

C_0 has eigenvalues with negative real parts (either real: $-s_1$, $-s_2$; or complex conjugate: $-s_1 \pm s_2 j$). By the center manifold theorem, there exists a center manifold $(v_3 = h_1(\theta, \mu, \rho, v_1, v_2), v_4 = h_2(\theta, \mu, \rho, v_1, v_2))^T$ with $h_i = Dh_i = 0$ at $\mu = \rho = v_1 = v_2 = 0$ such that the dynamics of equation (4.2.4) are topologically equivalent to those on the center manifold (see Kelley, 1967, for the required results and the proofs for time dependent center manifolds).

Differentiating $h = (h_1, h_2)^T$ with respect to time and using the chain rule, one obtains an equation which h must satisfy:

$$N[h] = Dh \left\{ B_0 \begin{bmatrix} v_1 \\ v_2 \end{bmatrix} + B_1\mu \begin{bmatrix} v_1 \\ v_2 \end{bmatrix} + B_2\mu\, h + S(1/\bar{\omega}_0 - \mu/\bar{\omega}_0^2)B_3 \begin{bmatrix} f_1 \\ f_2 \end{bmatrix} + \rho^2 B_3 \begin{bmatrix} \cos\theta \\ \sin\theta \end{bmatrix} \right\} - C_0 h - C_2\mu h - C_1\mu \begin{bmatrix} v_1 \\ v_2 \end{bmatrix} - \rho^2 C_3 \begin{bmatrix} \cos\theta \\ \sin\theta \end{bmatrix} - S(1/\bar{\omega}_0 - \mu/\bar{\omega}_0^2)B_3 \begin{bmatrix} f_1 \\ f_2 \end{bmatrix} = 0 \tag{4.2.5}$$

which is not solvable for h, but can be approximated arbitrarily well by a Taylor series near $(\mu, \rho, v_1, v_2) = 0$. h can be approximated up to order two if

$$DhB_0 \begin{bmatrix} v_1 \\ v_2 \end{bmatrix} - C_1\mu \begin{bmatrix} v_1 \\ v_2 \end{bmatrix} - C_0\, h - S/\bar{\omega}_0\, C_3 \begin{bmatrix} f_1 \\ f_2 \end{bmatrix} - \rho^2 C_3 \begin{bmatrix} \cos\theta \\ \sin\theta \end{bmatrix} = 0 \tag{4.2.6}$$

such that $N[h] = O(|\mu, \rho, v_1, v_2|^3)$. Solving equation (4.2.6) and substituting the results for h in $(\dot{v}_1, \dot{v}_2)^T$ of equation (4.2.4) yields the following equations which govern the dynamics on the center manifold:

$$\begin{bmatrix} \dot{v}_1 \\ \dot{v}_2 \end{bmatrix} = \begin{bmatrix} \sigma_1(\mu) & -\bar{\Omega} - \Omega_1(\mu) \\ \bar{\Omega} + \Omega_2(\mu) & \sigma_2(\mu) \end{bmatrix} + \begin{bmatrix} f_3(v_1, v_2) \\ f_4(v_1, v_2) \end{bmatrix} + \rho^2 B_3 \begin{bmatrix} \cos t \\ \sin t \end{bmatrix}$$

$$+ \begin{bmatrix} g_1(\mu, v_1, v_2, t) \\ g_2(\mu, v_1, v_2, t) \end{bmatrix} \tag{4.2.7}$$

where $\sigma_i(0) = \Omega_i(0) = 0$; f_3 and f_4 contain quadratic and cubic terms of v_1, v_2 with coefficients depending on μ which are non-zero when μ vanishes; and $g_i = \rho^2\ (O(\mu) + O(v_i))$. At this stage, it is clearly seen that for $\rho = 0$, equation (4.2.7) exhibits a Hopf bifurcation at $\mu = 0$. The latter two terms in equation (4.2.7) represent the small perturbation due to unbalance. By the normal form theorem (see Guckenheimer and Holmes, 1983 or Arnold, 1987), there exists a weakly non-linear change of coordinates which puts equation (4.2.7) into the standard normal form for a Hopf bifurcation. Written in complex variable form, $z = v_1 + j\ v_2$, this normal form is as follows :

$$\dot{z} = \lambda(\mu)z + b(\mu)z^2\bar{z} + \rho^2 g_3(t) + g_4(\mu, z, \bar{z}, \rho, t) \tag{4.2.8}$$

where $\lambda(\mu) = \sigma\mu + i(\bar{\Omega} + \Omega\mu) + O(\mu^2)$ (with $\sigma > 0$, $\Omega < 0$) is one of the eigenvalues of the linearized system (4.2.1) that crosses the imaginary axis at $\mu = 0$; $b(\mu) = (\alpha_1 + \alpha_2\mu) + i(\beta_1 + \beta_2\mu) + O(\mu^2)$; $\bar{z}$ is the complex conjugate of z; g_3 is periodic, i.e., $g_3(t + 2\pi) = g_3(t)$; and $g_4 = \rho^2(O(\mu) + O(|z|))$.

In the case $\rho = 0$, the zero solution of equation (4.2.8) undergoes a Hopf bifurcation at $\mu = 0$. The Hopf condition $\sigma > 0$ insures that the static equilibrium position is stable (unstable) if $\mu < 0$ ($\mu > 0$), or equivalently $\bar{\omega} < \bar{\omega}_0$ ($\bar{\omega} > \bar{\omega}_0$). The type of Hopf bifurcation occuring at $\mu = 0$ can be determined by examining the sign of Re $b(0) = \alpha_1$: $\alpha_1 < 0$ implies the existence of an attracting limit cycle arising at $\mu = 0$ (supercritical) while $\alpha_1 > 0$ implies the existence of a repelling limit cycle vanishing at $\mu = 0$ (subcritical) as μ is increased. A numerical computation of α_1 confirms and reproduces the bifurcation diagram of Figure 21.

The Poincare Map

Since this is a periodically forced problem, it would be convenient to look at the dynamics on the Poincare map which is obtained by sampling the response once per forcing period, $T = 2\pi$. In order to achieve this, the solution of equation (4.2.8) is written in an integral form as follows (after Gambaudo, 1985):

$$z(t) = e^{\lambda(\mu)t}\Big\{z(0) + \int_0^t e^{-\lambda(\mu)\eta}\Big[\,b(\mu)|z(\eta)|^2 z(\eta) + \rho^2 g_3(\eta) + g_4(\mu,\ z(\eta),\ \bar{z}(\eta),\ \rho,\ \eta)\Big]d\eta\Big\} \tag{4.2.9}$$

Hence a local expression of the Poincare map $P : C \to C$ (i.e., $z(0) \to z(2\pi)$) can be obtained by solving equation (4.2.9) utilizing a fixed point technique. It is given by

$$P = e^{\lambda(\mu)2\pi}\left[z + \frac{e^{4\pi \mathrm{Re}\lambda(\mu)} - 1}{2\mathrm{Re}\lambda(\mu)}\, b(\mu)|z|^2 z + \rho^2 I(\mu)\right]$$

$$+ \tilde{g}_4(\mu,\ z.\ \bar{z},\ \rho) \tag{4.2.10}$$

where
$$I(\mu) = \int_0^{2\pi} e^{-\lambda(\mu)\eta}\, g_3(\eta)d\eta = \frac{e^{-2\pi\lambda(\mu)} - 1}{\lambda^2(\mu) + 1}\,[-\, c\, -\, d\lambda(\mu)]$$

$$\tilde{g}_4(\mu,\ z.\ \bar{z},\ \rho) = \rho^2(O(\mu) + O(|z|))$$

and the constants $c = q_{14} + j\ q_{24}$, and $d = q_{12} + j\ q_{22}$ where q_{ij} is the (i,j) element of the matrix Q^{-1}.

The dynamics governed by the above equation (4.2.10) will be examined in a three parameter space : ρ for the amplitude of the unbalance, μ for the rotary speed variation from the Hopf bifurcation, and s for the frequency detuning of the critical eigenvalues associated with the Hopf bifurcation: $\bar{\Omega} = \Omega_0 + s$. Note that varying the system parameter S has the same effect as varying $\bar{\Omega}$ and hence Ω_0 and s. The discussion of this chapter includes two separate cases: the nonresonant ($\Omega_0 \notin \{p/q\}$) and resonant ($\Omega_0 \in \{p/q\}$) cases, with an emphasis on the latter.

As mentioned before, the dynamics for the <u>nonresonant</u> case are quite straightforward. Rather complicated and interesting dynamics occurs near <u>resonances</u> in which case small divisor terms play an important role in determining the response. Large amplitude vibration, jump phenomenon and the coexistence of multiple stable solutions are typically observed phenomena for the resonant case. Since equation (4.1.2) contains nonlinear terms up to order three, strongly resonant cases occur for q = 1, 2, 3. Higher order terms (order 4, 5, ...) are much less significant than the lower order terms in determining the response and hence are neglected in the equation. Thus, for $q \geq 4$ the natural frequency of the bifurcating cycle does not strongly interact with the excitation frequency. Here only the 1/1 and 1/2 resonances are considered. Other cases are left for future work.

It should be noted that fixed points of the Poincare map (4.2.10) represent periodic solutions with period 2π of equation (4.2.7), i.e., synchronous whirling; periodic cycles with rotation number p/q where p < q and p and q are relatively prime correspond to periodic solutions of equation (4.2.7) with period $2\pi q$, i.e., whirling subharmonics of order q, and that invariant circles correspond to two dimensional invariant tori, i.e., quasi-periodic motions (modulated whirling responses). The stability types also correspond.

The Nonresonant Case $\Omega_0 \notin (p/q)$

In this, the most common case, no resonance occurs and the perturbed dynamics are straightforward. Figures 22 and 23 show the bifurcation diagrams and the associated phase portraits of equation (4.2.10) in the three parameter space. Equation (4.2.10) has a single fixed point which undergoes a Hopf bifurcation at the Hopf bifurcation surface resulting in the disappearance (Figure 22) or birth (Figure 23) of an invariant circle as μ is increased across the surface, as might be generally expected. In terms of the dynamics of equation (4.2.7), the zero solution (i.e., the static equilibrium position (x_0, y_0)) is perturbed by the unbalance into a periodic response with period equal to that of the forcing, 2π, for $\mu < \mu_{cr}$. As the speed is increased across the Hopf bifurcation surface $\mu = \mu_{cr}$, this periodic motion becomes unstable and an invariant two dimensional torus (i.e., a quasi-periodic

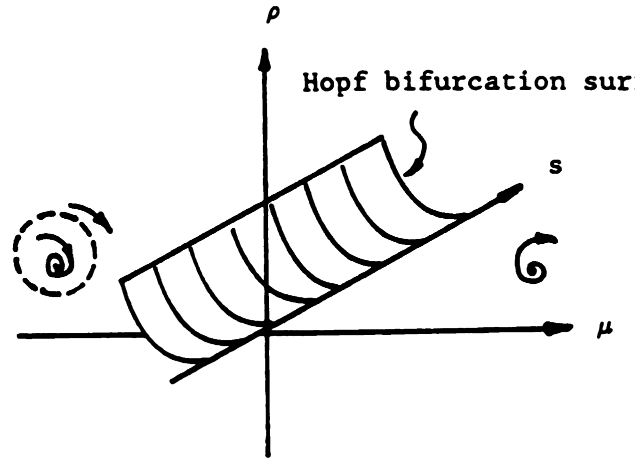

Figure 22. Phase portraits in parameter space - regions I and III of Figure 21.

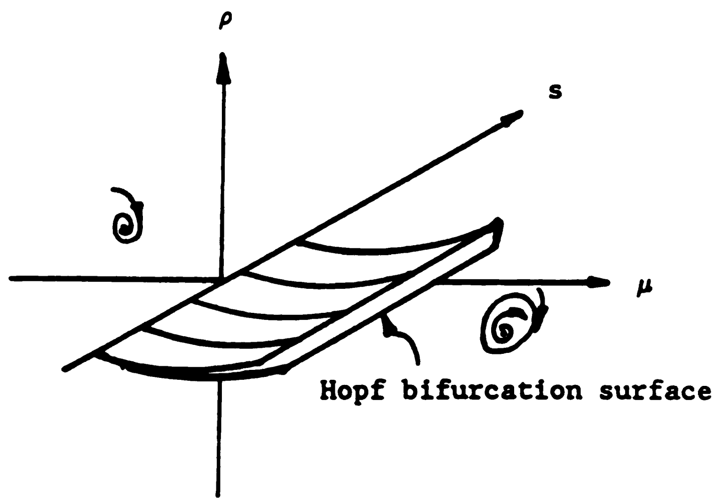

Figure 23. Phase portraits in parameter space - region II of Figure 21.

response) is born whose stability and existence is determined by the type of the corresponding unperturbed ($\rho = 0$) Hopf bifurcation, that is, an unstable (a stable, resp.) quasi-periodic response exists for parameters in region I and III (region II, resp.) of Figure 21.

It should be noted that the Hopf bifurcation surface in Figures 22 and 23 are obtained not by actual numerical computations of equation (4.2.10), but by observations from the results for the 1/1 (Figures 25 and 26) and 1/2 (Figure 29) resonant cases (studied below). Figure 22 is for the non-resonant case with parameters in regions I and III of Figure 21 in which subcritical Hopf bifurcation occurs. The response in Figure 29 with s away from 0 (i.e., away from the resonant case of 1/2) resembles that in Figure 22. Similar observations can also be found between Figures 25, 26 and Figure 23.

4.3 Dynamics of the Poincare Map in the 1/1 Resonant Case

For the perfectly balanced rotor system with S near $S_0 = 0.199875$ and $\bar{\omega}$ near $\bar{\omega}_0 = 1.138166$, which is in the region II of Figure 21, the bifurcating stable limit cycle arising at the stability boundary has a frequency near 1.0, in which case primary resonance is expected to occur when the periodic excitation due to unbalance is included. Letting $\Omega_0 = 1.0$ and $\bar{\Omega} = \Omega_0 + s$, the various responses of equation (4.2.10) will be determined for small values of the parameters (ρ, μ, s). The resulting bifurcation diagram is obtained by first specifying an s value (consequently, specifying the constants of equation (4.2.10)), then investigating the dynamics as parameters ρ and μ vary. This procedure is repeated for each different s value, hence the bifurcation diagram is completed in the (ρ, μ, s) space. Our treatment follows the ideas of Gambaudo (1985).

Substituting $\bar{\Omega} = \Omega_0 + s$ and using the fact that μ and s are small parameters, equation (4.2.10) can be reduced to :

$$P = (1 + c_1)z + c_2 b|z|^2 z + \rho^2 c_3 \tag{4.3.1}$$

where

$$c_1 = 2\pi\sigma\mu + 2\pi i(\Omega\mu + s), \quad c_2 = 2\pi(1 + 2\pi\sigma\mu), \text{ and}$$

$$c_3 = -2\pi[- c - d(\sigma\mu + i(1 + s + \Omega\mu))]/[2i + \sigma\mu + i(\Omega\mu + s)] \quad .$$

Let z_0 be a fixed point of the above equation. Substituting z_0 in equation (4.3.1) yields

$$c_4 z_0 + |z_0|^2 z_0 + \rho^2 c_5 = 0 \tag{4.3.2}$$

where $c_4 = c_1/c_2 b$ and $c_5 = c_3/c_2 b$. Let $\xi = |z_0|^2 > 0$, then ξ satisfies the following equation (from equation (4.3.2)):

$$\xi^3 + 2\mathrm{Re}(c_4)\xi^2 + |c_4|^2\xi - \rho^4|c_5|^2 = 0 \tag{4.3.3}$$

Equation (4.3.3) may have one, two, or three real solutions for ξ for each triad (ρ, μ, s), and the fixed point is given by

$$z_0 = -\rho^2 c_3 \,/\, (c_1 + c_2 b\xi) \quad . \tag{4.3.4}$$

The stability of the fixed point z_0 can be determined by the eigenvalues of $DP(z_0)$ (the Jacobian matrix of equation (4.3.1) evaluated at z_0). A saddle-node bifurcation of z_0 occurs when 1 is an eigenvalue of $DP(z_0)$, which occurs iff

$$3\xi^2 + 4\mathrm{Re}(c_4)\xi + |c_4|^2 = 0 \qquad . \tag{4.3.5}$$

The requirement of ξ to be real and positive and the compatibility of equation (4.3.3) and (4.3.5) give the saddle-node bifurcation curve SN in parameter space as shown in Figure 24. Note that for $s \leq 0$, there is only one fixed point, hence no such saddle-node curve exists. Similar conditions for the existence of a Hopf bifurcation of z_0 can also be written down (i.e., conditions at which $DP(z_0)$ has complex conjugate eigenvalues with modulus 1):

$$3\xi^2 + 4\mathrm{Re}(c_4)(1 + \frac{1}{c_1 \cdot b})\xi + |c_4|^2(1 + \frac{2\mathrm{Re}(c_1)}{|c_1|^2}) = 0 \tag{4.3.6}$$

$$(1 + c_4 + 2c_1c_3\xi)^2 \leq 1 \tag{4.3.7}$$

These equations are satisfied by z_0 and are associated with equation (4.3.3) to give the Hopf bifurcation curve HF. A complete examination of the fixed points in parameter space, their stabilities and possible local and global bifurcations of equation (4.3.1) leads to the bifurcation diagrams of Figures 25 and 26 and the associated following conclusions :

(1). For $s \leq 0$ (i.e., $\bar{\Omega} \leq 1.0$), there is only one fixed point which is initially stable and undergoes a Hopf bifurcation as μ crosses the HF line. A stable invariant circle is born thereafter as shown in

Figure 25. The rotation number (see Guckenheimer and Holmes, 1983) for this torus in terms of the dynamics of equation (4.2.7), which is essentially a measure of the ratio of the two frequencies contained in the response, is approximately 1.0 indicating that the response is a beating type motion (that is, amplitude modulated motion) with a long period envelope.

(2). For $s > 0$ (see Figure 26), P has only one fixed point outside SN; inside SN, P has three fixed points, one of which is a saddle.

(3). The Hopf bifurcation curve HF exists both outside and inside of SN.

(4). The points b_1 and b_2 correspond to the fixed points of P with 1 as a double eigenvalue of $DP(z_0)$. Hence, codimension two bifurcations occur at b_1 and b_2.

(5). Near points b_1 and b_2, P has homoclinic bifurcation curves emanating from b_1 and b_2 in the (ρ, μ) space - a saddle connection bifurcation which implies, by the Smale homoclinic theorem (1965) (see also Gambaudo, 1985, for the proof of existence of such homoclinic points), that equation (4.2.7) generically has infinitely many periodic and homoclinic orbits near the saddle connection curves (curves bordering regions 4-5 and 5-6). This implies that chaotic response may be observable near such parameter conditions.

(6). In region 1 there exists only one stable fixed point; in region 2 and 7 there exist only one unstable fixed point; in regions 3 and 8 there exist one saddle and two sinks, while regions 4, 5 and 6 have one saddle, one source and one sink. Stable limit cycles exist in regions 2, 4, 6, and 7.

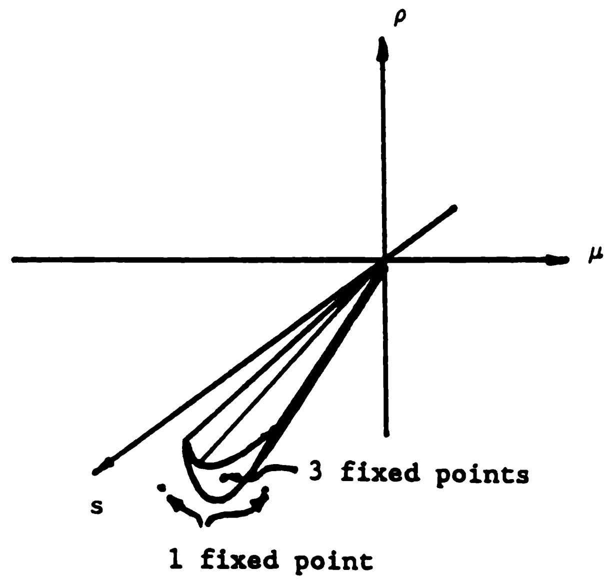

Figure 24. SN curves of equation (4.3.1) in parameter space.

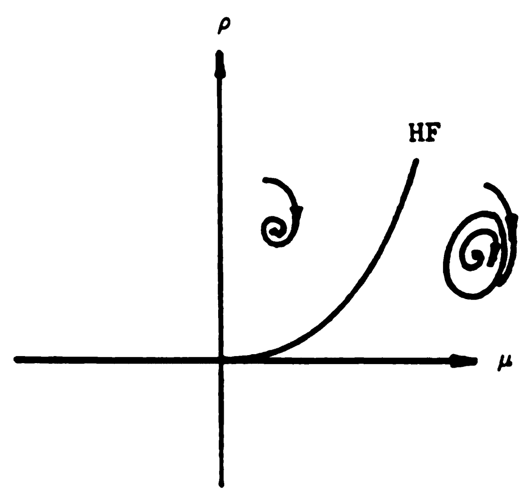

Figure 25. Bifurcation diagrams for $s \leq 0$.

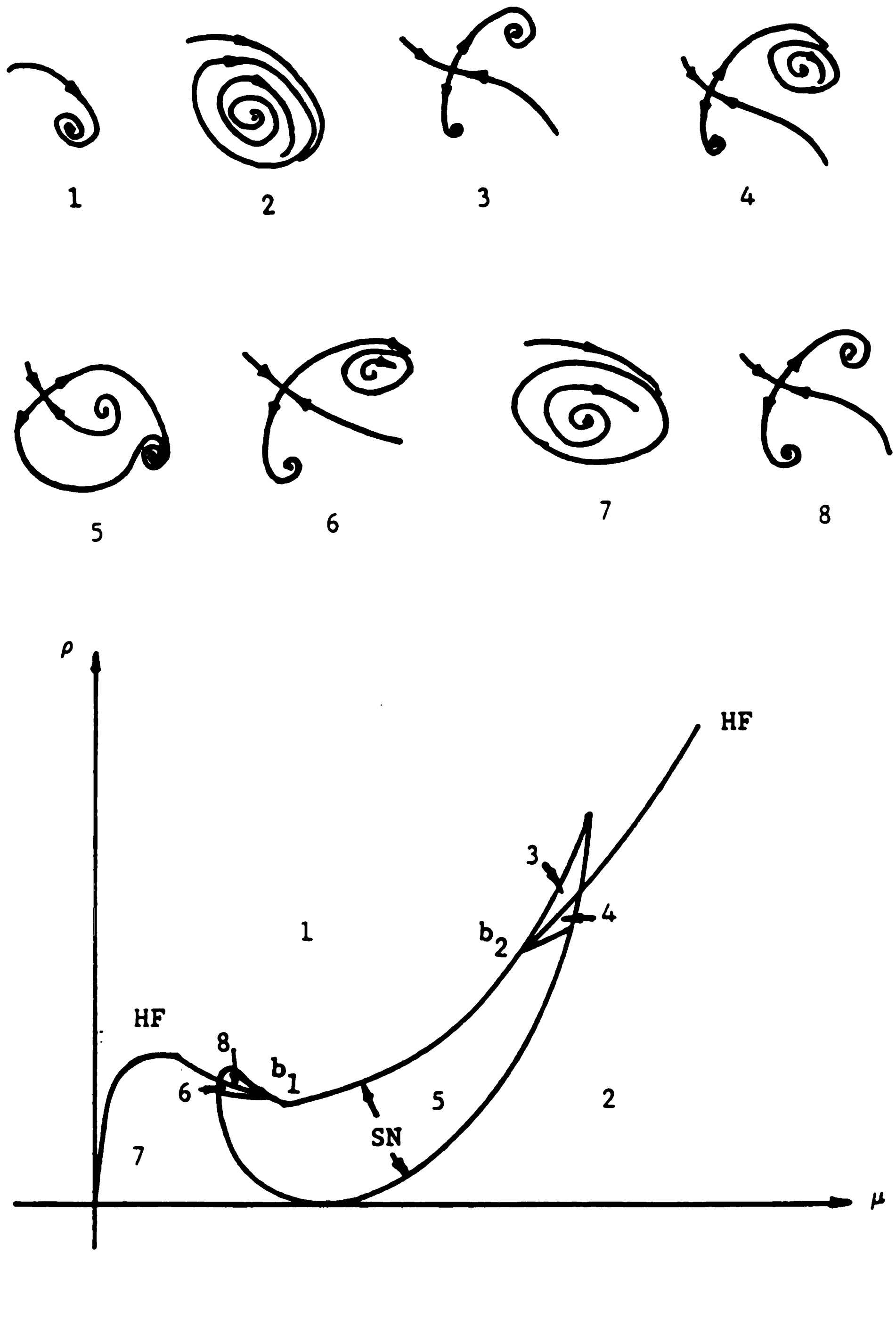

Figure 26. Bifurcation diagram for s > 0.

The corresponding dynamics of equation (4.2.7) in the neighborhood of S_0 and $\bar{\omega}_0$ can be readily realized from Figure 25 and 26 by recalling the fact that equation (4.3.1) is an approximation of the "time 2π map" of equation (4.2.7). For a rotor system with $S \le S_0$ and $S_0 - S << 1$ (figure 25), the response from equation (4.2.7) is similar to the nonresonant case of Figure 23. As $\bar{\omega}$ is increased from below $\bar{\omega}_0$, the system response is initially periodic with period 2π, then undergoes a Hopf bifurcation and becomes unstable as μ crosses the HF curve. A stable quasi-periodic motion occurs thereafter. For a rotor system with $S > S_0$ and $S - S_0 << 1$ (Figure 26), the system response is more complicated and phenomena typical of non-linear primary resonance are observed (Nayfeh and Mook, 1979). Depending on the levels of unbalance, different amplitude-frequency response curves can be obtained, much like those of Chapter III. Stable and unstable (source and/or saddle) periodic responses with period 2π and stable quasi-periodic motions are found to coexist and interact much the same way as in Chapter III. Saddle connections also occur between regions 4-5 and 5-6, suggesting the existence of irregular motions nearby.

It is of interest to look at the stable orbits in Figure 26 and to interpret the attendant rotor dynamics in terms of equation (4.2.7). Stable fixed points (which occur in regions 1, 3, 4, 5, 6, and 8) represent periodic responses with period 2π; stable invariant circles (which exist in regions 2, 4, 6 and 7) correspond to quasi-periodic motions which contain two frequencies: one is the forcing frequency, the other one is close to the frequency of the bifurcating cycle for the unforced problem which is approximately equal to 1.0; hence these quasi-periodic motions are beating type motions with long period envelopes. Multiple stable orbits coexist in regions 3, 4, 6, and 8 in which case initial conditions play a critical role in the observed response of the system.

4.4 Dynamics of the Poincare Map in the 1/2 Resonant Case

For the perfectly balanced rotor system with S near $S_0 = 0.0364$ and ω near $\bar{\omega}_0 = 2.57553$ (which is in region III of Figure 21), the bifurcating unstable limit cycle arising at the stability boundary has a frequency approximately equal to 1/2. In this case a subharmonic resonance is expected to occur when periodic excitation is applied. Substituting $\bar{\Omega} = 1/2 + s$ in equation (4.2.10) and using the assumption that $|\mu|$, $|s| << 1$ yields

$$P = -(1 + d_1)z - d_2 b|z|^2 z - \rho^2 d_3 \tag{4.4.1}$$

where $d_1 = c_1$, $d_2 = c_2$, and $d_3 = (-2 + c_1)[-c - d(\sigma\mu + i(\frac{1}{2} + s + \Omega\mu))]$. As in the previous section, the fixed points and their stabilities of equation (4.4.1) will be determined. Let $\xi_0 = |z_0|^2$ where z_0 is a fixed point, then the following equation is satisfied by ξ_0

$$\xi_0^3 + 2\mathrm{Re}(d_4)\xi_0^2 + |d_4|^2\xi_0 - \rho^4|d_5|^2 = 0 \tag{4.4.2}$$

where $d_4 = (2 + d_1) / d_2 b$ and $d_5 = d_3 / d_2 b$. A numerical study of equation (4.4.2) shows that there is only one real and positive solution for ξ_0 and the fixed point z_0 is given by

$$z_0 = -\rho^2 d_5 / (d_4 + \xi_0) \tag{4.4.3}$$

The stability of z_0 can be determined by the eigenvalues of the Jacobian matrix $DP(z_0)$ of equation (4.4.1). It is found that z_0 may change stability from stable to unstable either by a period doubling (flip) or a Hopf bifurcation. The period doubling bifurcation (with -1 as an eigenvalue of $DP(z_0)$) of z_0 is anticipated since the frequency of the bifurcating limit cycle for the balanced system is nearly one half of the forcing frequency. It is, therefore, convenient to consider the dynamics for this problem by using the second iterate of the Poincare map: $P^2 = P \cdot P$. Note that a flip bifurcation of z_0 for P corresponds to a pitchfork bifurcation of z_0 for P^2 in which two fixed points bifurcate from z_0; this is described in more detail below.

Letting $z = z_0 + z'$, which moves the origin of z' to z_0, equation (4.4.1) becomes

$$P' = -(1 + d_1 + 2\xi_0 d_2 b)z' - z_0^2 d_2 b\bar{z}' - d_2 b|z'|^2 z' - d_2 b(\bar{z}_0 z'^2 + 2z_0 z'\bar{z}') \tag{4.4.4}$$

Iterating P′ once and dropping the prime yields

$$P^2 = z + 2(d_1 + 2\xi_0 d_2 b)z + 2z_0^2 d_2 b\bar{z} + 2d_2 b|z|^2 z + O(\xi_0|z|^2) \tag{4.4.5}$$

where $O(\xi_0|z|^2)$ represents higher order terms which will be neglected. It is obvious that $z = 0$ is always a fixed point of equation (4.4.5); it represents the only non-zero solution of equation (4.4.1) and corresponds to a periodic response with period 2π for equation (4.2.7). The non-zero fixed points of P^2 correspond to periodic points with period two of the Poincare map P, which in turn represent periodic orbits with period 4π of equation (4.2.7). These consist mainly of two components (recall $z = z_0 + z'$): one from the forcing with period 2π, the other from the free response with period 4π.

Let $\xi_1 = z_1$, where z_1 is a fixed point of equation (4.4.5), then ξ_1 satisfies

$$\xi_1^2 + 2\mathrm{Re}(e_1)\xi_1 + |e_1|^2 - |e_2|^2 = 0 \tag{4.4.6}$$

where $e_1 = (d_1 + 2\xi_0 d_2 b) / d_2 b$ and $e_2 = z_0^2$. Equation (4.4.6) is quadratic in ξ_1, implying that there may be none, one, or two real and positive solutions for ξ_1. The fixed point z_1 is then given by

$$z_1 = - e_2\bar{z}_1 / (e_1 + \xi_1) \quad . \tag{4.4.7}$$

Since equation (4.4.7) possesses the symmetry of rotation by π, $z_{11} = v_1 + j\ v_2$ and $z_{12} = - v_1 - j\ v_2$ (rotation of z_{11} by π) are both fixed points for a given ξ_1 (Note that a non-zero fixed point z_{11} of P^2 is mapped on another fixed point z_{12} by P, and vice versa). Hence z_{11} and z_{12} on P^2 correspond to the periodic points with period two on P, which in turn represent periodic orbits with period 4π of equation (4.2.7).

According to equation (4.4.6) the number of fixed points of P^2 is determined to be as follows (see Figure 27):

(1). P^2 has only one fixed point, $z_1=0$: if $\mathrm{Re}(e_1)^2 - (|e_1|^2 - |e_2|^2) > 0$, $|e_1|^2 - |e_2|^2 > 0$ and $\mathrm{Re}(e_1) > 0$, or $\mathrm{Re}(e_1)^2 - (|e_1|^2 - |e_2|^2) < 0$.

(2). P^2 has three fixed points: if $\mathrm{Re}(e_1)^2 - (|e_1|^2 - |e_2|^2) > 0$ and $|e_1|^2 - |e_2|^2 < 0$.

(3). P^2 has five fixed points: if $\mathrm{Re}(e_1)^2 - (|e_1|^2 - |e_2|^2) > 0$,

$|e_1|^2 - |e_2|^2 > 0$ and $\mathrm{Re}(e_1) < 0$.

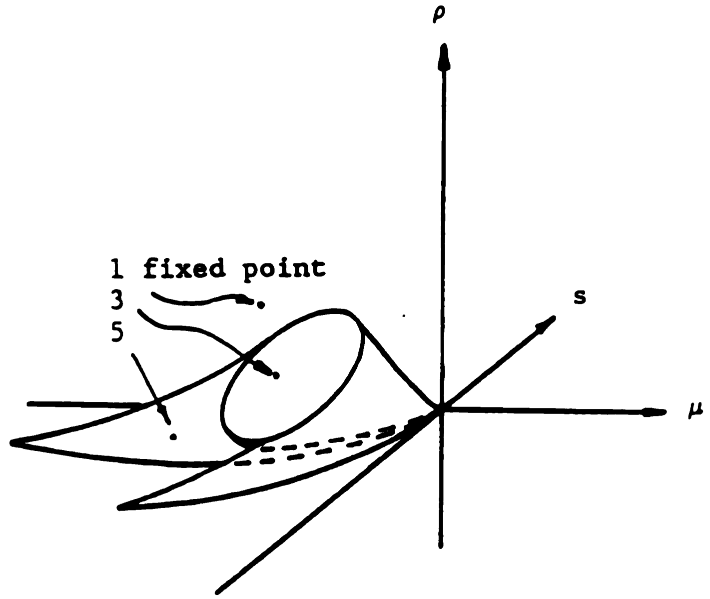

Figure 27. Bifurcation diagram of equation (4.4.5) in parameter space.

The stability types of the fixed points are determined by the eigenvalues of $DP^2(z_1)$. A study of these eigenvalues for a certain ρ value has been carried out and the results are shown in Figure 28. On curve PF the fixed point $z_1 = 0$ undergoes a pitchfork bifurcation while on the two curves marked SN the non-zero fixed points appear (or disappear) in saddle-node bifurcations. Line HF1 represents the Hopf bifurcation of $z_1 = 0$ while curve HF2 corresponds to the simultaneous Hopf bifurcations of two non-zero fixed points (two fixed points that are symmetric by a rotation of π). At points b_1, b_2 and b_3, 1 is a double eigenvalue of $DP^2(z_1)$, suggesting the existence of saddle connection bifurcations nearby.

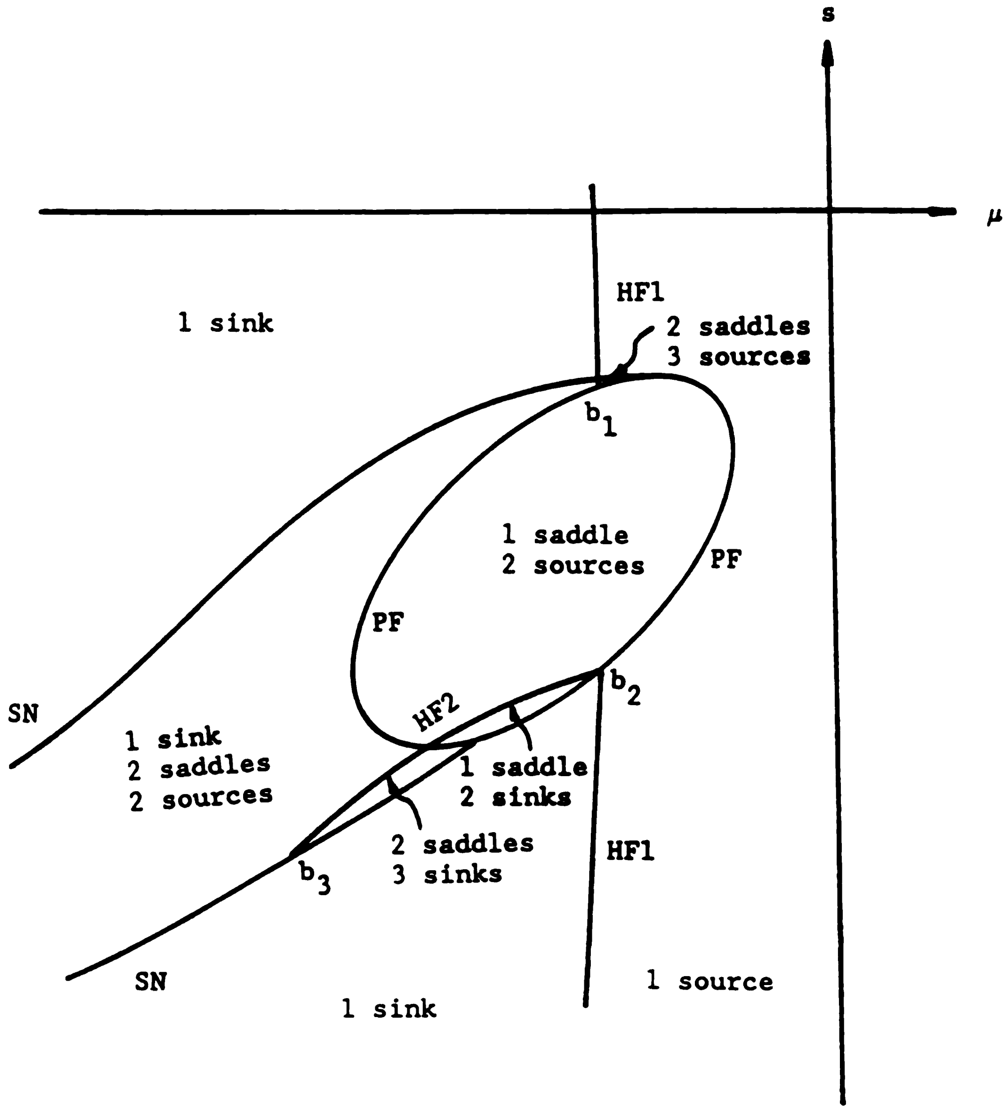

Figure 28. Stabilities of the fixed points of equation (4.4.5).

In fact, this case is much more complicated than the previous one. In addition to the local bifurcations just mentioned (pitchfork, saddle-node and Hopf bifurcations), a saddle-node bifurcation of invariant circles is also found to occur. The global bifurcations found are saddle connections of homoclinic as well as heteroclinic types. Based on the knowledge of these local and global bifurcations, as well as the type of stability of each fixed point, the phase portraits in parameter space (μ, s) may be determined; these are presented in Figure 29.

Other local bifurcations occur on the curves between regions 5-8 and 6-7 in Figure 29, these are saddle-node bifurcations of invariant circles. Global bifurcations occur between regions 8-9 and 10-11, saddle connections of homoclinic type; and between regions 6-11, 7-11 and 3-6, saddle connections of heteroclinic type. As in the previous section, equation (4.2.7) generically possesses infinitely many periodic and homoclinic (and/or heteroclinic) orbits near the saddle connection bifurcation curves.

It is again of interest to look at the stable orbits in Figure 29 and to interpret the attendant rotor dynamics in terms of equation (4.2.7). Stable zero solutions (which occur in regions 2, 3, 6, 7, 10, 11, 12 and 14) represent periodic response at the forcing period, 2π; stable nonzero fixed points (regions 12 and 13) indicate a periodic response with period 4π; stable invariant circles (regions 7, 8, 9 and 10) correspond to quasi-periodic motions, in which one of the frequencies is the forcing frequency and the other is approximately (not exactly) equal to 1/2, leading to amplitude modulated motions. Note that this amplitude modulated motion will not have as long a period envelope as that for the 1/1 resonant case. Figure 29 also clearly shows how the dynamics of equation (4.2.7) change as parameters (ρ, μ, s) vary.

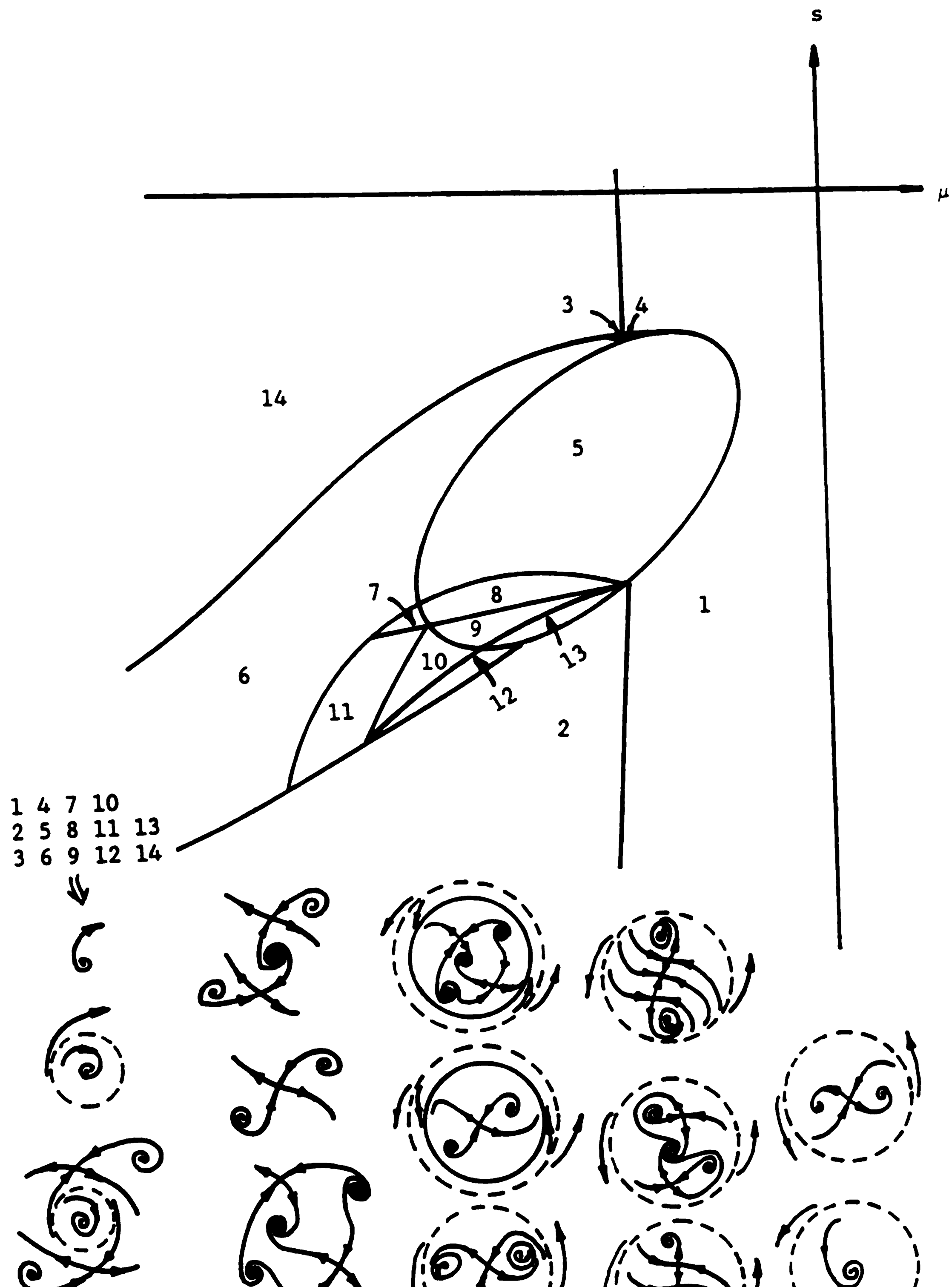

Figure 29. Phase portraits of equation (4.4.5).

4.5 Conclusions

An analytical approach has been presented which determines the effects of unbalance on oil whirl for a model rotor system supported in fluid film journal bearings. The main results, depicted in the bifurcation diagrams and the portraits of the associated Poincare maps, are presented in Figures 22, 23, 25, 26, 27 and 29. In order to interpret the shaft motions from these figures, the facts and correspondences given below should be kept in mind. Figures 22, 23, 25 and 26 are obtained from "time 2π" maps of equation (4.2.7) while Figures 27 and 29 are obtained from "time 4π" maps. The center manifold theorem assures that the shaft motions governed by equation (4.2.1) in the neighborhood of the threshold speed are topologically equivalent to those on the two dimensional center manifold governed by equation (4.2.7). The stability types of steady state solutions between the Poincare maps and equation (4.2.7) and between equation (4.2.7) and equation (4.2.1) also correspond. Hence the shaft motions governed by equation (4.2.1) whose origin is at (x_0, y_0) can be readily deduced by knowing these relations between equations (4.2.1), (4.2.7) and the Poincare maps.

It is noted that the results presented are valid only for small amount of unbalance and in the neighborhood of the threshold speed $\bar{\omega}_0$. For a relatively large amount of unbalance and/or speed well above or below the threshold speed the results may not be valid, and other methods of analysis are thus required to predict the response in this case. In fact, the works by Barrett, Akers and Gunter (1976), Gunter, Humphris and Springer (1983) and Hollis and Taylor (1987) were carried out for relatively large unbalances and/or for speeds well above or below the threshold speeds. Numerical integrations were employed in their works to investigate the responses and synchronous motions with period 2π, periodic orbits with period 4π and quasi-periodic motions have been found. Periodic orbits with period 4π arise due to the fact that the whirl frequency for the balanced shaft is approximately equal to one half of the rotational speed. Systematic parameter studies in the neighborhood of the threshold speed were not included in their investigations.

Preliminary computer simulations of equation (4.2.1) confirm the existence of the synchronous motions with period 2π and quasi-periodic responses in their corresponding parameter regions predicted in Figures 25 and 26 for the 1/1 resonant cases, but multiple stable solutions existing in regions 3, 4, 6 and 8 have not been found to coexist. For the 1/2 resonant case, only the stable synchronous responses and large amplitude quasi-periodic motions are obtained from the simulations. These large amplitude quasi-periodic motions are predictable from the unforced problem, in which case Myers (1984) has shown existence of a large stable limit cycle enclosing the bifurcating unstable limit cycle. These phenomenon are expected, since the directions of the outer portions of the local phase flow in each region of Figure 29 are directed outward and are rotational. These large amplitude quasi-periodic motions are undesirable in view of system performance and hence should be avoided. More simulations are currently being conducted in order to obtain and verify the results predicted for the 1/1 and 1/2 resonant cases.

The dynamics of the rotor predicted in Figure 26 and 29 are valid in a relatively small parameter space, hence it would be extremely difficult to observe many of these responses in practice. It is, however, important to recognize their existence and their possible effects on the dynamics of the system. Harmonic, subharmonic and quasi-periodic motions are possible motions for this system under various parameter conditions.

In both models described in chapters III and IV, mass unbalance introduces a periodic forcing term which allows the response of the system to be studied in the context of a perturbed Hopf bifurcation. Mathematical work on this subject can be found in the papers by Kath (1981), Rosenblat and Cohen (1981) and Bajaj (1986). More recently, Sri Namachchivaya and Ariaratnam (1987) have analyzed secondary bifurcations for these resonances. Gambaudo (1985) presents the most detailed and complete study of this periodically perturbed Hopf bifurcations. In fact, the latter part of this chapter (from equation (4.2.7)) follows closely his work, especially for 1/1 and 1/2 resonant cases. For the 1/1 resonant case, Figures 24 and 26 are similar to (actually,twisted images of) Figures 4 and 16 in his work. Figure 29 is similar to Figure 25 in his work, for the 1/2 resonant case, except that his case is for the perturbation of a supercritical Hopf bifurcation while Figure 29 is for a subcritical Hopf bifurcation. In each of the corresponding regions between Figure 29 and his Figure 25, the stability type is opposite and phase flow is reversed.

CHAPTER V

DISCUSSION AND CONCLUSIONS

In this dissertation methods of dynamical systems and bifurcation theories have been used to investigate the non-linear behavior of symmetric rotor models. These approaches are analytic in nature, and are supported by computer simulations. The results are presented in terms of bifurcation diagrams and associated phase portraits in parameter space and clearly illustrate how the dynamics of the rotor change as system parameters are varied. Though these methods are employed locally in the neighborhood of bifurcation points, the system's global behaviors can often be realized by knowing these local dynamics together with some knowledge about global behavior, obtained either from applying other methods (e.g. Lyapunov methods) or from computer simulations. In any case, most of the complicated and interesting dynamics of these systems occur near the bifurcation points.

Though rotordynamic instabilities caused by internal damping and fluid film journal bearing forces have been the subjects of many investigations, few rigorous and complete studies have been carried out; the exceptions include the works by Myers (1984), Gardner et al. (1985) and Hollis and Taylor (1986). In this dissertation, these instabilities and the attendant post-critical behavior are thoroughly examined as a function of system parameters. We then go on to investigate the dynamics of the rotor system with the existence of mass unbalance. This periodically perturbed problem has received little attention, not because it is unimportant, but mainly due to the lack of suitable methods. An analytical approach has been applied to derive the response for these systems. The results presented in terms of bifurcation diagrams and phase portraits have proven the utility of the method and enable one to clearly visualize the rotor dynamics as system parameters are varied. Although the results are not complete, they are new.

In Chapters II and III the model used to investigate the effects of internal damping and mass unbalance on the rotordynamic instability and resonance is a relatively simple one (a flexible continuous rotating shaft); the type of damping and structural non-linearities used were chosen to illustrate a procedure by which the response may be computed, and to provide what are hoped to be qualitatively typical results. More complicated models which incorporate the effects of asymmetric stiffness, gyroscopic forces, applied axial loads and torques and even non-linear rheological models of the shaft material may be adopted in which case more exotic dynamics of the system will be expected; these are left for future work. It should be noted that if the non-linearities are of the softening type ($\alpha < 0$) the response will be quite different. Our main conclusion for the analysis of this model is as follows: in order to fully understand the effects of structural non-linearities on the resonant behavior of a rotating shaft, one must include the effects of structural damping. The results obtained by neglecting internal dissipation are very different from those obtained for non-zero internal damping.

In the context of the study of the effects of mass unbalance on instability, only the 1/1 resonant case has been studied in Chapter III (because the whirl frequency, Ω_1, of the bifurcating cycle which is born at $\Omega = \Omega_1^*$ is close to the rotational frequency Ω). However, as was pointed out in the discussion section of Chapter III, if the ratio $\mu_e/\mu_i\Omega_1$ is not small, other types of resonance may occur. In fact, subharmonic resonant cases of p/q for $q \leq 5$ are possible for this single mode model. It would be quite interesting to carry out studies of all these resonant cases, especially for the strongly resonant cases $q \leq 3$, and to compare with those of bearing problems in Chapter IV and/or Gambaudo's work (1985). This is also left for future work.

The model used in Chapter IV to study the rotordynamic instability due to fluid film journal bearings was originally proposed by Myers (1984). It is a simple model (a long bearing operating with a half film) and was chosen because it provides simple analytic expressions for the hydrodynamic forces (equation (4.1.2)). The use of a more accurate model would significantly complicate the determination of the coefficients of equation (4.2.1), but is not expected to alter the *qualitative* character of the bifurcations of the problem. It would merely alter the values of the threshold speed, the whirl frequency, and/or the type of Hopf bifurcation for a particular system.

As mentioned in Chapter IV, preliminary computer simulations confirm the results presented in Chapter IV, but difficulties have been encountered in showing the coexistence of multiple stable solutions predicted in the analysis; this is not surprising since some regions of the bifurcation diagram are extremely small in the parameter space and a careful choice of parameters and initial conditions is crucial to obtain the desired stable motions. The details of the bifurcation diagrams are important in the understanding of the rotor dynamics in a more complete sense, but may not all be easily observed in practice. This is due to the narrow parameter ranges over which certain motions will occur, and to the fact that they also have small initial condition sets which result in that particular motion. Engineers working in rotordynamic systems should be aware of all the possible responses that a rotor system might have, however, and be prepared to handle the situations should a problem occur. In fact, the existence of these "possible but unlikely" motions can cause difficulties in experimental and/or simulation studies, and can lead to results which are difficult to reproduce. More simulations are currently being conducted; laboratory experiments are left for future work.

In both models considered, it may well occur that irregular amplitude modulations of the motion are observed in simulation or experimental studies, these are most likely to occur near the saddle connection bifurcations. Such chaotic behavior has been found by Hollis and Taylor (1986) for the journal bearing system for certain sets of parameter values, but more work needs to be done in order to provide predictive criteria for the chaotic motions found in rotor systems.

Other sources of rotordynamic instabilities are not covered in this thesis, but are as important in applications; these include aerodynamic forces, gyroscopic forces, magnetic and electrodynamic forces, dry friction, and labyrinth seals. It is expected that the interaction between unbalance and instability will be qualitatively similar in those situations.

LIST OF REFERENCES

LIST OF REFERENCES

Arnold, V. I., 1987, Geometric Methods in the Theory of Ordinary Differential Equations, Springer-Verlag, New York.

Ariaratnam, S. T., Sri Namachchivaya, N. 1986, "Periodically Perturbed Nonlinear Gyroscopic Systems," Journal of Structural Mechanics, Vol. 14, pp. 153-175.

Badgley, R. H., Booker, J. F., 1969, "Turborotor Instability: Effect of Initial Transients on Plane Motion," Journal of Lubrication Technology, October, pp. 625-633.

Baja, A. K., 1986, "Resonant Parametric Perturbations of the Hopf Bifurcation," Journal of Mathematical Analysis and Applications, Vol. 115, pp. 214-224.

Barrett, L. E., Akers, A., Gunter, E. J., 1976, "Effect of Unbalance on a Journal Bearing Undergoing Oil Whirl," Proc. Instn. Mech. Engrs., Vol 190, pp. 535-544.

Barrett, L. E., Allaire, P. E., Gunter, E. J., 1980, "A Finite Length Bearing Correction Factor for Short Bearing Theory," Journal of Lubrication Technology, Vol. 102, pp. 283-290.

Bellman, R. E., 1970, Introduction to Matrix Analysis, McGraw-Hill, New York.

Bolotin, V. V., 1963, Nonconservative Problems of the Theory of Elastic Stability, Pergamon Press, Inc., New York.

Brindley, J., Elliott, L., McKay, J. T., 1983, "The Role of Cavitation in Whirl Instability in a Rotor Bearing - 1 The Π-Film Model," Journal of Applied Mechanics, Vol. 50, December, pp.877-885.

Bucciarell, L. L., 1982, "On the Instability of Rotating Shafts Due to Internal Damping," Journal of Applied Mechanics, Vol. 49, pp. 425-428.

Carr, J., 1981, Applications of Center Manifold Theory, Springer-Verlag, Inc.

Childs, D., Moes, H., van Leeuwan, H., 1977, "Journal Bearing Impedance Descriptions for Rotordynamic Applications," Journal of Lubrication Technology, April, pp. 198-214.

Crandall, S. H., 1980, "Physical Explanations of the Destabilizing Effcts of Damping in Rotating Parts," in Rotordynamic Instability Problems in High Performance Turbo Machinery, NASA CP 2133, pp. 369-382.

Dimentberg, F. M., 1951, "Transverse Vibrations of a Rotating Shaft with Disks Attached, in the Presence of Frictional Resistance," Sb. "Poperechnye Kolebani'a I Kriticheskie Skorosti," Izd-vo. Akad. Nauk. USSR, No. 1.

Ehrich, F. F., 1964, "Shaft Whirl Induced by Rotor Internal Damping," Journal of Applied Mechanics, Vol. 31, pp. 279-282.

Gambaudo, J. M., 1985, "Perturbation of a Hopf Bifurcation by an External Time-Periodic Forcing," Journal of Differential Equations, Vol. 57, pp. 172-199.

Gardner, M., Myers, C., Savage, M., 1985, "Analysis of Limit-Cycle Response in Fluid-Film Journal Bearings Using the Method of Multiple Scales," Q. J. Mech. Appl. Math., Vol. 38, pp. 27-45.

Genin, J., Maybee, J. S., 1970, "Whirling Motion of a Viscoelastic Continuous Shaft," International Journal of Engineering Science, Vol. 8, pp. 457-464.

Golubitsky, M., Schaeffer, D., 1978, "Bifurcation Analysis Near a Double Eigenvalue of a Model Chemical Reaction," MRC Rep. 1859, University of Wisconsin.

Golubitsky, M., Schaeffer, D., 1979, "A Theory for Imperfect Bifurcation via Singularity Theory," Communications on the Pure and Applied Mathematics. Vol. 32, pp. 21-98.

Guckenheimer, J., Homles, P., 1983, Nonlinear Oscillations, Dynamical Systems and Bifurcations of Vector Fields, Springer-Verlag, Inc.

Gunter, E. J., and Trumpler, P. R., 1969, "The Influence of Internal Friction on the Stability of High Speed Rotors with Anisotropic Support," Journal of Engineering for Industry, November, pp. 1105-1113.

Gunter, E. J., Humphris, R. R., Springer, H., 1983, "Influence of Unbalance on the Nonlinear Dynamical Response and Stability of Flexible Rotor-Bearing Systems," Rotor Dynamical Instability, The Applied Mechanics, Bioengineering, and Fluid Engineering Conference, Houston, Texas.

Hagg, A. C., 1946, "The Influence of Oil-film Journal Bearings on the Stability of Rotating Machines," Journal of Applied Mechanics, Vol. 13, No. 3, pp. 211-220

Hendricks, S. L., 1986, "The Effect of Viscoelasticity on the Vibration of a Rotor," Journal of Applied Mechanics, Vol. 53, pp. 412-416.

Henry, D., 1981, Geometric Theory of Semi-linear Parabolic Equations. New York: Springer-Verlag, Inc.

Ho, C. H., Scott, R. A., Eisley, J. G., 1975, "Non-planar, Non-linear oscillations of a beam - I. Forced Motions," International Journal of Non-linear Mechanics. Vol. 10, pp. 113-127.

Hollis, P., Taylor, D. L., 1986, "Hopf Bifurcation to Limit Cycles in Fluid Film Bearings," Journal of Tribology, Vol. 108, pp. 184-189.

Hollis, P., Taylor, D. L., 1987, "Poincare' Maps of a Journal Bearing," preprint.

Holmes, P. J., Marsden, J., 1978, "Bifurcations to divergence and Flutter in Flow-Induced Oscillations: an Infinite-Dimensional Analysis," Automatica. Vol. 14, pp. 367-384.

Holmes, P. J. and Rand, D. A., "Bifurcations of the Forced van der Pol Oscillator," Quarterly of Applied Mathematics, Vol. 35, pp. 495-509.

Iooss, G., 1979, Bifurcation of Maps and Applications, North-Holland.

Ishida, Y., Ikeda, T., Yamamoto, T., 1987, "Transient Vibration of a Rotating Shaft with Nonlinear Spring Characteristics during Acceleration through a Major Critical Speed," JSME International Journal, Vol. 30, No. 261, pp. 458-466.

Jeffcott, H. H., 1919, "The Lateral Vibration of Loaded Shafts in the Neighborhood of a Whirl Speed: The Effect of Want of Balance," Philosphical Magazine, Ser. 6, 37, 304.

Johnson, J. M. and Bajaj, A. K., 1986, "Amplitude Modulated and Chaotic Dynamics in Resonant Motions of Strings," Journal of Sound and Vibration, Vol. 128, pp. 87-107.

Kath, W. L., 1981, "Resonance in Periodically Perturbed Hopf Bifurcation," Studies in Applied Mathematics, Vol. 65, pp. 95-112.

Kelley, A., 1967, "The Stable, Center-Stable, Center, Center-Unstable, Unstable Manifolds," Journal of Differential Equations, Vol. 3, pp. 546-570.

Kimball, A. L., 1924, "Internal Friction Theory of Shaft Whirling," General Electric Review, Vol. 27, No. 4, pp. 244-251.

Knobloch, I. M., 1986, "On the Degenerate Hopf Bifurcation with 0(2) symmetry," Contemporary Mathematics, Vol. 56, pp. 193-201.

Knobloch, I. M., Guckenheimer, J., 1983, "Convective Transitions induced by a Varying Aspect Ratio," Physical Review A, Vol. 27 , pp. 408-417.

Lund, J. W., Saibel, E., 1967, "Oil Whip Whirl Orbits of a Rotor in Sleeve Bearings," Journal of Engineering for Industry, November, pp. 813-823.

Merkin, D. R., 1984, "On the Stability of Stationary Motions of Rotating Rotor Axis Mounted on Nonlinear Bearings," Prikl. Matem. Mekhan. U.S.S.R., Vol. 47, No. 3, pp. 321-326.

Moroz, I. M., Holmes, P., 1985, "Double Hopf Bifurcation and Quasiperiodic Flow in a Model for Baroclinic Instability," Journal of Atmospheric Science, Vol. 1, November, pp. 3147-3159.

Muszynska, A., 1974, "Non-Linear Excited and Self-Excited Precessional Vibrations of Symmetrical Rotors," Proceedings of the IUTAM Symposium, Lyngby, Denmark, August.

Myers, C. J., 1981, Ph.D. Thesis, University of Leeds.

Myers, C. J., 1984, "Bifurcation Theory Applied to Oil Whirl in Plain Cylindrical Journal Bearings," Journal of Applied Mechanics, Vol. 51, pp. 244-250.

Nayfeh, A. H., Mook, D. T., 1979, Nonlinear Oscillations, Wiley-Interscience.

Newkirk, B. L., 1924, "Shaft Whipping," General Electric Review, Vol. 27, pp. 169-178.

Newkirk, B. L., Taylor, N. D., 1925, "Shaft Whirling Due to Oil Action in Journal Bearings," Genaral Electric Review, Vol 28, No. 8.

Pozniak, E. L., 1958, "Influence of Resistance on the Stability of Rotating Shafts," Sb. "Problemy Prochnosti V Mashinostroenii," Izd-vo. Akad. Nauk USSR, No.1.

Reddi, M. M., Trumpler, P. R., 1962, "Stability of the High Speed Journal Bearing Under Steady Load, 1 The Incompressible Film," Journal of Engineering for Industry, August, pp. 351-358.

Robertson, D., 1935, "Hysteretic Influences on the Whirling of Rotors," Proc. Insti. Mech. Engrs., Vol 131, pp. 513-533.

Rosenblat, S., Cohen, D. S., 1981, "Periodically Perturbed Bifurcation. II. Hopf Bifurcation," Studies in Applied Mathematics, Vol. 64, pp. 143-175.

Schecter, S., 1987, "The Saddle-Node Separatrix-Loop Bifurcation," SIAM Journal on Mathematical Analysis, Vol. 18, No 4, pp. 1142-1156.

Smale, S., 1965, "Diffeomorphism with Many Periodic Points, Differential and Combinatorial Topology," Princeton University Press, Princeton, New Jersey.

Smith, D. M., 1933, "The Motion of a Rotor Carried by a Flexible Shaft in Flexible Bearings," Proceedings of the Royal Society of London, Vol. A142, pp. 92-118.

Sri Namachchivaya, N., Ariaratnam, S. T., 1987, "Periodically Perturbed Hopf Bifurcation," SIAM Journal of Applied Mathematics, Vol. 47, No. 1, pp. 15-39.

Takens, F., 1974, "Singularities of Vector Fields," Publ. Math. IHES, Vol. 43, pp. 47-100.

Taylor, D. L., 1980, "Limit Cycle Analysis of Rotors with Fluid Film Bearings," Proceedings Joint Automatic Control Conference, August, San Francisco.

Thomson, W. T., Younger, F. C., Gordon, H. S., 1977, "Whirl Stability of the Pendulously Supported Flywheel System," Journal of Applied Mechanics, Vol. 44, pp. 322-328.

Tondl, A., 1965, Some Problems of Rotor Dynamics, Publishing House of the Czechoslovak Academy of Sciences, Prague.

Torby, J., 1979, "The Effect of Structural Damping Upon the Whirling of Rotors," Journal of Applied Mechanics, Vol. 46, pp. 469-470.

Vance, J. M., 1987, Rotordynamics of Turbomachinery, John Wiley & Sons, New York.

Wiggins, S., 1988, Chaos and Global Bifurcations: Analytical Methods, Springer-Verlag.

Zhang, W., Ling, F. H., 1986, "Dynamic Stability of the Rotating Shaft made of Boltzmann Viscoelastic Solid," Journal of Applied Mechanics, Vol. 53, pp. 424-429.